This report was produced in cooperation with South Carolina Sea Grant Consortium

Morphology and Textures of Modern Sediments on the inner shelf of South Carolina's Long Bay from Little River Inlet to Winyah Bay

By J.F. Denny, W.E. Baldwin, W.C. Schwab, P.T. Gayes, R.A. Morton, and N.W. Driscoll

Open-File Report 2005-1345

U.S. Department of the Interior
U.S. Geological Survey

U.S. Department of the Interior
DIRK KEMPTHORNE, Secretary

U.S. Geological Survey
Mark D. Myers, Director

U.S. Geological Survey, Reston, Virginia 2007
Revised and reprinted: 2007

For product and ordering information:
World Wide Web: http://www.usgs.gov/pubprod
Telephone: 1-888-ASK-USGS

For more information on the USGS—the Federal source for science about the Earth, its natural and living resources, natural hazards, and the environment:
World Wide Web: http://www.usgs.gov
Telephone: 1-888-ASK-USGS

Suggested citation:
J.F. Denny, W.E. Baldwin, W.C. Schwab, P.T. Gayes, Morton, R.A., and N.W. Driscoll, 2007, Morphology and Textures of Modern Sediments on the inner shelf of South Carolina's Long Bay from Little River Inlet to Winyah Bay, CD-ROM. [Revised 2007]

Contents

Figures

Tables

Conversion Factors

Inch/Pound to SI

Multiply	By	To obtain
Length		
foot (ft)	0.3048	meter (m)
mile (mi)	1.609	kilometer (km)
mile, nautical (nmi)	1.852	kilometer (km)
yard (yd)	0.9144	meter (m)

Vertical coordinate information is referenced to the Mean Lower Low Water (MLLW).
Horizontal coordinate information is referenced to WGS84.

Morphology and Textures of Modern Sediments on the inner shelf of South Carolina's Long Bay from Little River Inlet to Winyah Bay

By J.F. Denny[1], W.E. Baldwin[1], W.C. Schwab[1], P.T. Gayes[2], R.A. Morton[3], N.W. Driscoll[4]

Abstract

High-resolution sea-floor mapping techniques, including sidecan-sonar, seismic-reflection, swath bathymetric systems, and bottom sampling, were used to map the geologic framework offshore of the northern South Carolina coast in order to provide a better understanding of the physical processes controlling coastal erosion and shoreline change. Four general sea floor environments were identified through analysis of sidescan-sonar, swath bathymetry, and surface sediment texture: inlet shoal complexes, shoal-detached shoals, hardground, and mixed zones. Inlet shoal complexes generally lie offshore of modern inlet systems, with the exception of a shore-detached shoal lying offshore of Myrtle Beach. The shoals show 1 – 3 m in relief and comprise the largest accumulations of modern sediment within the inner shelf survey area. Surficial sediments within the shoal complexes are characterized by a low-backscatter, moderately sorted fine sand. Hardground areas are characterized by exposures of Cretaceous and Tertiary strata and Pleistocene channel-fill deposits. These areas display little to no bathymetric relief and are characterized by high- surface texture and backscatter. These areas are characterized by a thin layer of modern sediment (< 1 m) and exposures of Cretaceous strata and Pleistocene channel-fill deposits.

Textural and geomorphic variations suggest a long-term net southerly flow within the study area. The general acoustic and textural character of the inner shelf within Long Bay suggests long-term erosion, reworking and continued modification of inner-shelf deposits by modern nearshore processes.

Introduction

The northeastern South Carolina coast (Figure 1) is a heavily developed region that supports a thriving tourism industry, large local populations and extensive infrastructure. The economic stability of the region is closely tied to the health of its beaches; primarily in providing support for local tourism and protection from storm events. Despite relatively low long-term shoreline erosion rates (~ 1 m/yr in some areas) (Anders and others, 1985; Morton and Miller, 2005), and the implied stability of the beaches, the economic impact of storm events to coastal communities has been

[1] USGS, Woods Hole Science Center, Woods Hole, Massachusetts
[2] Coastal Carolina University, Center for Marine and Wetland Studies, Conway, South Carolina
[3] USGS, Center for Coastal and Watershed Studies, St. Petersburg, Florida
[4] Scripps Institution of Oceanography, University of San Diego, San Diego, California

costly. For example, Hurricane Hugo made landfall on the central South Carolina coast in 1989. High winds and storm surge inflicted roughly $6 billion in property loss and damages and remains the costliest storm event in South Carolina history (Gayes, 1991). Localized erosion, commonly occurring around tidal inlets and erosion "hot spots", has also proved costly. Construction and maintenance of hard structures and beach nourishment, designed to mitigate the effects of erosion, have become annual or multi-annual expenditures (Gayes, 1991; Putney and others, 2004). Providing a better understanding of the physical processes controlling coastal erosion and shoreline change will allow for more effective management of coastal resources.

In 1999, the U.S. Geological Survey (USGS), in partnership with the South Carolina Sea Grant Consortium (SCSGC), began a study to investigate inner continental shelf and shoreface processes. Previous work shows that modern beach behavior and morphology of coastlines with limited sediment supply are heavily influenced by the structure and composition of older geologic strata located beneath and seaward of the shoreface (Milliman and others, 1972; Pilkey and others, 1981; Riggs and others, 1995, 1996, 1998; Schwab and others, 1997; 2000; Thieler and others, 1995, 2001; Boss and others, 2002). The objectives of the USGS/SCSGC cooperative program are: **1)** to provide a regional synthesis of the shallow geologic framework underlying the shoreface and inner continental shelf and define its role in coastal evolution and modern beach behavior; **2)** to identify and model the physical processes affecting coastal ocean circulation and sediment transport and to define their role in shaping the modern shoreline; and **3)** to identify sediment sources and transport pathways; ultimately leading to construction of a regional sediment budget. This study builds upon the work of Baldwin and others (2004), by describing inner shelf morphology and surficial sediment distribution and qualitatively assessing modern sediment transport pathways.

Setting

Long Bay is a large arcuate embayment that lies along the northeastern South Carolina coast, bound to the north and south by the Cape Fear and Santee Delta/Cape Romaine shoal complexes, respectively (Figure 1). This study focuses on the Grand Strand, a 100-km stretch of coastline within the apex of Long Bay that extends from Little River Inlet in the north to the mouth of Winyah Bay estuary in the south. This area of mainland coast is characterized by few barrier islands and associated tidal inlets, except at its northern and southern extents.

Presently, little modern fluvial sediment enters the Grand Strand region (Hayes, 1994; Patchineelam and others, 1999). To the south, the Pee Dee River system and its tributaries drain the Piedmont and coastal plain to the Winyah Bay estuary. Patchineelam and others (1999) and Hayes (1994) suggest that placement of dams along the Pee Dee River and trapping of fine-grained sediment within the bay and adjacent salt marshes severely restrict sediment input into the littoral system. The contribution of sediment from Winyah Bay to the study area is further limited by a southerly long-shore current, as evidenced by southerly spit growth at the entrance of Winyah Bay (Hayes, 1994; Gayes and others, 2003). North of the Grand Strand, the Cape Fear River enters Long Bay. However, the Cape Fear shoal complexes and spits appear to be efficient sediment sinks, limiting fluvial input from the Cape Fear River system to the southern portions of Long Bay (Denison, 1998; Patchineelam and others, 1999).

Long Bay is characterized as a mixed-energy environment, more heavily dominated by waves than tides. Tidal ranges are < 2 meters, and mean wave heights range between 1.2 to 1.3 meters (Hayes and others, 1993; Hayes, 1994). Long Bay represents a transition zone between the wave-dominated, microtidal North Carolina barrier-island coast to the tidally controlled, mesotidal

barrier coast of southern South Carolina and Georgia (Brown, 1977; Hayes and others, 1993; Hayes, 1994).

Winds within Long Bay vary somewhat seasonally, but yearly averages show that winds generally align with the southwest/northeast orientation of the coast (Brown, 1977; Blanton and others, 1985). During the winter, spring, and summer, northeast and southwest winds generally prevail, with north/northeast winds dominating in the fall.

Regional Geologic Setting

The Grand Strand region lies along the southern flank of the Mid-Carolina Platform High or Cape Fear Arch, the central axis of a structural high (Carolina Platform) that underlies portions of the Mid-Atlantic and Georgia Bight (Klitgord and others, 1988; Riggs and Belknap, 1988; Riggs and others, 1985; see Figure 2 in Baldwin and others, 2006) (Figure 1). The Mid-Carolina Platform High is an upward doming, subsurface feature that extends from Cape Lookout, N.C. to Cape Romaine, S.C. and positioning along its flank has influenced the thickness and distribution of post-Cretaceous strata throughout Long Bay (Riggs and others, 1985; Riggs and Belknap, 1988; Prowell and Obermeier, 1991). Later Cretaceous and Tertiary strata are absent throughout much of the region, indicating either a lack of deposition or erosion or partial preservation of these strata due to the combined influences of structural control and fluctuations in eustatic sea-level (Riggs and others, 1985; Poag and Valentine, 1988; Gohn, 1988; Riggs and Belknap, 1988; Colquhoun, 1972, 1995; Colquhoun and others, 1991; Ward and others, 1991, Baldwin and others, 2006). The discontinuous cover of Quaternary sediments observed within Long Bay is deposited unconformably on older, truncated Cretaceous and Tertiary strata and Pleistocene channel-fill deposits (Ward and others, 1991; Baldwin and others, 2004, 2006), marking erosion and deposition throughout repeated regressive and transgressive cycles.

Recent work by Baldwin and others (2004) show the study area is composed of outcropping Cretaceous and Tertiary strata with a thin, patchy and discontinuous veneer of Holocene sediment (Figure 2). Cretaceous and Tertiary strata are deeply incised by channels formed during sea-level lowstands as Piedmont and coastal plain rivers drained across the inner continental shelf and cut into older, subaerially exposed units. Gayes and others (1992) and Baldwin and others (2004) mapped smaller, less continuous channels that are thought to represent more recent drainage associated with tidal inlets, ephemeral swashes, or tidal creeks. Pleistocene channel-fill and Cretaceous and Tertiary strata are truncated by a regional unconformity that probably represents, in part, erosion during the most recent marine transgression (Gayes and others, 1992; Baldwin and others, 2004, 2006). Holocene sediment overlying the transgressive unconformity is generally thickest adjacent to modern inlet systems (Figure 3). Over much of the study area, however, the transgressive unconformity lies at the sea floor and the thickness of Holocene sediment cover is below the resolution of geophysical surveys.

Inland of the study area, the thickest Quaternary deposits exist as a series of relict barrier-island complexes extending across the lower coastal plain, marking previous sea-level high-stands. These deposits decrease in age and elevation toward the coast (Colquhoun, 1972; Colquhoun and others, 1991; Dubar and others, 1974; Dubar and Dubar, 1980; Owens 1989), with the modern shoreline consisting of Holocene sediment attached to a composite Pleistocene headland deposited during earlier sea-level high-stands (Brown, 1977; Colquhoun and others, 1991; Colquhoun, 1995; Putney and others, 2004).

Methods

In 1999, the USGS began an offshore geophysical mapping program between Little River Inlet and Winyah Bay (Figure 1). The study area covers 700 km^2 of the inner continental shelf from the seaward limit of breaking waves to ~10 km offshore. Six geophysical surveys were conducted over a five year period (1999 – 2003): October-November, 1999 aboard the *R/V Atlantic Surveyor* (Hill and others, 2000a, 2000b; Roberts and others, 2002); March 2000 aboard the *R/V Megan Miller* (Dadisman and others, 2001a, 2001b); June 2002 aboard the *R/V Atlantic Surveyor;* May 2001, 2002, and 2003 aboard the *R/V Coastal II*.

Geophysical data were acquired using a 100-105 kHz chirp sidescan-sonar system, a 2-7 kHz chirp sub-bottom profiler, a 300 Hz – 3 kHz boomer sub-bottom profiler, and a 234-kHz interferometric sonar during the offshore surveys aboard the *R/V Atlantic Surveyor* and the *R/V Megan Miller*. During the nearshore surveys aboard the *R/V Coastal II*, geophysical data were acquired using a 100/500 kHz dual-frequency sidescan-sonar system, a 500 Hz – 12 kHz chirp sub-bottom profiler, and a 234-kHz interferometric sonar. A full description of data acquisition and processing routines applied to the sub-bottom data is presented in Baldwin and others (2004).

Sidescan-sonar data were acquired at a 0.125-s sample rate, yielding a 400-m swath width. Data were digitally recorded at a 2 kHz sample rate, yielding ~ 0.2 m pixel resolution following the methodology of Danforth and others (1991). Data were further processed and digitally mosiacked based on procedures described in Paskevich (1992) and Danforth (1997). The composite sidescan-sonar mosaic was generated at a 4m/pixel resolution and exported from the processing software as a georeferenced Tagged Image File Format (TIFF), and incorporated into a Geographic Information System (GIS).

Swath bathymetric data were acquired with a 234-kHz interferometric sonar at a 0.133-s ping rate and digitally logged at a 2 kHz sample rate. The swath width of the interferometric sonar varied as a function of depth but generally achieved 7 – 10 times water depth, or 50 – 150 meters. A Motion Reference Unit (MRU) mounted directly above the sonar head recorded vessel motion (pitch, heave, roll, and yaw); attitude information was used to rectify bathymetric soundings. Additionally, a Sound Velocity Profiler (SVP) was used during nearshore surveys to measure the speed of sound in the water column. The sound-velocity structure is needed in order to accurately model the ray path to correct for refraction. Because an SVP was not available for use during offshore surveys, an average sound velocity of 1490 m/s was used. Vertical resolution for all surveys is approximately 1% of water depth. Bathymetric data were rectified for tidal fluctuations based on the ADCIRC circulation model (see *http://www.marine.unc.edu/C_CATS/adcirc/adcirc.htm*) and referenced to Mean Lower Low Water. Data were further processed using multibeam processing software developed at the University of New Brunswick (see *http://www.unb.omg.edu*). Fully processed bathymetric data were gridded at a 100 meter cell size and incorporated into a GIS.

Surface grab samples were collected by Coastal Carolina University using a Shipek grab sampler during the 2000 – 2002 field seasons (Figure 1). Locations were chosen based on variations in backscatter patterns observed in the sidescan-sonar mosaic (Figure 4). A total of 722 grab samples were collected during three cruises aboard the NOAA *Ferrel* (2000 and 2001) and *Nancy Foster* (2002) (Appendix A). Grain-size analyses for samples collected in 2000 were conducted by the USGS following the methodology of Poppe and others (1985). Surface samples collected in 2001 and 2002 were analyzed at Coastal Carolina University following a similar methodology.

Ship position for all surveys was determined through use of Differential Global Positioning System (DGPS) navigation. Slant-range position of the sidescan-sonar towfish was acquired through use of an acoustic ranging unit. Ship position, towfish altitude, and slant-range position are used to triangulate towfish layback (i.e. straight-line distance behind the vessel). Towfish position is assumed to be ± 5 m. The interferometric sonar was deployed on a rigid side-mount during all surveys. Offsets between the sonar head and the DGPS antenna were measured and the horizontal accuracy of bathymetric data is within ± 1 – 2 m. Grab sample locations were navigated through use of DGPS and are accurate to ± 1 – 2 m.

Shore-parallel survey tracklines were spaced 300 m apart to ensure overlap of adjacent sidescan-sonar swaths and complete coverage of the sea floor. The swath width of the interferometric sonar ranged from ~ 50 – 150 meters; thus only partial bathymetric coverage of the sea floor was achieved. In order to generate a bathymetric grid that accurately represents the regional sea-floor morphology, interpolation routines were used to fill data gaps between tracklines. All data were imported to a GIS for ease of display, analysis and interpretation.

Mapping Results

Bathymetry

The inner shelf of Long Bay exhibits a low-relief, gently seaward-dipping sea floor. Water depths range from 4 m in nearshore areas (< 1 km offshore) to 14 m at the seaward edge of the survey area (10 km offshore) (Figure 5). Average sea floor gradients vary across the shelf. The steepest slopes of 1 - 4 m/km occur in nearshore areas (landward of the 7-m isobath) and decrease to 0.5 -1 m/km in offshore areas. The gentle seaward dip is interrupted in many locations by isolated bathymetric highs defined here as large-scale shoals, associated with modern inlets or shore-detached, and smaller-scale, low-relief ridges present throughout the study area (Table 1). Shoals and ridges were identified using swath bathymetry and seismic-reflection profiles. Figure 3 outlines the location of inlet-associated and shore-detached shoals. Ridge crests are outlined on Figure 5 and ridge morphology is summarized in Table 2.

Shoals

Inlet-Associated

Offshore of Waites Island, an inlet shoal complex abuts the shoreface and extends along the coast from Little River Inlet to North Myrtle Beach. Variations in shoreface profiles illustrate the along- and cross-shore extent of the shoal complex (Figure 6). Seaward of Waites Island, the shoreface has a gentle slope with average gradients of ~2 - 4 m/km in < 7 meter water depth. To the southwest, the shoreface steepens and exhibits average gradients of ~6 – 8 m/km in < 7 meter water depth, marking the southern terminus of the shoal complex.

Offshore of Murrells Inlet a series of well-developed, shore-perpendicular shoals extend from the shoreface to the offshore extent of the survey area, ranging from ~ 5 – 12 m water depth (Figure 5). The shoals generally are 1 – 2 m high, 4 – 5 km wide, and 10 km long and show some asymmetry with slightly steeper NE-facing sides (Figure 7).

Offshore of North Inlet, a third inlet shoal complex extends from the nearshore bounds of the survey (1 km offshore; ~ 5 m water depth) to the ~ 8-m isobath (~ 5 km offshore) and along the coast from the southern edge of Pawley's Island south to North Island (Figure 3). Average gradients offshore of North Inlet are 2 – 4m/km in < 8 m water depth (Figure 5).

Shore-detached

A large, shore-oblique, N/NE-S/SW trending shoal extends from the shoreface offshore of northern Myrtle Beach to the offshore edge of the study area, in water depths ranging from ~7 – 12 m (Figure 5). The shoal is ~2 m high, 5 – 6 km wide, and 11 km long and shows no discernable asymmetry (Figure 8).

Ridges

Small-scale, low-relief ridges range from the shoreface to the offshore extent of the survey area from North Myrtle Beach to Winyah Bay (Figure 5). These features average < 1 m high and ~1 km wide and range in length from 0.5 to 3 km. Orientation varies from shore-perpendicular to shore-oblique, with shore-perpendicular features lying primarily offshore of Myrtle Beach. Little to no asymmetry is observed along these shore-normal features.

Between Pawley's Island and the southern extent of the survey area, the inner shelf is characterized by a NE-SW bathymetric fabric produced by a series of shore-oblique sand ridges (Figure 5). Directly offshore of Pawley's Island, the ridges are moderately- to poorly-developed (~ 1 to 2 m in height, < 0.5 km in width, and 1 km in length), have little to no asymmetry, and trend NE-SW from the shoreface to the 9-m isobath (Figure 9). The ridges become well-developed offshore of North Island (~ 2 to 6 m high, 0.5 to 1 km wide, and 1 to 6 km long), where they exhibit definitive asymmetry (steep southern facing slopes), and trend NE-SW from the shoreface to the offshore extent of the survey area (Figure 10). More subtle bathymetric highs, directly offshore of North Inlet and just north of the mouth of Winyah Bay, represent the smaller inlet shoal complexes associated with North Inlet and Winyah Bay.

Sidescan-Sonar

The variation in acoustic backscatter within the sidescan-sonar imagery reveals the complexities of the sea floor within Long Bay (Figure 4). High backscatter, or a strong acoustic return, is represented by light tones and low backscatter, or a weak acoustic return, is represented by dark tones. Three primary regimes have been identified based on dominant backscatter characteristics of the sea floor: 1) uniform areas of low backscatter, 2) uniform areas of moderate to high backscatter, and 3) patchy areas of mixed low and high backscatter.

1) Areas of Low Backscatter

Two expanses of uniform low backscatter lie offshore of Myrtle Beach and Murrells Inlet and correspond to localized bathymetric highs; the shore-detached shoal and inlet shoal complex, respectively (Figures 4 and 5). Low backscatter extends from the shoreface to the offshore extent of the survey in both locations. The shore-detached shoal offshore of Myrtle Beach is bound by areas of moderate to high backscatter, with more abrupt backscatter gradients to the north and west than to its south/southeast. To the north, a series of cross-hatched shore-normal and shore-parallel thin bands of high-backscatter (< 500 m in length) abut the shoal. To the west, a well defined transition from low to high backscatter borders the shoal. A more gradual transition exists along its south/southeastern boundary, where backscatter grades from low to a region of patchy low to moderate backscatter that extends to the seaward edge of the survey area (Figure 8).

The inlet shoal complex offshore of Murrells Inlet is characterized by large expanses of low backscatter with isolated areas of moderate backscatter (Figure 7). Sharp transitions exist between the low backscatter expanses and adjacent moderate to high backscatter areas along the

south/southwest and north/northeast borders of the complex. The low-backscatter expanses correspond to the south/southwest sides and crests of the shore-perpendicular shoals, while the north/northeast sides and trough are characterized by moderate backscatter (Figure 11). Narrow bands of shore-oblique, moderate backscatter extend from the shoreface to the offshore extent of the survey area and average <100 m wide and ~1 km long. The moderate backscatter signature corresponds to the trough of a series of low-relief ridges superimposed upon the larger shoal complex (Figure 5). The low-relief ridge crests and sides are characterized by low backscatter (Figure 7).

2) Areas of Moderate to High Backscatter

Two expanses of moderate to high backscatter lie offshore of Surfside Beach and between Pawley's Island and the mouth of Winyah Bay (Figure 4). Little bathymetric variability is present within the high-backscatter region offshore of Surfside Beach; the area is characterized by a gently, seaward dipping sea floor and complex patterns of shore-normal and sinuous high-backscatter (Figure 12). The area is bordered by the low-backscatter expanse of the Murrells Inlet shoal complex to the south, and patchy regions of low to moderate backscatter to the north.

The high-backscatter area offshore of Pawley's Island shows slight bathymetric variability. Small-scale, shore-oblique ridges (< 1 m relief) lie inshore of the 8-m isobath and are characterized by high backscatter on the southern side and moderate backscatter along the northern side and trough (Figure 9). Offshore of the 8-m isobath to the seaward edge of the survey area, relatively uniform high backscatter covers a gently, seaward dipping sea floor, with few bathymetric perturbations. Offshore of North Island to the south, large-scale, shore-oblique ridges show moderate backscatter on the southern sides and high backscatter along the northern sides and troughs (Figure 10).

3) Areas of Mixed Low, Moderate, and High Backscatter

Localized areas of low, moderate, and high backscatter on the inner shelf are located primarily from Myrtle Beach north to Little River Inlet (Figure 4). The complex backscatter patterns correspond to a series of low-relief ridges trending roughly northwest (NW) to southeast (SE). In water depths less than 9-m off Myrtle Beach, low backscatter covers the SW-facing sides and crests of the ridges, and moderate to high backscatter cover the NE-facing sides and trough (Figure 11). The transition from low to high backscatter across these features is gradual. More abrupt backscatter transitions are present inshore of the 9-m isobath, where shore-normal bands of low and high backscatter extend seaward from the shoreface (Figure 13). High backscatter appears to be concentrated within the trough of shore-normal low-relief ridges, with low backscatter along the crest. In some locations, shore-parallel ripples were resolved within the high backscatter troughs. Figure 14 displays ripple crests present within one trough and illustrate the characteristically sharp transition between high to low backscatter at trough margins.

Complex patterns of moderate to high backscatter are present offshore of North Myrtle Beach north to Little River Inlet, where the sea floor displays a gentle, seaward-dipping slope. Little bathymetric variability appears to be associated with the shore-normal regions of low and high backscatter offshore of the 9-m isobath.

Grain Size

The surface sediments of the inner shelf within Long Bay primarily consist of poorly sorted sands (Appendix A). Grain size distribution within the study area ranges from very coarse sand (-1 phi) to a coarse silt (6 phi), with a mean grain size of medium sand (1.6 phi) (Figure 15). Sorting ranges from well sorted (0.39 phi) to very poorly sorted (2.94 phi), with a mean of poorly sorted (1.09 phi).

In order to evaluate the relationship between variations in textural properties of the surficial sediment and acoustic backscatter, mean backscatter values were extracted from the sidescan-sonar imagery using a 10-m radius around sample locations and plotted against mean grain size divided by sorting (Figure 16). The 10-m radius was chosen to account for navigational uncertainty in sample locations. Samples were excluded from analysis if the 10-m radius encompassed backscatter transitions, for example an abrupt boundary between high and low backscatter. Ninety-nine samples fell along backscatter transitions, leaving 623 samples for analysis.

There is a wide range of scatter and no statistically significant correlation between mean grain size divided by standard deviation versus mean backscatter (Figure 16). However, a qualitative relationship exists between grain size distribution and sorting, variations in backscatter and sea floor morphology (Figures 4, 5 and 15). For example, the surficial sediments within the low backscatter expanses of the inlet shoal complexes and the shore-detached shoal consist predominately of moderately sorted, fine sand (mean sorting = 0.8 phi; mean grain size = 2.34 phi). In contrast, the surface sediments within the moderate to high backscatter, gently sloping regions offshore of Surfside Beach and Pawley's Island consist of poorly sorted, medium to coarse sand (sorting = 1.33 phi; mean grain size = 1.05 phi). The less expansive regions of mixed low to moderate backscatter display variable bathymetry (low-relief ridges and areas of gently sloping sea floor) and are characterized by poorly sorted, medium sands (sorting = 1.05 phi; mean grain size = 1.6 phi).

Grain size and sorting distributions along the low-relief ridges offshore of Myrtle Beach further exemplify these patterns. Surficial sediment generally becomes finer along a transect that begins in the high backscatter trough, rises up the gentle north-facing slope, and ends at the crest. Sorting follows a similar pattern along the same transect, with relatively poorly sorted material in the trough and slightly better sorted material on the north-facing slope and crest. Although the vertical exaggeration of the perspective views within Figures 17 and 18 is extreme (200x) and ridges only show ~ 1 m of vertical relief over horizontal distances of ~ 2 km, the general association of fining grain size and improved sorting to position on the ridge (i.e. crest, trough, or flank) appears to be characteristic of the study area (Figure 11). Textures are generally finer and better sorted on the crests and north-facing slopes, whereas textures are coarser and less well sorted in the troughs and south-facing slopes.

Discussion

Integrated analysis of sidescan-sonar imagery, swath bathymetry, and surface sediment texture reveals a complex range of sea floor environments offshore of the Grand Strand. Through the work of this study and that of Baldwin and others (2004), the environments of the inner shelf are broadly characterized as: 1) inlet shoal complexes; 2) shore-detached shoals; 3) hardground areas; and 4) mixed zones (Figure 19).

Inlet Shoal Complexes

Inlet shoal complexes lie offshore of Waites Island, Myrtle Beach, Murrells Inlet, North Island, and the mouth of Winyah Bay. With the exception of the shore-oblique shoal offshore of Myrtle Beach, all shoal complexes are associated with modern inlet systems (Figure 3). Baldwin and others (2004) show that these shoal complexes represent the greatest accumulation of modern sediment within the study area (Figures 3, 5, 7-10), and unconformably overlie Cretaceous and Tertiary strata and Pleistocene channel-fill deposits (Figures 7 and 8).

The inlet shoal complex offshore of Waites Island is characterized by fine to medium sand, moderate to low backscatter, and a gently, seaward-dipping shoreface (Figure 6). Baldwin and others (2004) mapped up to 6 m of modern sediment within the shoal complex (Figure 3) and suggest that the relatively thick accumulation of sediment is associated with the Waites Island transgressive barrier and Little River and Hog Inlets that bound the island to the north and south, respectively.

Modern sediment deposits (~ 1 – 3 m thick) within the Murrells Inlet shoal complex (Figure 3) are characterized by uniform low backscatter and contain surficial sediments that predominately consist of fine sand (Figure 15). Where the surficial sediments are thin, underlying Pleistocene channel deposits are exposed at the sea floor. These exposures generally consist of coarse sand and are defined by complex patterns of high-backscatter that extend from the shoreface to the offshore extent of the survey area. Pleistocene deposits are also exposed in the troughs of a series of shore-oblique sand ridges superimposed on the larger shore-perpendicular shoals. Fine sands (< 3 m thick) comprise the low-backscatter ridge crests (Figure 4 and 15).

Baldwin and others (2004) mapped small shallow channels lying above the transgressive unconformity directly offshore of Murrells Inlet. The shallow channels show less cross-shelf continuity than the larger channels that cut into Cretaceous and Tertiary strata below the transgressive unconformity (Baldwin and others, 2004; 2006). While the larger channels have been interpreted to represent the result of downcutting by Pleistocene rivers during previous sea-level low-stands, the shallow channels are interpreted to represent younger drainage, including tidal creeks, tidal inlets and/or local swashes (Baldwin and others, 2004). The thick modern sediment deposits, presence of younger channels and proximity to the modern tidal-inlet indicate the Murrells Inlet shoal complex likely represents the landward retreat of the inlet system (Baldwin and others, 2004). The series of shore-oblique ridges cross-cutting the shoals suggests that sediments within the complex are being reworked by modern nearshore processes.

From Pawley's Island to the mouth of Winyah Bay, Pleistocene channel-fill deposits and Tertiary strata are exposed at the sea floor between thick deposits of modern sediment (Figures 3, 9 and 10) (Baldwin and others, 2004). The thickest sediment deposits are contained within low to moderate backscatter, shore-oblique ridges that extend across the survey area. Pleistocene channel-fill deposits are exposed within the adjacent troughs and display complex patterns of high-backscatter within the sidescan-sonar imagery (Figures 8-10). Tertiary strata exposed at the sea floor in isolated locations offshore of Pawley's Island are also characterized by expanses of high backscatter. Surficial grain size distribution shows the region to be generally composed of coarse sand, with concentrations of medium sand along ridge crests and coarse sand within the trough (Figure 15). Proximity to the Winyah Bay estuary and the greater Santee Delta/Cape Romaine shoal complex probably accounts for the large accumulations of modern sediment within this portion of the study area. These sediments appear to be actively reworked by modern processes, as evidenced by the series of relatively large (> 3 m) shore-oblique ridges.

Shore-detached Shoals

The NE-SW trending shore-oblique low backscatter shoal offshore of Myrtle Beach is characterized by up to 3 m of well-sorted, medium sand and represents the only large accumulation of modern sediment on the inner shelf not associated with an active inlet system (Baldwin and others, 2004). Two of the larger swash systems in the region (Whitepoint and Singleton Swash) lie directly landward of the shoal (Figure 3). Upland morphology indicates that these swashes likely represent the remnants of a relict tidal inlet that could have provided the sedimentary source for the shore-detached shoal. Inshore of the shoal, Baldwin and others (2004) mapped shallow channels above the transgressive unconformity, and interpret their formation to drainage of back-barrier creeks, swash or tidal inlet systems. Calibrated radiocarbon dates, based on shell and organic material extracted from the upper ~1.2 - 1.5 m of the shoal deposit, constrain its age to Holocene (4070 +/- 40 BP – 8040 +/- 150 BP; P.T. Gayes, pers. comm.)(Figure 8, Appendix B). Due to the presence of modern swash systems on the adjacent upland, younger channels inshore of the shoal, and the Holocene age of the shoal deposit, we interpret this feature to represent the remnants of an ebb-tidal delta complex produced by an inlet system that did not survive the most recent marine transgression.

Hardground Areas

Hardground areas are characterized by complex patterns of high-backscatter within the sidescan-sonar imagery, little bathymetric variation, and coarse surficial texture (Figures 4, 5 and 15). Two expansive regions of hardground lie within the study area: offshore of Surfside Beach and Pawley's Island. Little to no modern sediment is present in these areas; Cretaceous and Tertiary strata and Pleistocene channel-fill deposits are exposed at the sea floor (Baldwin and others, 2004) (Figures 2 and 3). Surficial sediment samples consisting of poorly sorted, coarse sand were collected within the hardground areas (Figure 1), suggesting that a thin layer of modern sediment may exist but is most likely below the resolution of the geophysical systems (~ < 0.5 m). Any mobile fraction is most likely transported away from the area as deposition of fine sediment would be inhibited by near-bottom turbulence associated with the rough substrate. Baldwin and others (2004), show that the exposed strata within these areas have undergone differential erosion, probably during repeated regressive and transgressive cycles. This appears to be reflected in the complex high-backscatter patterns displayed within the sidescan-sonar imagery (Figure 12).

Studies along the Atlantic seaboard have shown that erosion of the inner shelf may provide a local source of sediment to sediment-starved regions (Pilkey and Field, 1972; Milliman and others, 1972; Pilkey and others, 1981; Hine and Snyder, 1985; Demarest and Leatherman, 1985; Schwab and others, 1997, 2000; Thieler and others, 1995, 2001). Riggs and others (1996) have shown that degradation of relict strata in neighboring Onslow Bay (Figure 1) provides a local source of sediment to the coastal system. Ojeda and others (2004) and Gayes and others (2003) suggest that hardground areas within Long Bay may also contribute sediment to the coastal system through active erosion by biological and mechanical processes. However, the coarse-grained nature of the sediments within the hardground areas implies that erosion may primarily occur during storm events, when conditions for entrainment and transport of coarse material would prevail (Gayes, 1991).

Mixed Zones

The northern half of the survey area, with the exception of the shore-detached shoal offshore of Myrtle Beach and the inlet shoal complex offshore of Waites Island, is characterized by small-scale spatial variations in backscatter and bathymetry and surface sediments ranging from fine to coarse sand (Figures 4, 5 and 15). Where modern sediment is absent, Cretaceous strata and Pleistocene channel-fill deposits lie at, or near, the sea floor (Figure 2). These broad expanses of outcrop exhibit complex moderate to high backscatter patterns and coarse surface texture. Where modern sediment exceeds 0.5 m in thickness, these strata locally appear within the trough and northern side of low-relief ridges (Figures 3 and 11). Uniform low-backscatter defines the fine to medium sand crest and southern face of these features (Figure 17). Offshore of Myrtle Beach (< 9-m water depth), wave-orbital ripples are observed within the coarse-grained, high-backscatter trough of smaller-scale, shore-normal, low-relief ridges (Figure 14). Little to no asymmetry is associated with these features.

The backscatter variations and grain size distribution of the shore-normal, low-relief ridges offshore of Myrtle Beach are similar to the sorted bedforms (previously, 'rippled scour depressions') mapped in other inner shelf environments (Thieler and others, 1995; Schwab and others, 2000; Goff and others, 2005). Murray and Thieler (2004) adopt the term 'sorted bedforms' to describe asymmetric, low-relief, shore-normal features offshore of Wrightsville Beach, N.C., and propose their development occurs by way of complex interactions between dominant along-shore flow (interaction of waves and currents) and poorly sorted bottom sediments. Gutierrez and others (2005) analyzed near-bed current measurements within the sorted bedforms offshore of North Carolina. Their findings support the work of Murray and Thieler (2004) and suggest that the differences in bed roughness within the coarse grained trough and finer grained crest are enhanced during strong wind and wave events. Increased turbulence inhibits deposition of fine sand within coarse grained areas, thus providing a mechanism for maintenance of the coarse to fine grained segregation characteristic of sorted bedforms (Grant and Madsen, 1986; Murray and Thieler, 2004).

Asymmetry was noted in the morphology of sorted bedforms mapped offshore of Martha's Vineyard (Goff and others, 2005), southern Long Island (Schwab and others, 2000), and North Carolina (Thieler and others, 2001), yet the shore-normal, low-relief ridges offshore of Myrtle Beach show no asymmetry (Figure 11). Additionally, varying thicknesses of mobile sediment were present within other inner shelf settings (Thieler and others, 1995; Schwab and others, 2000; Goff and others, 2005). Figure 13, shows that little to no modern sediment was mapped offshore of Myrtle Beach; the transgressive unconformity lies at the sea floor, capping Cretaceous strata and Pleistocene channel-fill deposits (Baldwin and others, 2004). The low-backscatter signature and fine grained texture of sediments sampled along the crest of the shore-normal, low-relief ridges is similar to the surficial character of modern sediment deposits throughout the survey area and may suggest the presence of a thin (< 0.5 m) layer of modern sediment that is below the resolution of the seismic systems.

The shore-normal, low-relief ridges appear to be influenced by modern nearshore processes, as evidenced by the presence of wave-orbital ripples, a common feature of the sorted bedforms (Thieler and others, 1995; Schwab and others, 2000; Goff and others, 2005). However, based on the thin to absent layer of modern sediment and the exposure of underlying geologic strata throughout the area, the general morphology and surficial character of these features appears to be mostly controlled by the underlying geology. If more sediment were available within the coastal system, sorted bedforms more characteristic of those mapped along the inner shelf of the U.S. Atlantic coast would likely develop.

Mixed areas show a range in sediment cover from no cover (i.e. exposed strata) to ~ 1 meter or greater. This variability is thought to reflect an increased temporal and spatial sediment flux as compared to the relatively stable shoal complexes (sediment accumulation) and hardground areas (erosion or non-deposition). Sediment flux is most likely driven by proximity to a source (i.e. shoals, shoreface, etc.), variability of nearshore hydrodynamics due to seasonal and climactic forcing, and location (i.e., proximity to inlets). Ongoing physical oceanographic studies will aid in defining the magnitude and temporal signature of sediment flux within these areas.

Sediment Transport

Qualitative assessments of sediment transport directions can be inferred from the general morphology and textural variations within the inner shelf. Perspective views of the regional morphology and backscatter and textural variations characteristic of the study area are displayed within Figures 11, 17 and 18. Within all ridge like features, high-backscatter, poorly sorted, coarse-grained trough and NE sides lie adjacent to low-backscatter, moderately-sorted, medium- to fine-grained crest and SW sides. These textural and morphologic signatures may reflect the long-term erosion of the inner shelf. Similar processes were described by Schwab and others (2000) and Twichell and others (2003), where reworking of inner-shelf deposits results in selective transport of finer grained sediments, leaving a coarse-grained winnowed lag. Based on geomorphic and textural evidence within Long Bay, net long-term transport of fine-grained sediments appears to be to the southwest, producing a winnowed lag on the northeast side of low-relief ridges (Figure 19). However, local perturbations to long-term net southerly flow may exist. Cross-cutting bedforms directly landward of the shore-detached shoal offshore of northern Myrtle Beach (Figure 8) suggest that there may be some cross-shelf component to flow. Recent work by Gutierrez and others (2006) show that in the study area cross-shelf flow may persist under certain prevailing wind conditions.

Conclusion

Analysis of sidescan-sonar imagery, swath bathymetry, and surface sediment texture reveals four general sea floor environments within Long Bay: inlet shoal complexes, shore-detached shoals, hardgrounds, and mixed zones. Generally, inlet shoal complexes lie offshore of modern inlet systems, with the exception of a shore-detached shoal lying offshore of Myrtle Beach. The shoal complexes comprise the greatest accumulations of modern sediment within the inner shelf and represent the most significant bathymetric highs. They consist of moderately sorted fine sand and are defined by low-backscatter within the sidescan-sonar imagery. Hardground areas lie offshore of Surfside Beach and Pawley's Island and are characterized by exposures of Cretaceous and Tertiary strata and Pleistocene channel-fill deposits reflected as high-backscatter within the sidescan-sonar imagery. Little to no bathymetric variability is displayed within these areas, and surficial sediments generally contain poorly sorted coarse sand. Mixed zones show small-scale spatial variations in bathymetry, surface texture, and backscatter. These areas are characterized by a thin layer of modern sediment, generally less than 1.5 m, and exposures of Cretaceous strata and Pleistocene channel-fill deposits corresponding to low and high backscatter, respectively. The variability in sediment cover is thought to reflect an increased temporal and spatial sediment flux driven by proximity to sediment source and changes in nearshore hydrodynamics due to seasonal and climactic forcing.

Variations in surface texture and acoustic backscatter appear to be related to sea floor morphology within Long Bay. Low-relief, ridge-like features characteristic of the study area display a high-backscatter, poorly sorted, coarse-grained NE face and trough, with a low-backscatter, moderately to well sorted, medium to fine sand crest and SW face. Textural and geomorphic variations suggest a long-term net southerly flow within the study area. The general acoustic and textural character of the inner shelf within Long Bay suggests long-term erosion, reworking and continued modification of inner-shelf deposits by modern nearshore processes.

References Cited

Anders, F.J., Reed, D.W., and Meisburger, E.P., 1985, Shoreline Movements, Report 2, Tybee Island, Georgia, to Cape Fear, North Carolina, 1851-1983, USACE Technical Report, CERC-83-1, 164p.

Baldwin, W.E., Morton, R. A., Denny, J.F., Dadisman, S.V., Schwab, W.C., Gayes, P.T., and Driscoll, N.W., 2004, Maps Showing the Stratigraphic Framework of South Carolina's Long Bay from Little River to Winyah Bay, U.S. Geological Survey Open-File Report, 2004-1013.

Baldwin, W.E., Morton, R.A., Putney, T.R., Katuna M.P., Harris, M.S., Gayes, P.T., Driscoll, N.W., Denny, J.F., and Schwab, W.C., 2006, Migration of the Pee Dee River System inferred from Ancestral Paleochannels underlying the South Carolina Grad Strand and Long Bay inner shelf, GSA Bulletin, v.118, no. 5/6, p. 533-549.

Blanton, J.O, Schwing, F.B., Weber, A.H., Pietrafesa, L.J., and Hayes, D.W., 1985, Wind stress climatology in the South Atlantic Bight, *in* Oceanography of the Southeastern U.S. Continental Shelf, Atkinson, L.P., Menzel, E.W., and Bush, K.A., eds., American Geophysical Union, Washington, D.C.

Boss, S.K., Hoffman, C.W., and Cooper, B., 2002, Influence of fluvial processes on the Quaternary geologic framework of the continental shelf, North Carolina, USA, Marine Geology, v. 183, p. 45-65.

Brown, P.J., 1977, Variations of South Carolina coastal morphology, Southeastern Geology, v.18, no. 4, p. 249-264.

Colquhoun, D.J., 1972, Charleston Harbor, South Carolina estuarine values study – Physical and chemical identification of sediments deposited in Charleston Harbor: Report to U.S. Army Corps of Engineers, Charleston, South Carolina District, p. 53, 19 sheets.

Colquhoun, D.J., Johnson, G.H., Peebles, P.C., Huddlestun, P.F., and Scott, T., 1991, Quaternary geology of the Atlantic Coastal Plain, *in* Morrison, R.B., ed. Quaternary nonglacial geology: Conterminous U.S.: Boulder, Colorado, Geological Society of America, The Geology of North America, v. K-2, p. 629-650.

Colquhoun, D.J., 1995, A review of Cenozoic evolution of the southeastern United States Atlantic coast north of the Georgia Trough, Quaternary International, v. 26, p. 35-41.

Dadisman, S.V., Hill, J.C. and Schwab, W.C., 2001a, Archive of Datasonics SIS-1000 chirp sub-bottom data collected during USGS cruise MGNM00014, central South Carolina, 13-30 March 2000. USGS Open-File Report 00-462, 4 CD-ROMs.

Dadisman, S.V., Hill, J.C. and Schwab, W.C., 2001b, Archive of boomer sub-bottom data collected during USGS MGNM00014, central South Carolina, 13-30 March 2000. USGS Open-File Report 00-462, 4 CD-ROMs.

Danforth, W.W., O'Brien, T.F., and Schwab, W.C., 1991, USGS image processing system: Near real-time mosaicking of high-resolution sidescan-sonar data: Sea Technology, January, p. 54-59.

Danforth, W.W., 1997, Xsonar/Showimage: A complete system for rapid sidescan-sonar processing and display: USGS Open-File Report 97-686, p. 77.

Demarest, J.M., and Leatherman, S.P., 1985, Mainland influence on coastal transgression: Delmarva Peninsula, Marine Geology, v. 63, p. 19 – 33.

Denison, P., 1998, Beach renourishment/groin field construction project: Bald Head Island, NC: Shore and Beach, Jan 1998, p. 2-9.

DuBar, J.R., and DuBar, S.S., 1980, Neogene biostratigraphy and morphology of northeastern South Carolina, *in* Frey, R.W., ed., Excursions in Southeastern Geology: Geological Society of America 1980 Annual Meeting Guidebook, Field Trip No. 9, Atlanta, GA: Falls Church, VA, p. 179 – 189.

DuBar, J.R., Johnson, H.S. Jr., Thom, B. and Hatchell, W.O., 1974, Neogene stratigraphy and morphology, south flank of the Cape Fear Arch, North and South Carolina, *in* Oaks, R.Q. and DuBar, J.R., eds., Post-Miocene Stratigraphy central and southern Atlantic Coastal Plain: Utah State University Press, Logan, UT, p. 139-173.

Gayes, P.T., 1991, Post Hurricane Hugo nearshore sidescan-sonar survey; Myrtle Beach to Folly Beach, South Carolina, *in*: Finkl, C.W., Pilkey, O.H., (Eds.), Journal of Coastal Research, Special Issue 8, 95-111.

Gayes, P.T., Nelson, D.D., and Ward, T., 1992, Ancestral channels of the ancient Pee Dee river on the inner continental shelf off Murrells Inlet, South Carolina, South Carolina Geology, v. 32, no. 1 & 2, p. 53 – 56.

Gayes, P.T., Schwab, W.C., Driscoll, N.W., Morton, R.A., Baldwin, W.E., Denny, J.F., Harris, M.S., Wright, E.E., and Katuna, M.P., 2003, Sediment dispersal pathways and conceptual sediment budget in Long Bay: a southeast U.S. sediment starved embayment, Coastal Sediments '03 Conference Proceedings, Clear Water Beach, Florida, 18 – 23 May, 2003, p 14.

Goff, J.A., Mayer, L.A., Traykovski, P., Buynevich, I., Wilkens, R., Raymond, R., Glang, G., Evans, R.L., Olson, H., and Jenkins, C., 2005, Detailed investigation of sorted bedforms, or

"rippled scour depressions," within the Martha's Vineyard Coastal Observatory, Massachusetts, Continental Shelf Research, v. 25, p. 461-484.

Gohn, G.S., 1988, Late Mesozoic and early Cenozoic geology of the Atlantic Coastal Plain: North Carolina to Florida, Sheridan, R.E., and Grow, J.A., eds., The Atlantic continental margin: Boulder, Colorado. The Geological Society of America, The Geology of North America, v. 1-2, p. 107-130.

Grant, W.D., and Madsen, O.S., 1986, The continental-shelf bottom boundary layer. Annual Review of Fluid Mechanics 18, 265-305.

Gutierrez, B.T., Voulgaris, G., and Thieler, E.R., 2005, Exploring the persistence of sorted bedforms on the inner-shelf of Wrightsville Beach, North Carolina, Continental Shelf Research, v. 25, p. 65-90.

Gutierrez, B.T., Voulgaris, G., Work, P.A., 2006, Cross-shore variation of wind-driven flows on the inner shelf in Long Bay, South Carolina, United States, Journal of Geophysical Research, v. 111, C0315, p. 1-16.

Hayes, M.O., Sexton, W.J., Colquhoun, D.J, and Eckard, T.L., 1993, Evolution of the Santee/Pee Dee delta complex, South Carolina, USA, in Kay, R. ed., Deltas of the World, American Society of Civil Engineers, New York, NY, USA, p. 54-64.

Hayes, M.O., 1994, The Georgia Bight barrier system, *in* Davis, R.A., Jr. ed. Geology of Holocene Barrier Island Systems, New York: Springer-Verlag, p. 233-304.

Hill, J.C., Schwab, W.C., Dadisman, S., Danforth, W.W., Denny, J.F., O'Brien, T.F., and Parolski, K., 2000a, Archive of chirp data collected during USGS cruise ATSV99044 Myrtle Beach, South Carolina, 29 October – 14 November 1999. USGS Open-File Report 00-040, 9 CD-ROMs.

Hill, J.C., Schwab, W.C., Dadisman, S.V., Danforth, W.W., Denny, J.F., O'Brien, T.F., and Parolski, K.F., 2000b, Archive of boomer sub-bottom data collected during USGS cruise ATSV99044 Myrtle Beach, South Carolina, 29 October – 12 November 1999. USGS Open-File Report 00-153, 18 CD-ROMs.

Hine, A.C., and Snyder, S.W., 1985, Coastal lithosome preservation: evidence from the shoreface and inner continental shelf off Bogue Banks, North Carolina, Marine Geology, v. 63, p. 307-330.

Klitgord, K.D., Hutchinson, D.R., and Schouten, H., 1988, U.S. Atlantic continental margin: structural and tectonic framework, *in* Sheridan, R.E., and Grow, J.A., eds., The Atlantic continental margin: Boulder, Colorado. The Geological Society of America, The Geology of North America, v. 1-2, p. 19-55.

Milliman, J.D., Pilkey, O.H., and Ross, D.A., 1972, Sediments of the Continental Margin off the Eastern United States, Geological Society of America Bulletin, v. 83, p. 1315-1334.

Morton, R. A., and Miller, T. L., 2005, National assessment of shoreline change: Part 2: Historical shoreline changes and associated coastal land loss along the U.S. Southeast Atlantic coast: U.S. Geological Survey Open-file Report 2005-1401 (http://pubs.usgs.gov/of/2005/1401/).

Murray, A.B., and Thieler, E.R., 2004, A new hypothesis and exploratory model for the formation of large-scale inner-shelf sediment sorting and "rippled scour depressions", Continental Shelf Research, v. 24, p. 295-315.

National Oceanographic and Atmospheric Administration (NOAA) – National Geophysical Data Center (NGDC), 2001, Coastal relief model – U.S. southeast Atlantic coast: Boulder, Colorado, NOAA-NGDC, v.2, CD-ROM.

Ojeda, German Y., Gayes, P.T., Van Dolah, R.F., and Schwab, W.C., 2004, Spatially quantitative seafloor habitat mapping: example from the northern South Carolina inner continental shelf, Estuarine Coastal and Shelf Science, v. 59, p. 399-416.

Owens, J.P., 1989, Geologic map of the Cape Fear region, Florence 1° x 2° quadrangle and northern half of the Georgetown 1° x 2° quadrangle, North Carolina and South Carolina: U.S. Geological Survey, Miscellaneous Investigations Series Map I-1948-A, scale 1:250000.

Paskevich, V., 1992, Digital mapping of side-scan sonar data with the Woods Hole Image Processing System software: USGS Open-File Report 92-536, p. 87.

Patchineelam, S.M., Kjerfve B., and Gardner, L. Robert, 1999, A preliminary sediment budget for the Winyah Bay estuary, South Carolina, USA, Marine Geology, v. 162, p. 133-144.

Pilkey, O.H., and Field, M.E., 1972, Onshore transportation of continental shelf sediment, *in* Swift, D.J.P, Duane, D.B., and Pilkey, O.H., eds., Shelf Sediment Transport: Process and Pattern, Duane, Hutchinson and Ross, Inc., Pennsylvania, p. 429 – 446.

Pilkey, O.H., Blackwelder, B.W., Knebel, H.J., and Ayers, M.W., 1981, The Georgia Embayment continental shelf: Stratigraphy of a submergence, Geological Society of America Bulletin, v. 92, p. 52-63.

Poag, W.C., and Valentine, P.C., 1988, Mesozoic and Cenozoic stratigraphy of the U.S. Atlantic continental shelf and slope, in Sheridan, R.E., and Grow, J.A., eds., The Atlantic continental margin: Boulder, Colorado, The Geological Society of America, The Geology of North America, v. 1-2, p. 67-86.

Poppe, L.J., Eliason, A.H., and Fredricks, J.J., 1985, APASA – An Automated Particle Size Analysis System: USGS Circular 963, p. 7.

Prowell, D.C. and Obermeier, S.F., 1991, Evidence of Cenozoic tectonism, *in* Horton, J.W., Jr., and Zullo, V.A., eds., The Geology of the Carolinas: Carolina Geological Society Fiftieth Anniversary Volume, p. 309-318.

Putney, T.R., Katuna, M.P., and Harris, M.S., 2004, Subsurface stratigraphy and geomorphology of the Grand Strand, Georgetown and Horry Counties, South Carolina: Southeastern Geology, v. 42, no. 4, p.217-236.

Riggs, S.R., Snyder, S.W.P., Hine, A.C., Snyder, S.W., Ellington, M.D., and Mallette, P.M., 1985, Geologic framework of phosphate resources in Onslow Bay, North Carolina continental shelf: Economic Geology and Bulletin of the Society of Economic Geologists, v. 80, p. 716-738.

Riggs, S.R., and Belknap, D.F., 1988, Upper Cenozoic processes and environments of he continental margin sedimentation: eastern United States, *in*, R.E. Sheridan and J.A. Grow, eds., The Geology of North America v 1-2, The Atlantic Continental Margin: U.S. Geological Society of America, Boulder, CO, p. 131-176.

Riggs, S.R., Cleary, W.J., and Snyder, S.W., 1995, Influence of inherited geologic framework on barrier shoreface morphology and dynamics: Marine Geology, v. 126, p. 213-243.

Riggs, S.R., Snyder, S.W., Hine, A.C., and Mearns, D.L., 1996, Hardbottom Morphology and relationship to the geologic framework: Mid-Atlantic continental shelf, Journal of Sedimentary Research, v. 66, no. 4, p. 830-846.

Riggs, S.R., Ambrose, W.G., Cook, J.W., Snyder, S.W., and Snyder, S.W., 1998, Sediment production on sediment-starved continental margins: the interrelationship between hardbottoms, sedimentological and benthic community processes, and storm dynamics, Journal of Sedimentary Research, v. 68, no. 1, p. 155-168.

Roberts, C., Hammar-Klose, E., and Schwab, W.C., 2002, Archive of sidescan-sonar data and DGPS navigation data collected during USGS cruise ATSV99044, South Carolina coast, 29 October – 14 November, USGS Open-File Report 02-103, 5 DVD-ROMs.

Schwab, W.C., Allison, M.A., Corso, W., Lotto, L.L., Butman, B., Buchholtz ten Brink, M., Denny, J.F., Danforth, W.W., and Foster, D.S., 1997, Initial Results of high-resolution sea-floor mapping offshore of the New York-New Jersey metropolitan area using sidescan sonar, Northeastern Geology & Environmental Sciences, v. 19, no. 4, p. 243-262.

Schwab, W.C., Thieler, E.R., Allen, J.R., Foster, D.S., Swift, B.A., and Denny, J.F., 2000, Influence of inner-continental shelf geologic framework on the evolution and behavior of the barrier-island system between Fire Island Inlet and Shinnecock Inlet, Long Island, New York, Journal of Coastal Research, v. 16, no. 2, p.408-422.

Thieler, E.R., Brill, A.L., Cleary, W.J., Hobbs, C.H., and Gammisch, R.A., 1995, Geology of the Wrightsville Beach, North Carolina shoreface: Implications for the concept of shoreface profile of equilibrium, Marine Geology, v. 126, p. 271-287.

Thieler, E.R, Pilkey, O.H., Cleary, W.J., and Schwab, W.C., 2001, Modern sedimentation on the shoreface and inner continental shelf at Wrightsville Beach, North Carolina, U.S.A., Journal of Sedimentary Research, v. 71, no. 6, p.958-970.

Twichell, D., Brooks, G., Gelfenbaum, G., Paskevich, V., and Donahue, B., 2003, Sand ridges off Sarasota, Florida: A complex facies boundary on a low-energy inner shelf environment, Marine Geology, v. 200, p. 243-262.

Ward, L.W., Bailey, R.H., and Carter, J.G., 1991, Pliocene and early Pleistocene stratigraphy, depositional history, and molluscan paleobiogeography of the coastal plain, *in* Horton, J.W., Jr., and Zullo, V.A., eds., The geology of the Carolinas: Knoxville, Tennessee, Carolina Geological Society Fiftieth Anniversary Volume, University of Tennessee Press, p. 274-289.

Acknowledgements

We thank Tom O'Brien, William Danforth, Dave Nichols, Shawn Dadisman, Jenna Hill, Charles Worley, Barry Irwin, Walter Barnhardt, Paul Byham, Richard Goldberg, Elizabeth Johnston, Neil Gielstra, German Ojeda, and Jamie Phillips for their support during field operations. Additionally, we thank the crews of the *R/V Atlantic Surveyor*, *R/V Megan Miller*, and the *R/V Coastal II* for their support during field efforts. We thank Dave Twichell and Walter Barnhardt for their thorough reviews of this document.

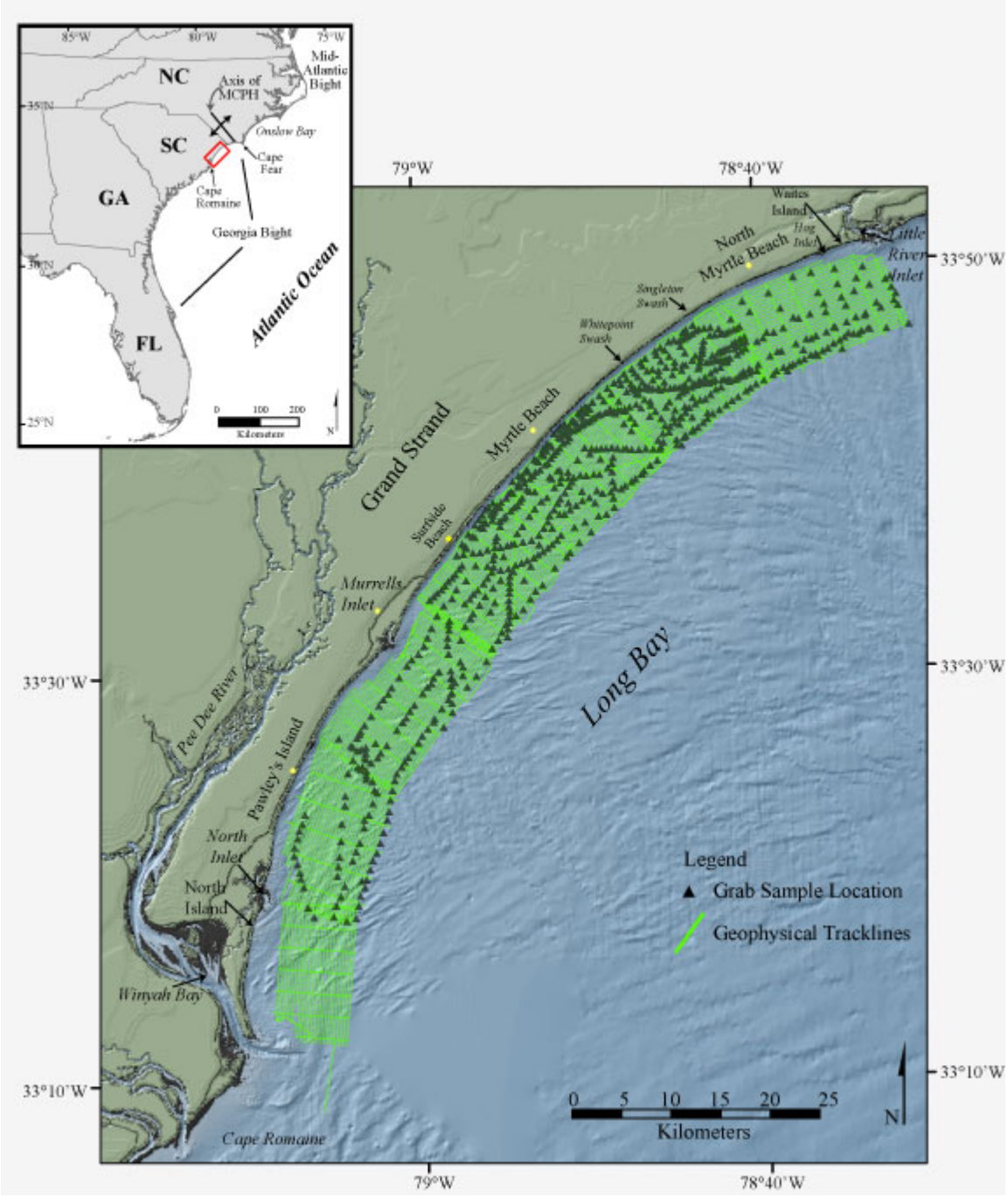

Figure 1. Location map of the study area showing geophysical tracklines and surficial grab sample locations. Inset map shows major water bodies, coastal landforms, and the regional orientation and axis of the Mid-Carolina Platform High (MCPH). The background shaded relief imagery is a digital elevation model of the northeastern South Carolina coastal plain (NOAA-NGDC, 2001).

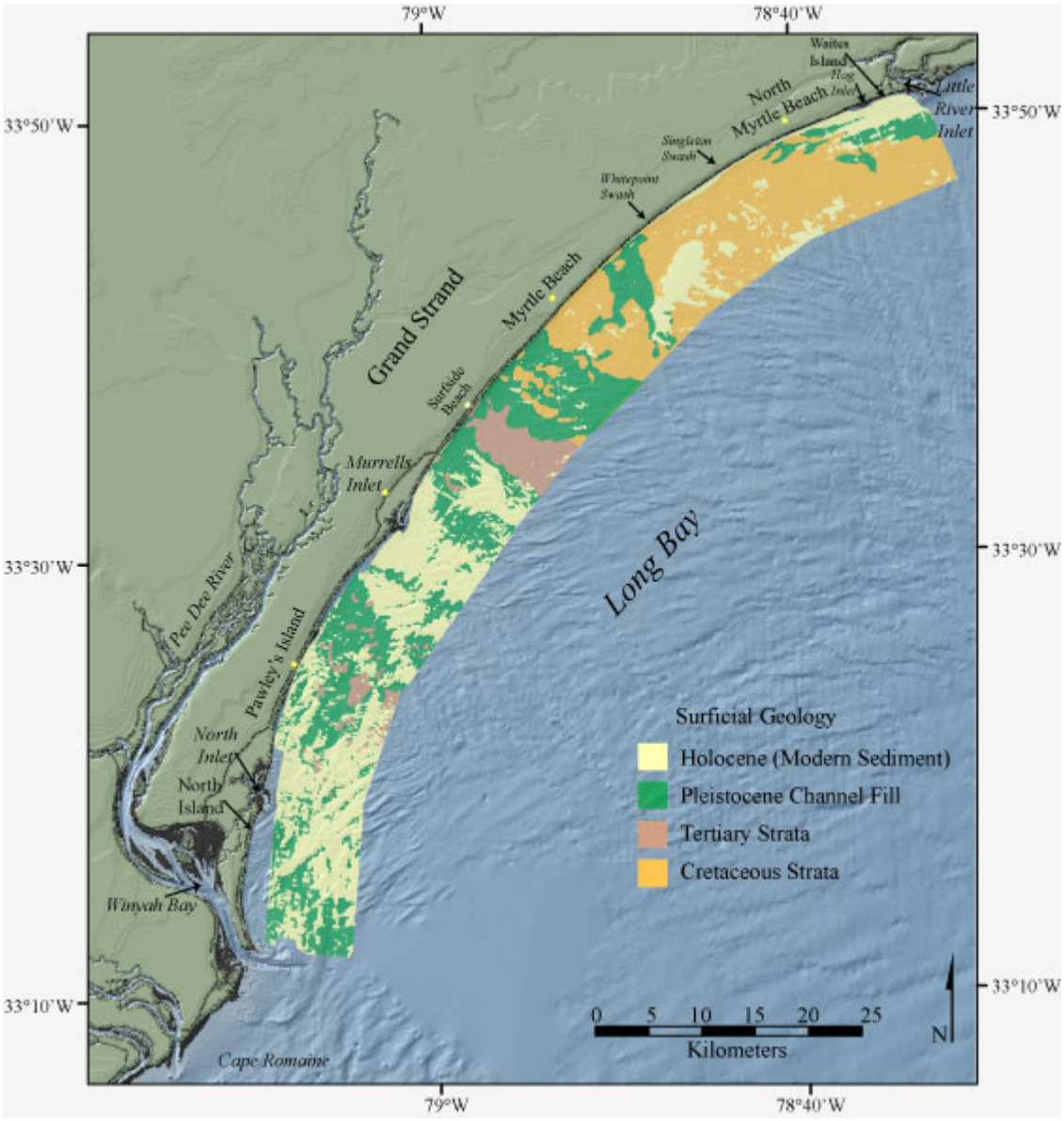

Figure 2. Surficial geologic map of the study area based on Baldwin and others (2004). The inner shelf consists of exposures of Cretaceous and Tertiary strata, Pleistocene channel-fill deposits, and discontinuous deposits of modern sediment. The background shaded relief imagery is a digital elevation model of the northeastern South Carolina coastal plain (NOAA-NGDC, 2001).

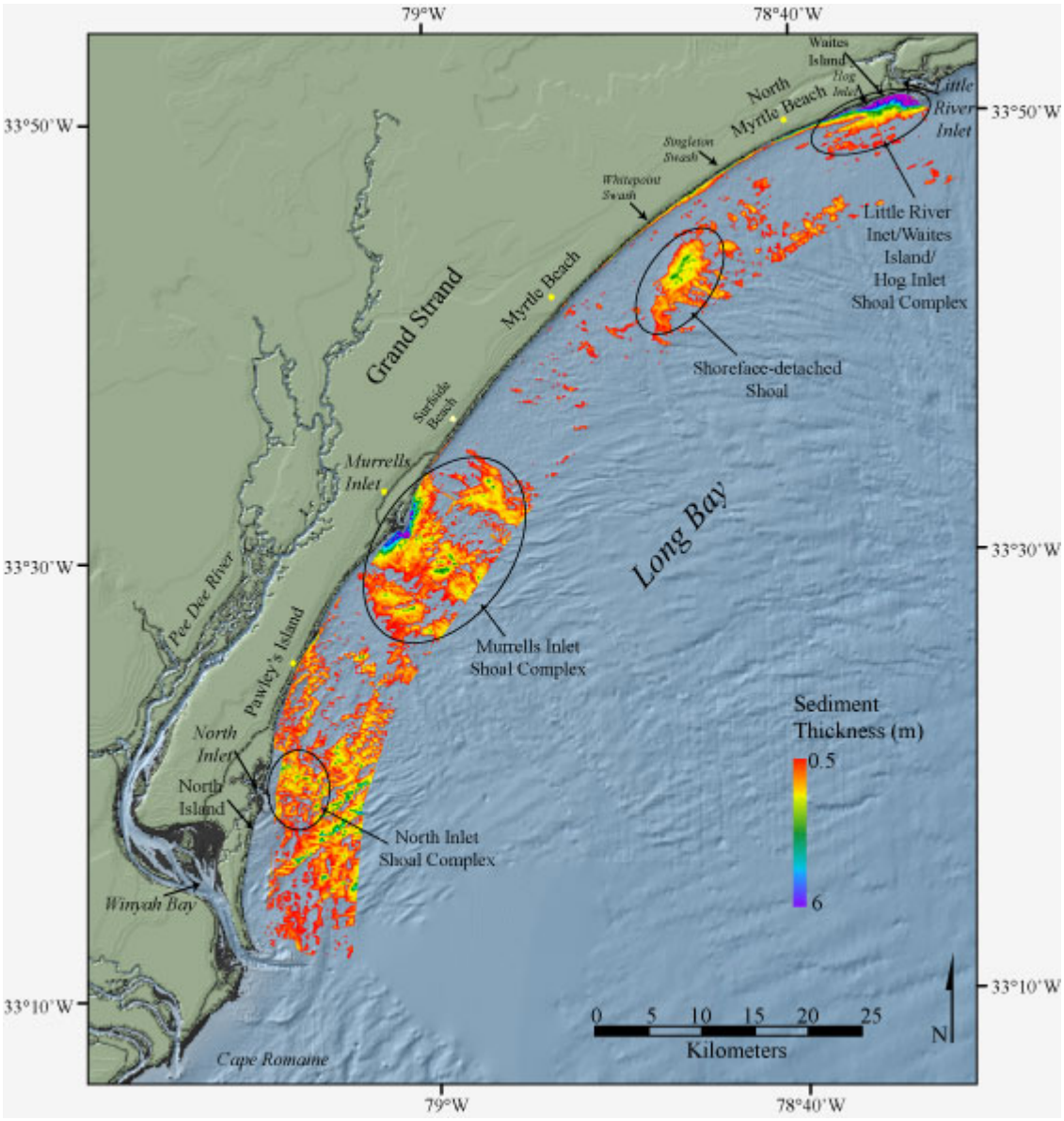

Figure 3. Map showing the thickness of modern sediment within the study area. Sediment thickness was mapped through interpretation of chirp seismic reflection data. Inlet shoal complexes and shore-detached shoals are outlined. Thicknesses are reported in meters (assuming a velocity of 1500m/sec). Areas where the sea floor bathymetry is visible indicate areas of surficial sediment < 0.5 m thick. Figure modified from Baldwin and others (2004, their Figure 17). The background shaded relief imagery is a digital elevation model of the northeastern South Carolina coastal plain (NOAA-NGDC, 2001).

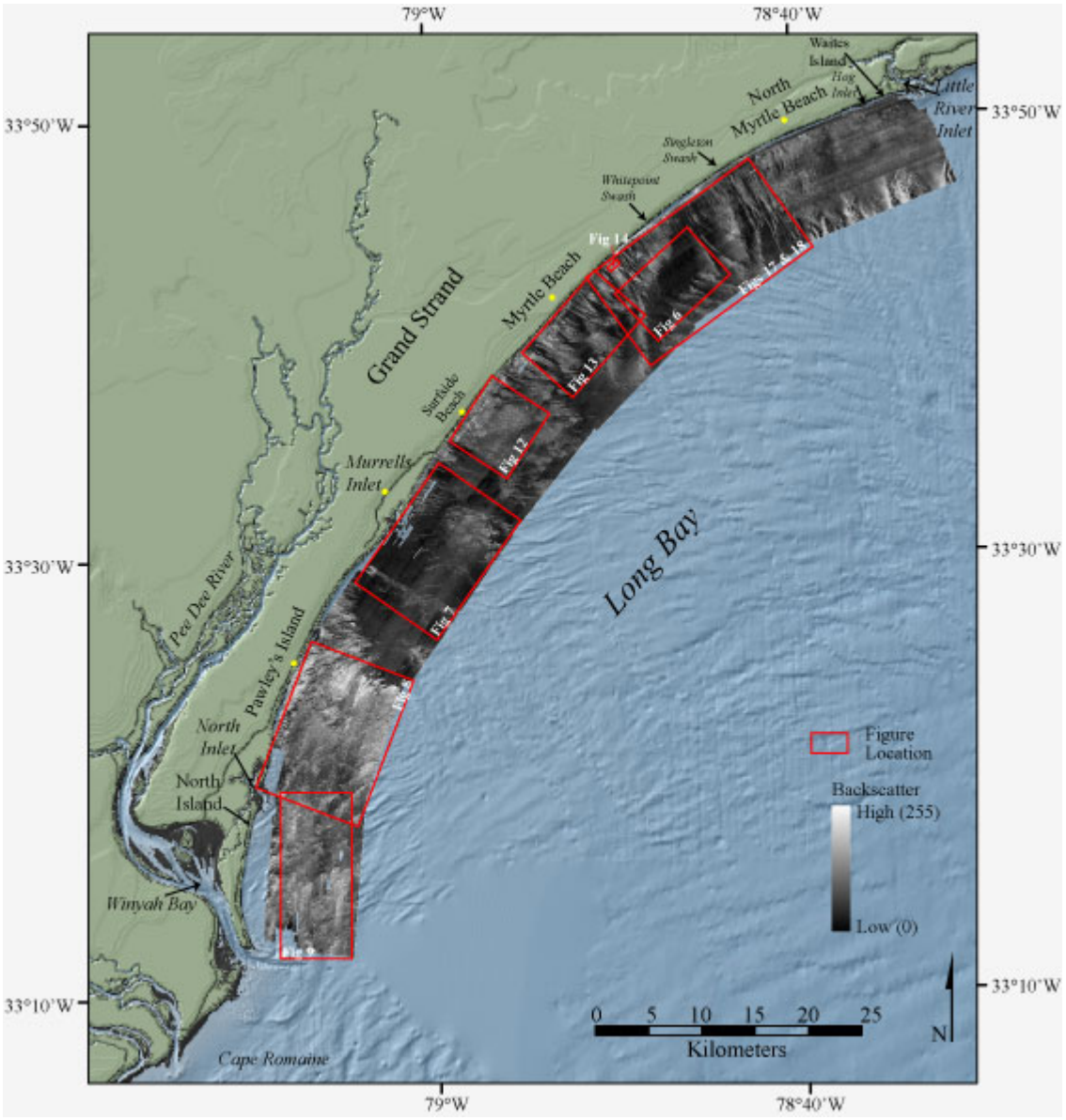

Figure 4. Sidescan-sonar image of the study area and figure locations. High backscatter is represented as light tones within the imagery, low-backscatter is represented by dark tones.

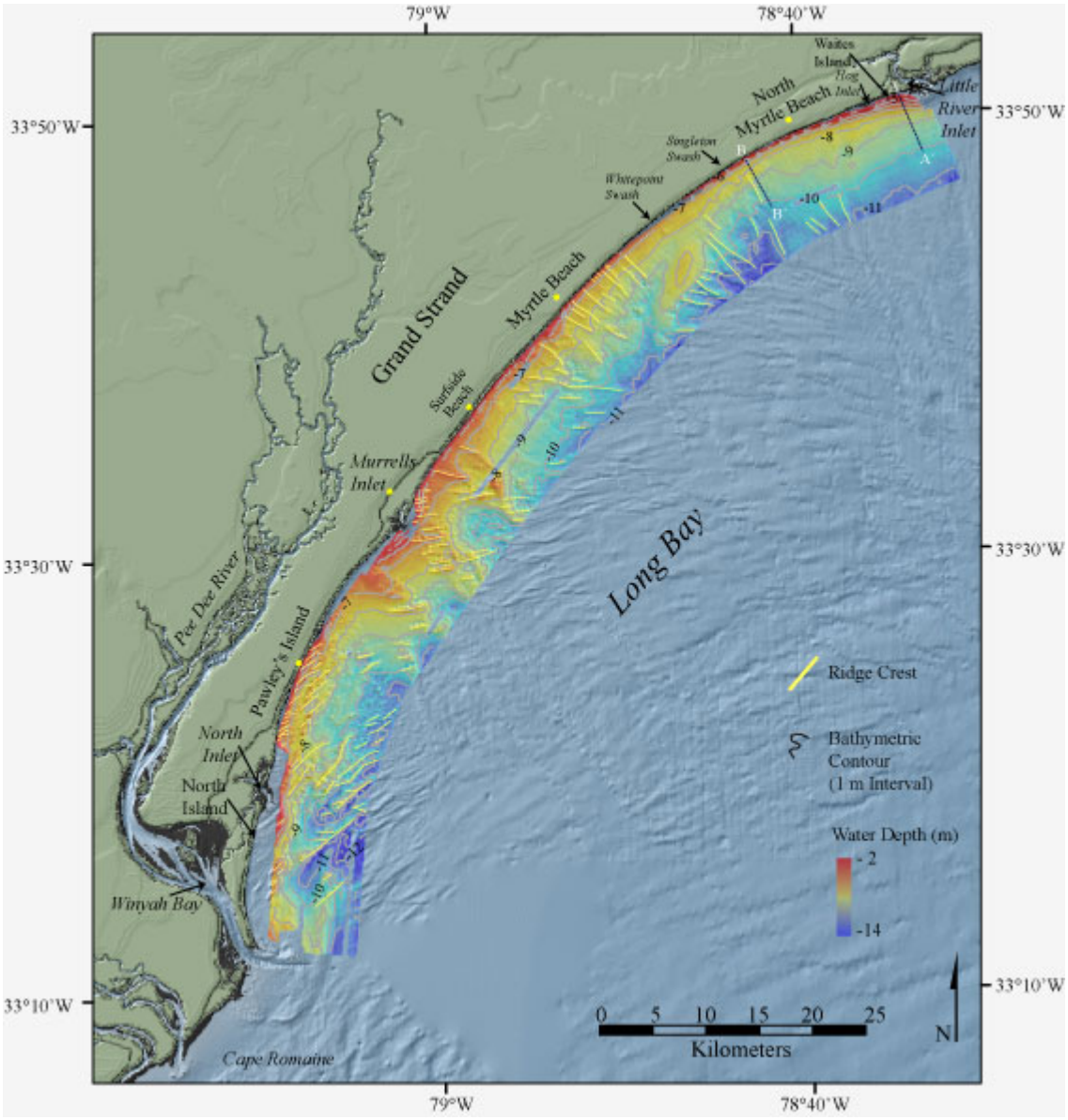

Figure 5. Map showing the bathymetry within the study area. Contour interval is 1 m. Ridge crests are displayed. Location of shoreface profiles A-A' and B-B' in Figure 6 are displayed. Depth in the study area ranges from 2 to 14 meters. The background shaded relief imagery is a digital elevation model of the northeastern South Carolina coastal plain (NOAA-NGDC, 2001).

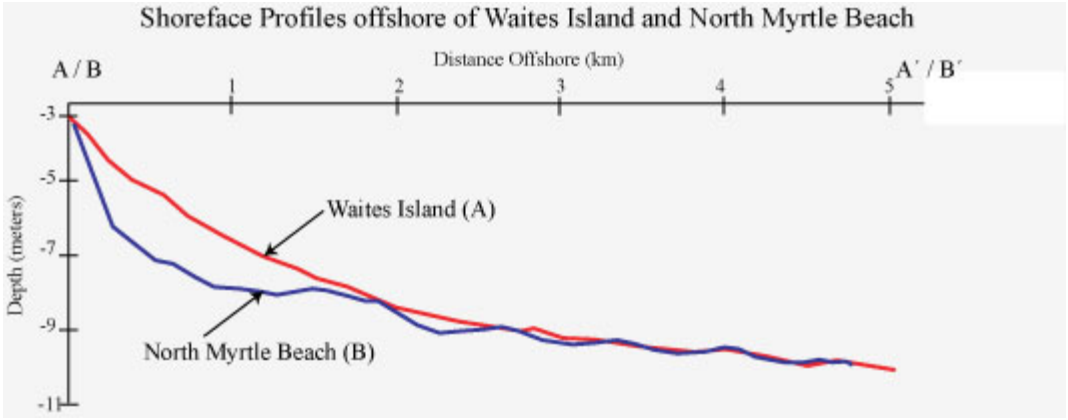

Figure 6. Bathymetric profiles across the shoreface and inner shelf of Long Bay. Figure 4 identifies the location of profile transects. A) The smooth shoreface offshore of Waites displays a gentle slope due to influence of the inlet shoal complex associated with Little River Inlet. B) The more irregular shoreface offshore of North Myrtle Beach is steeper where it lies outside the influence of the inlet shoal complex.

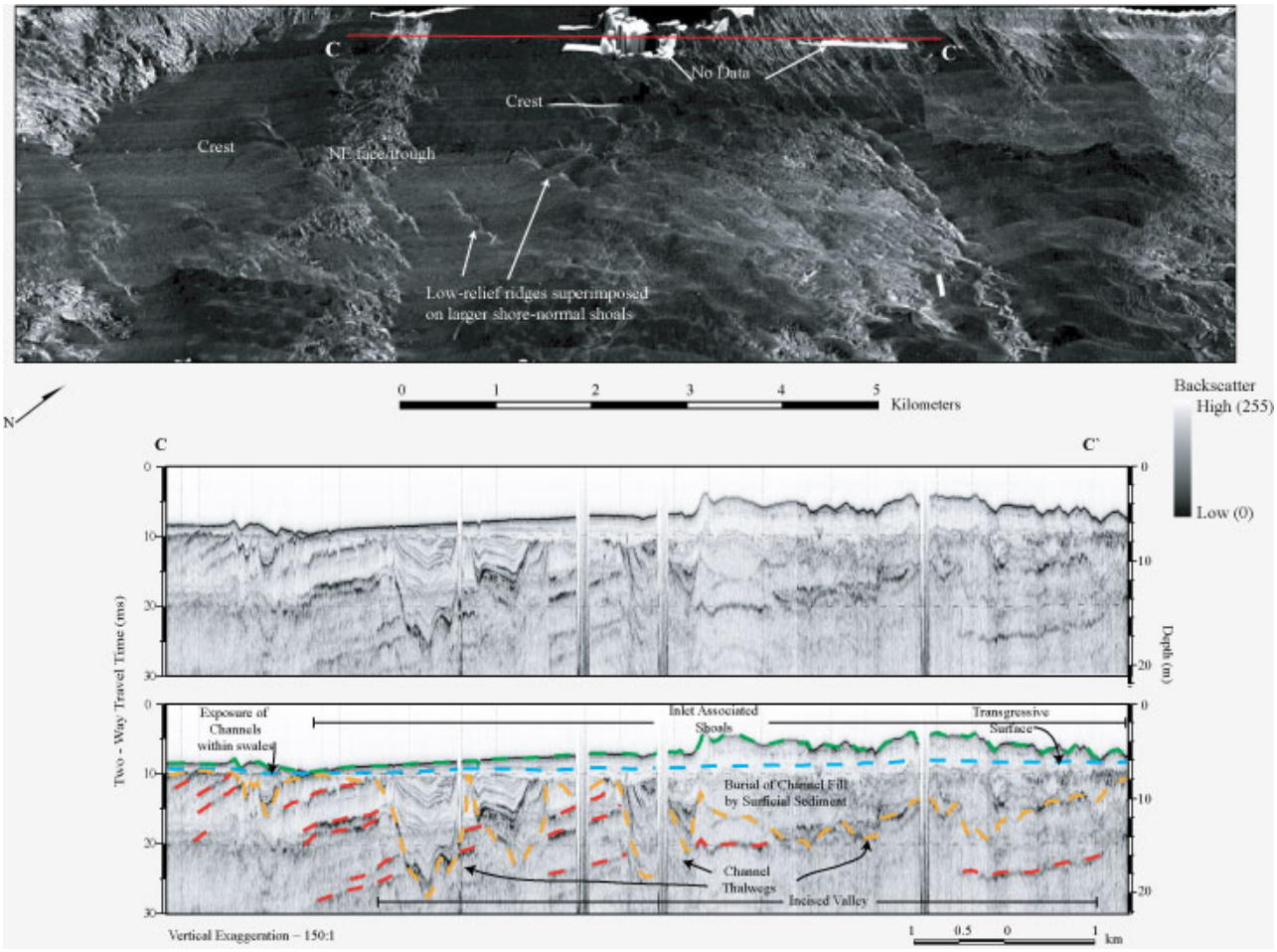

Figure 7. Sidescan-sonar imagery and chirp seismic-reflection profile across the inlet shoal complex offshore of Murrells Inlet. See Figure 4 for figure location. Top: Perspective view of sidescan-sonar imagery draped over bathymetry, showing shore-oblique, low-relief ridges and the crest of the larger shore-normal shoals. Bottom: Chirp seismic-reflection profile shows the shoal complex overlying the transgressive surface, which truncates Pleistocene channels (yellow) and Cretaceous strata (red). Depth is approximate and assumes a seismic velocity of 1500 m/sec. Figure modified from Baldwin and others (2004, their Figure 13).

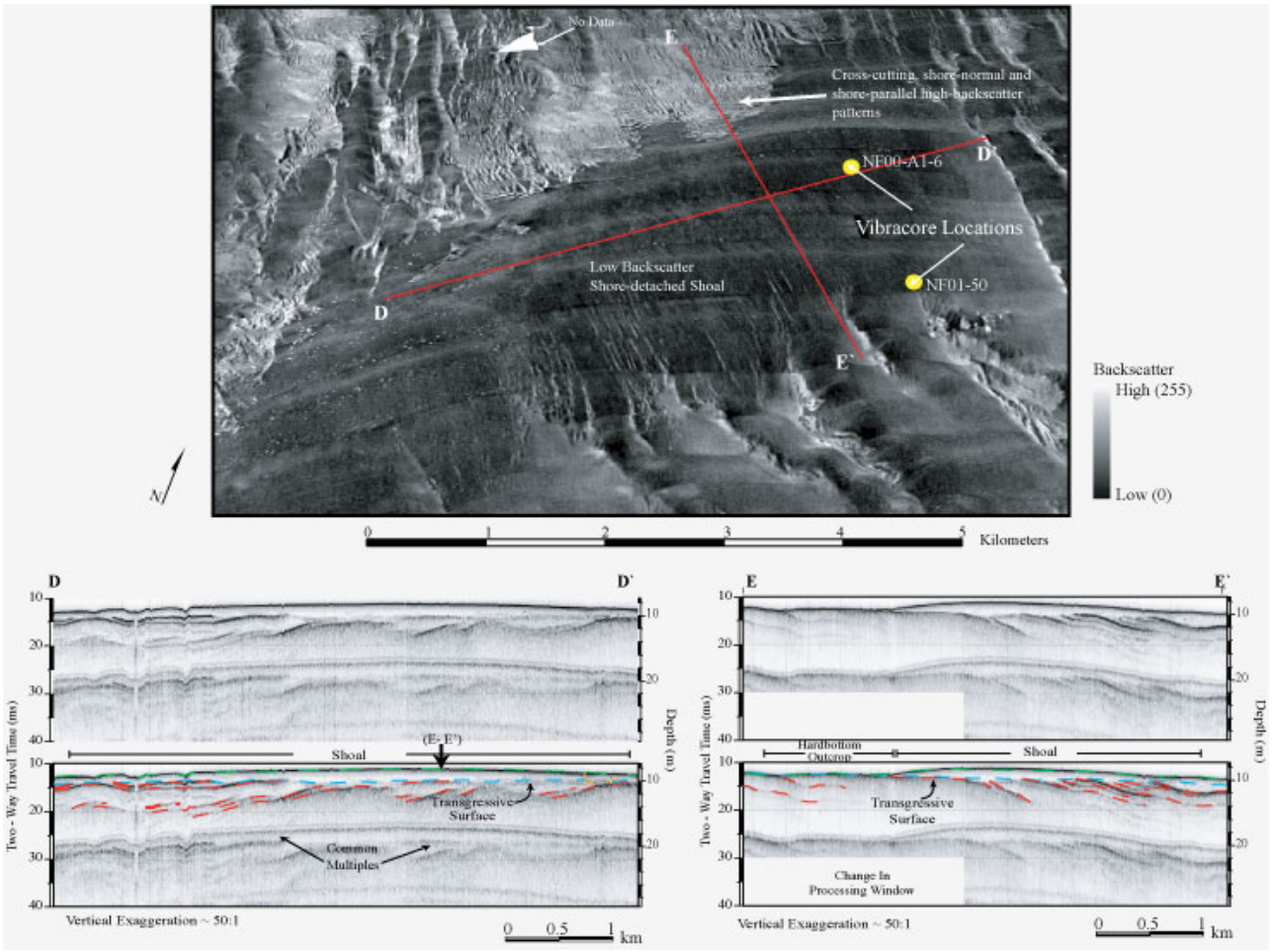

Figure 8. Sidescan-sonar imagery and chirp seismic-reflection profiles on the inner shelf offshore of northern Myrtle Beach. See Figure 4 for figure location. Top: Perspective view of sidescan-sonar imagery draped over bathymetry showing the low-backscatter, shore-oblique shoal and adjacent high-backscatter areas. A complex pattern of shore-normal and shore-parallel high-backscatter lies directly shoreward of the shoal. Yellow circles denote core locations: see Appendix B for core descriptions. Bottom: Chirp seismic-reflection profiles across shoal show the thickness of sediment associated with the shoal (area between green and blue), and the transgressive surface (blue) and truncated Cretaceous strata underlying the shoal (red). Depth is approximate and assumes a seismic velocity of 1500 m/sec. Figure modified from Baldwin and others (2004, their Figure 18).

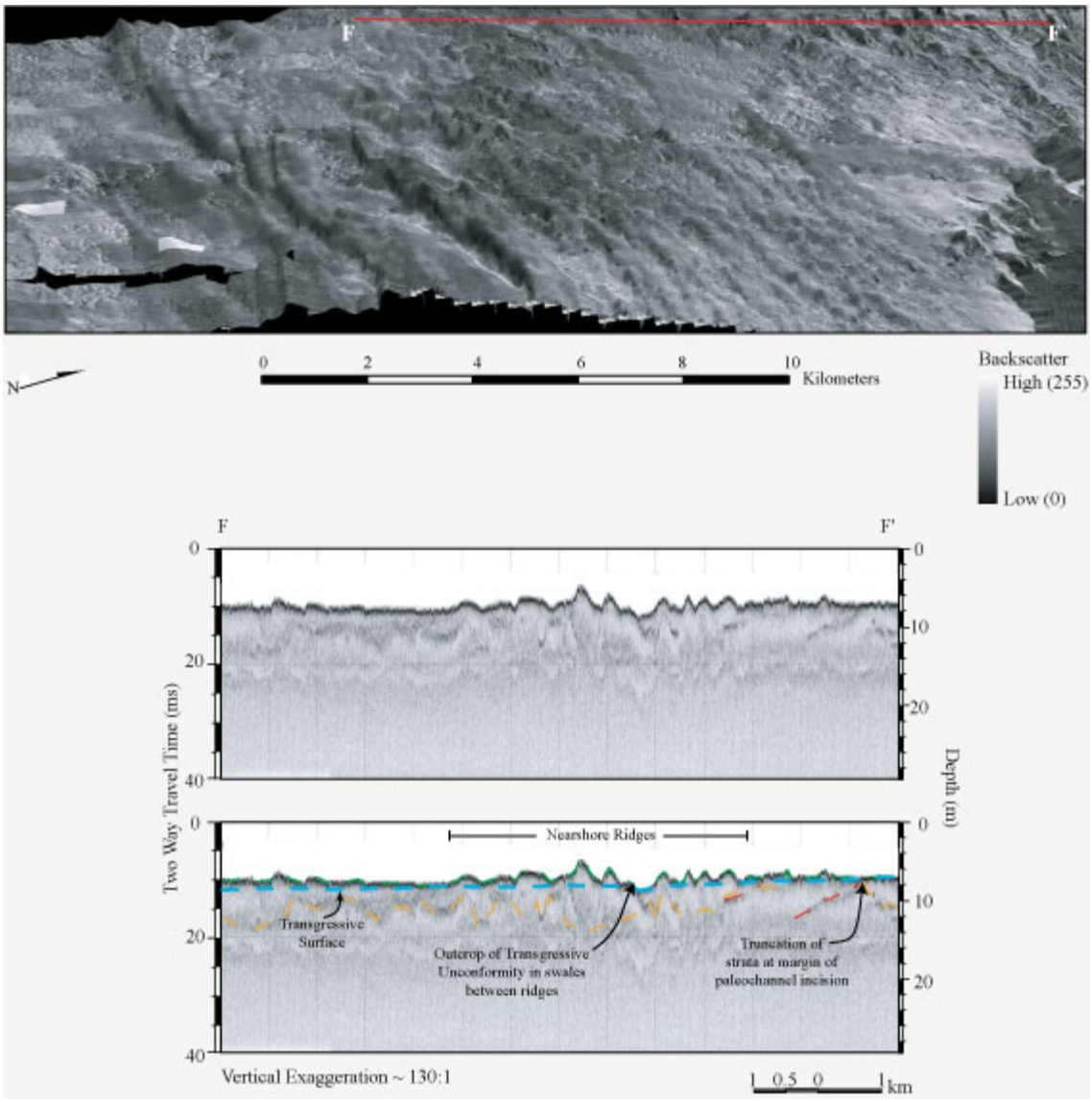

Figure 9. Sidescan-sonar imagery and chirp seismic-reflection profile on the inner shelf offshore of Pawley's Island. See Figure 4 for figure location. Top: Perspective view of sidescan-sonar imagery draped over bathymetry, showing the moderate to high backscatter ridges characteristic of the area. Bottom: Chirp seismic-reflection profile shows ridges of modern sediment with the transgressive surface (blue) exposed in the trough. Depth is approximate and assumes a seismic velocity of 1500 m/sec. Figure modified from Baldwin and others (2006, their Figure 20).

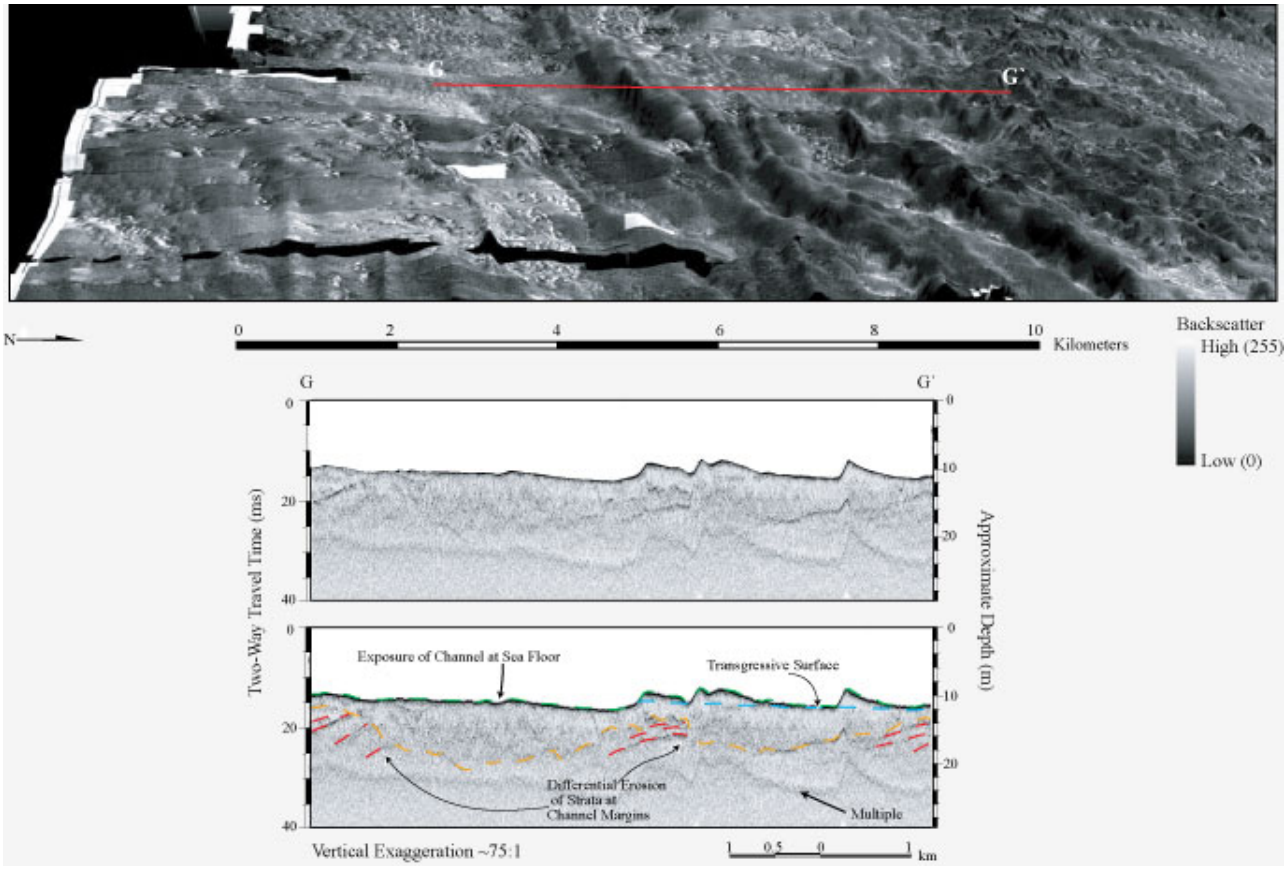

Figure 10. Sidescan -sonar imagery and chirp seismic-reflection profile on the inner shelf offshore of North Island. See Figure 4 for figure location. Top: Perspective view of sidescan-sonar imagery draped over bathymetry, showing the moderate to high backscatter ridges characteristic of the area. Bottom: Chirp seismic-reflection profile shows large, asymmetric ridges of modern sediment with steeper sides facing south, and the transgressive surface (blue) exposed in the swales. Depth is approximate and assumes a seismic velocity of 1500 m/sec. Figure modified from Baldwin and others (2006, their Figure3 in Data Repository).

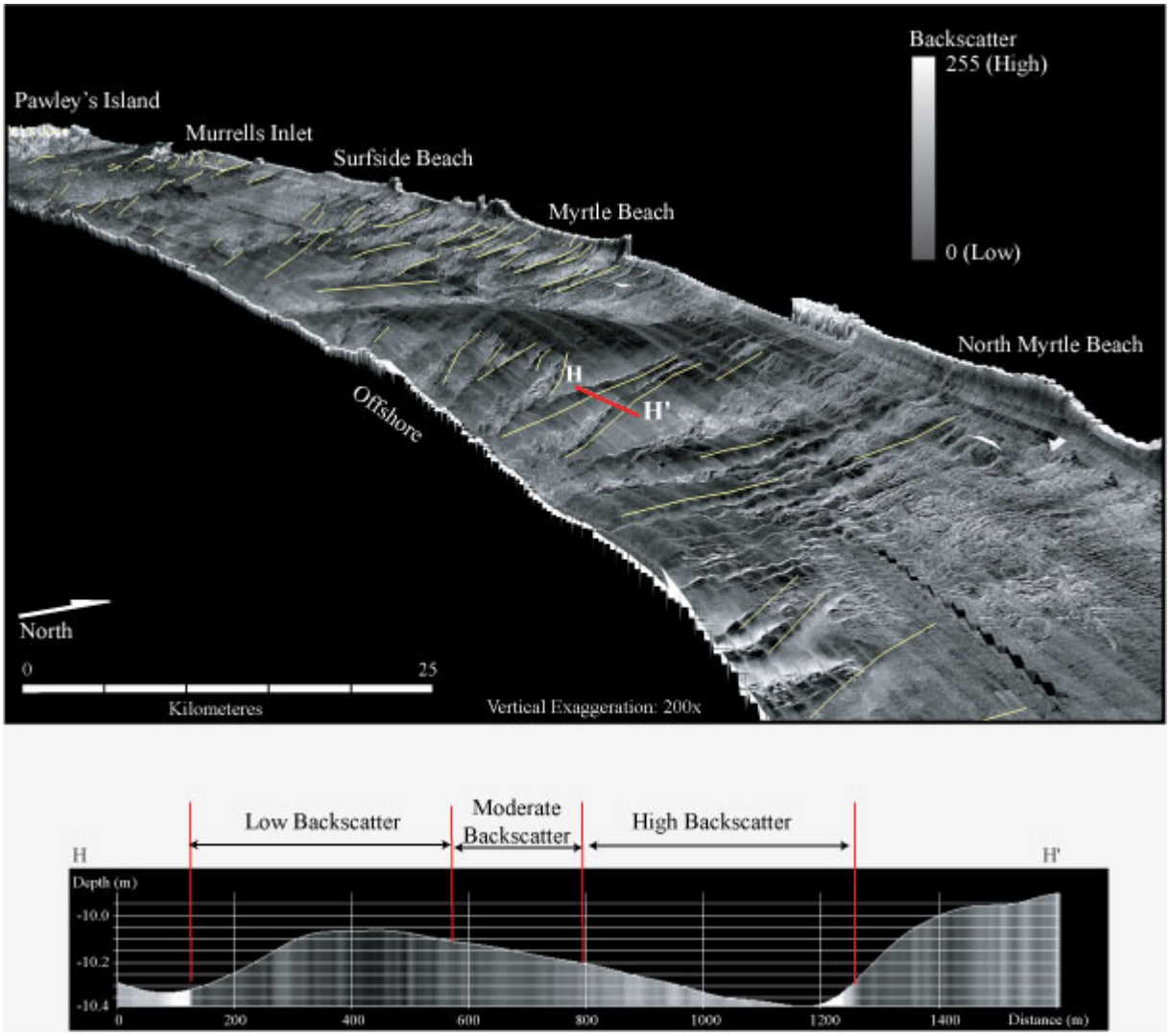

Figure 11. Top: Perspective view of sidescan-sonar imagery draped over bathymetry looking towards the southwest. Yellow lines indicate the crests of low-relief ridges. Vertical exaggeration is 200 x. Bottom: Shore-parallel bathymetric profile across a characteristic low-relief ridge showing variation in backscatter in relation to ridge morphology. High-backscatter covers the trough and NE side of the ridge, and moderate to low backscatter covers the crest and SW side. Depth is in meters. Distance is in kilometers. Note asymmetry of ridge with steeper slope facing to the southwest.

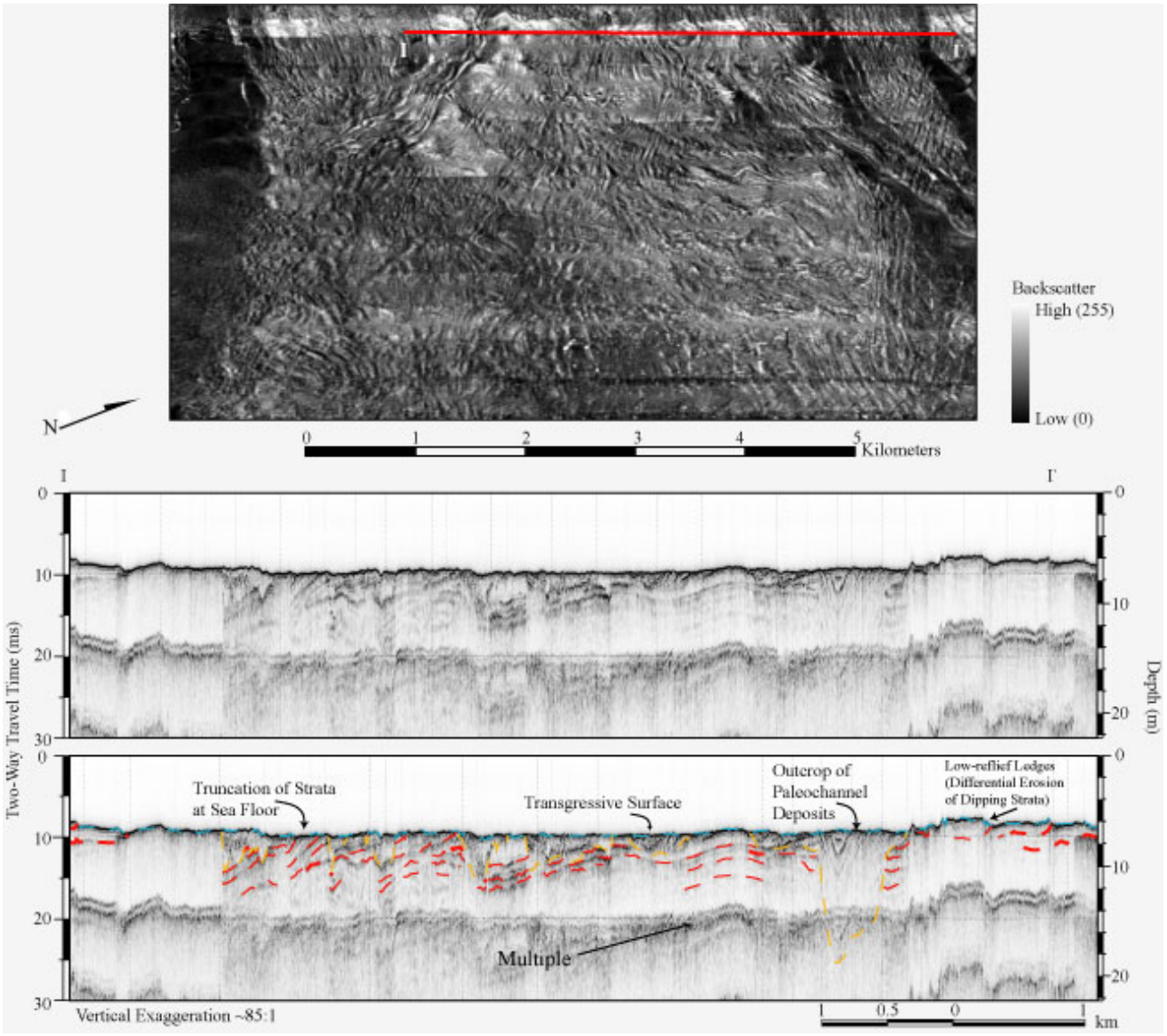

Figure 12. Sidescan-sonar imagery and chirp seismic-reflection profile on the inner shelf offshore of Surfside Beach. See Figure 4 for figure location. Top: Perspective view of sidescan-sonar imagery draped over bathymetry, showing the complex patterns of high backscatter characteristic of the area. Bottom: Chirp seismic-reflection profile showing thin to absent modern sediment and the transgressive surface (blue) exposed at the sea floor. Depth is approximate and assumes a seismic velocity of 1500 m/sec. Figure modified from Baldwin and others (2004, their Figure 9).

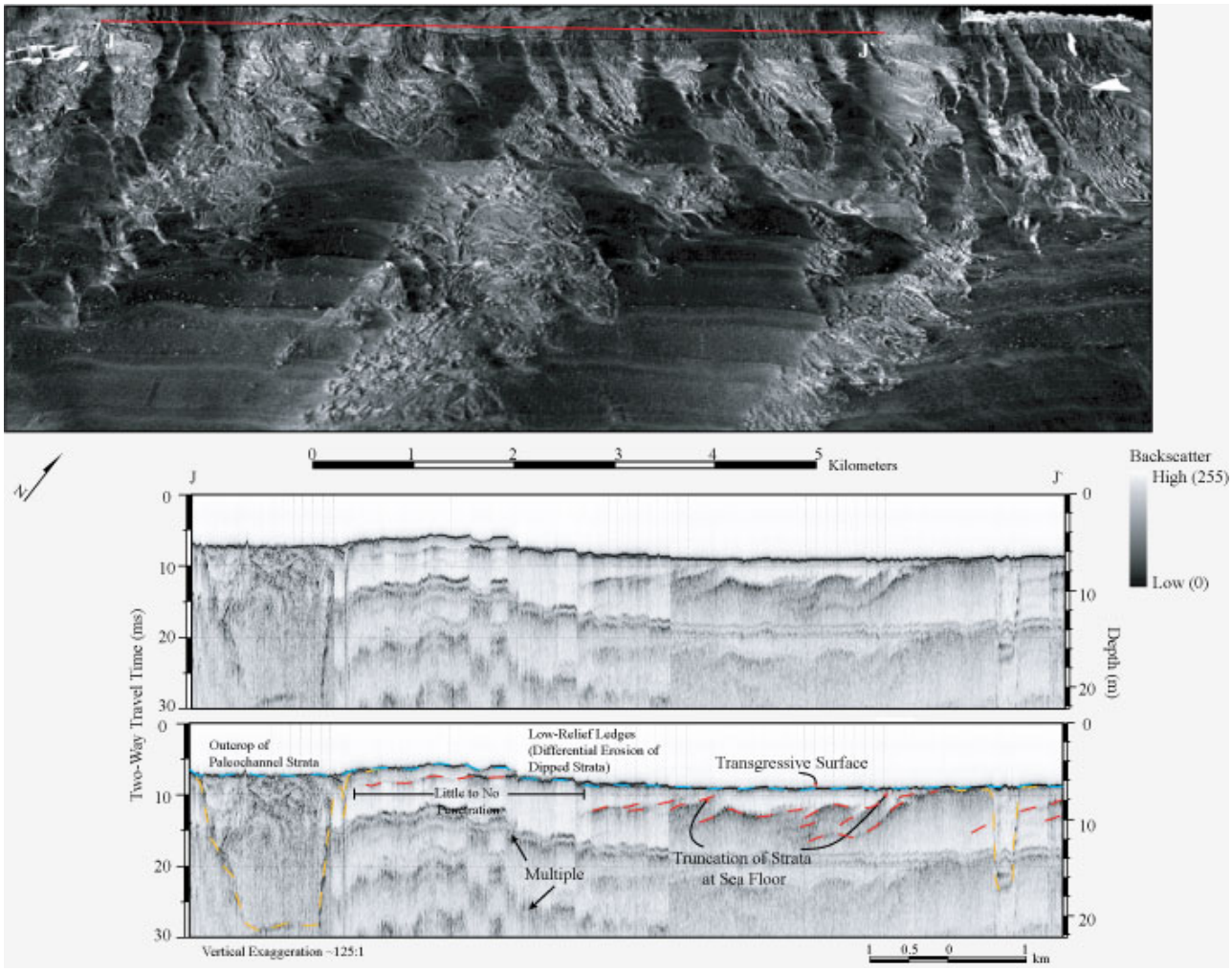

Figure 13. Sidescan-sonar imagery and chirp seismic-reflection profile directly offshore of Myrtle Beach. See Figure 4 for figure location. Top: Perspective view of sidescan-sonar imagery draped over bathymetry, showing the complex patterns of high and low backscatter characteristic of the area. Low-relief, shore-normal ridges are displayed in the nearshore. Bottom: Chirp seismic-reflection profile directly offshore of Myrtle Beach. Profile displays Pleistocene channels (yellow) and Cretaceous strata (red) exposed at the sea floor and differential erosion of outcropping Cretaceous strata. Transgressive surface (blue) and seafloor are outlined (green). Vertical scales show milliseconds (Two-way travel time) and approximate depth assuming a seismic velocity of 1500 m/sec. Figure modified from Figure 12, Baldwin and others (2004).

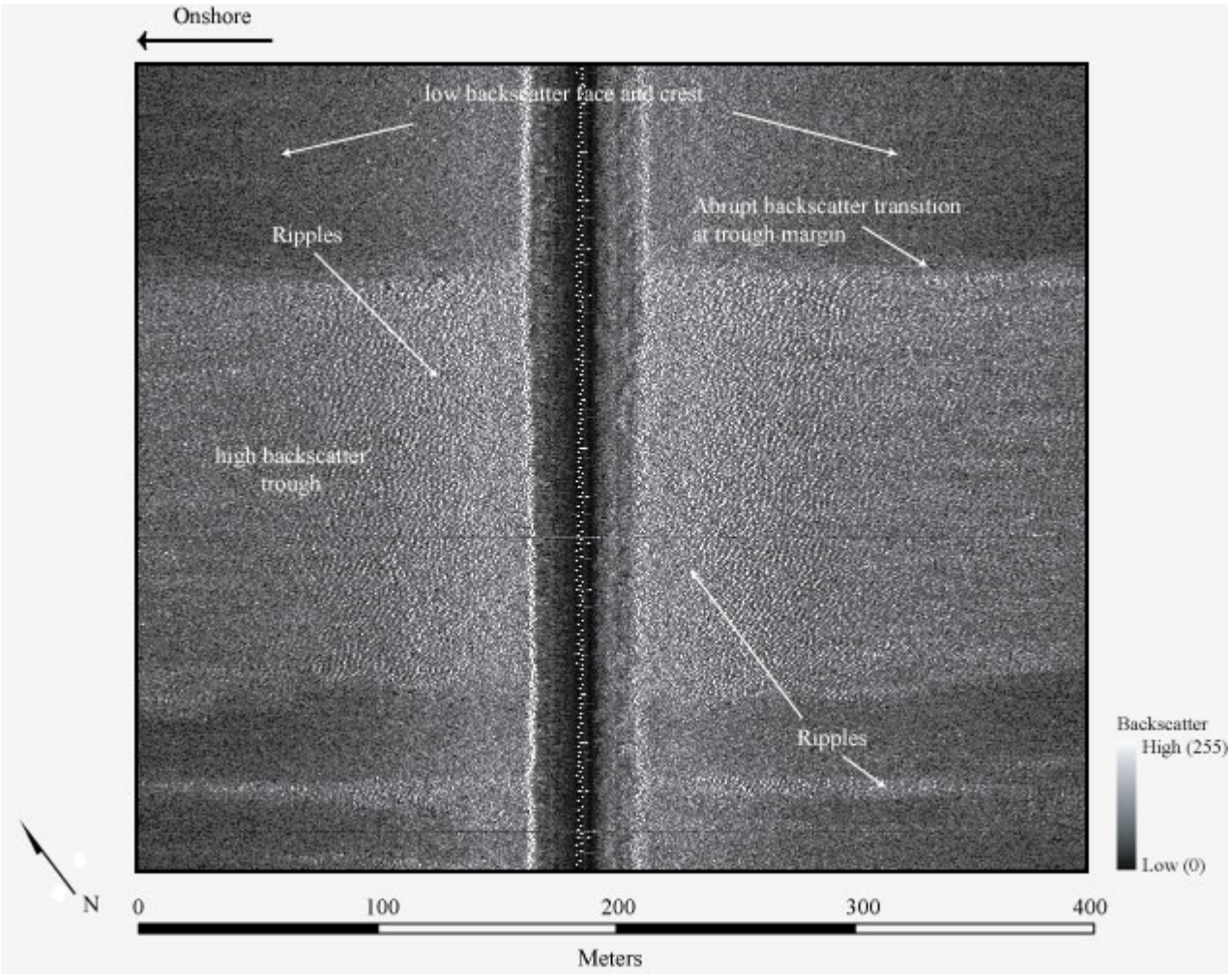

Figure 14. Sidescan-sonar image displaying the wave-orbital ripples within the high-backscatter shore-perpendicular lineations offshore of Myrtle Beach. Low backscatter crests and abrupt backscatter transitions at the trough margins are displayed. See Figure 4 for figure location.

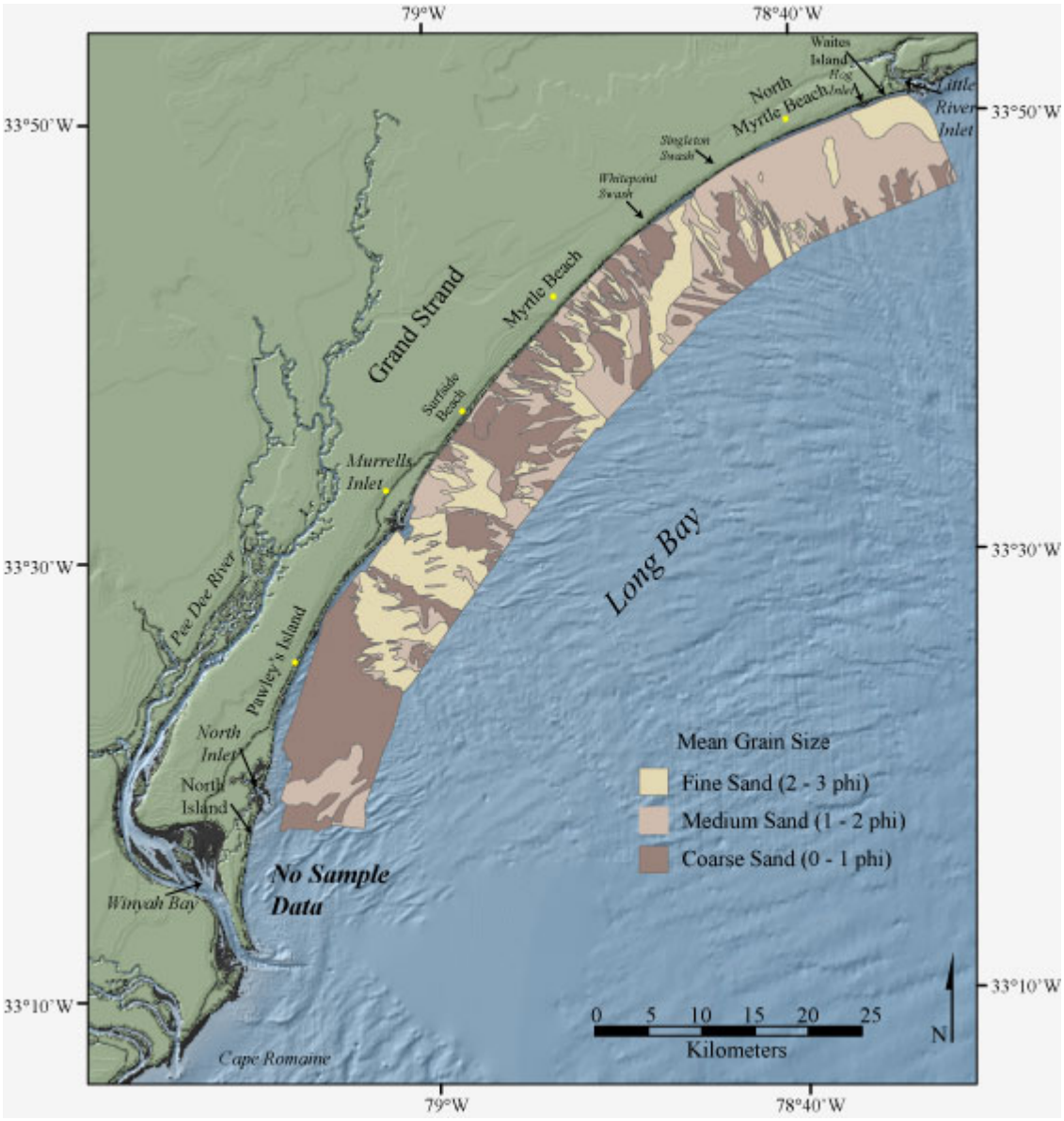

Figure 15. Map showing the mean grain size of surficial sediments in the study area. No sample data were available for the area south of North Inlet.

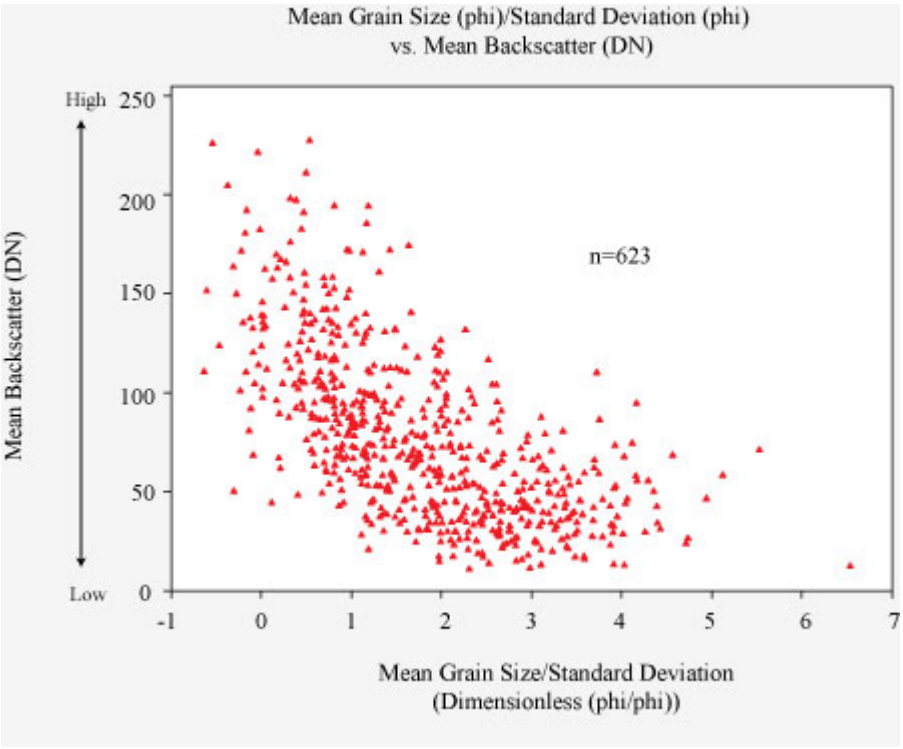

Figure 16. Plot showing mean grain size/standard deviation versus mean backscatter for surficial sediment samples collected within the study area. No statistically significant correlation exists between variables. Backscatter values were extracted from the sidescan-sonar imagery in a 10-m radius around sample location. Samples falling on backscatter transitions were excluded from analyses (99 out of 722).

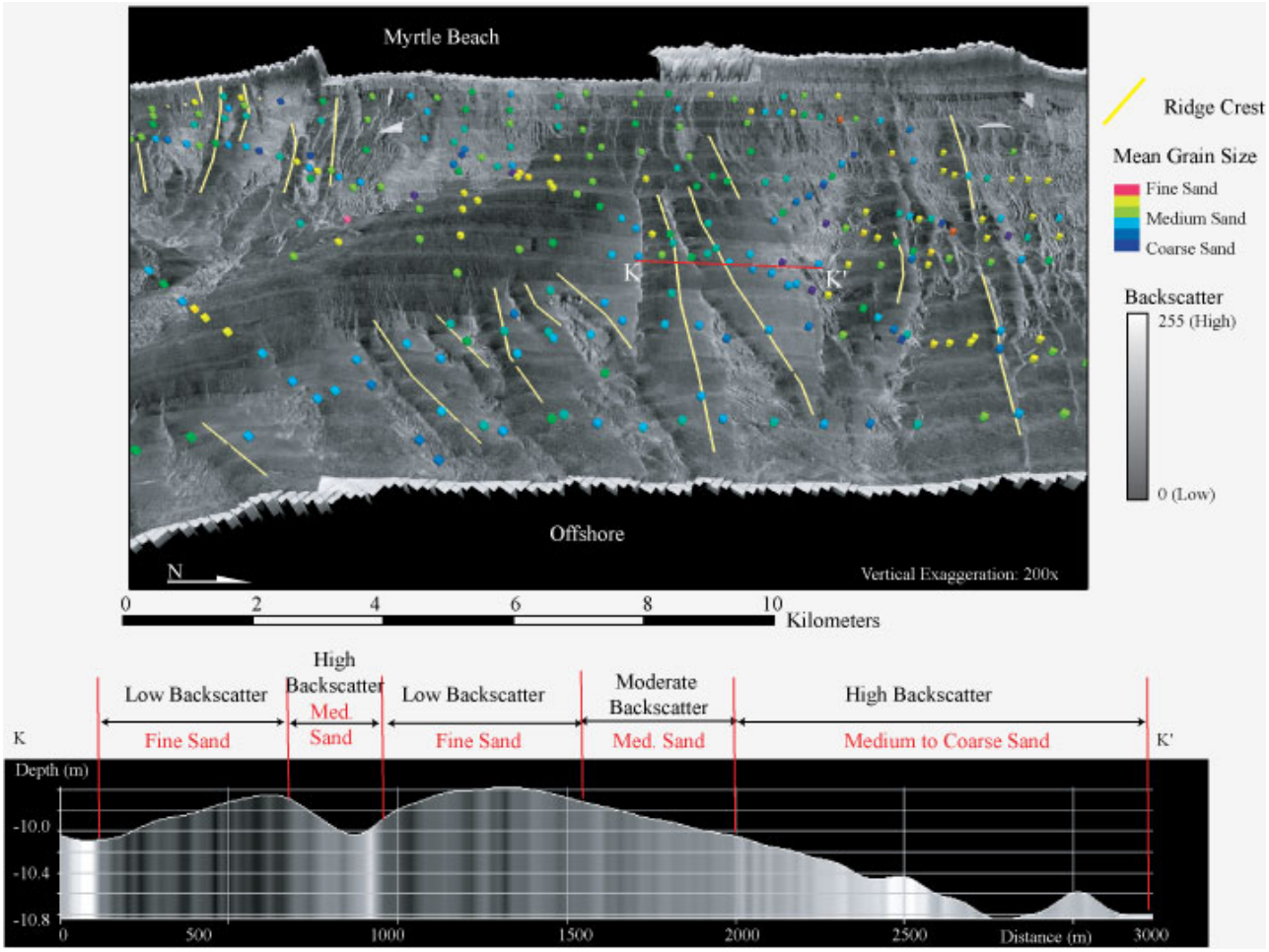

Figure 17. Top: Perspective view of sidescan-sonar imagery draped over bathymetry looking towards Myrtle Beach. Mean grain size of samples is indicated by color-coded spheres. Vertical exaggeration is 200 x. Bottom: Shore-parallel bathymetric profile along a characteristic low-relief ridge showing variations in backscatter and mean grain size of surficial sediment in relation to ridge morphology. Finer sediments fall on the crest and SW side of low-relief ridges; coarse grained sediments fall on NE side and within the trough.

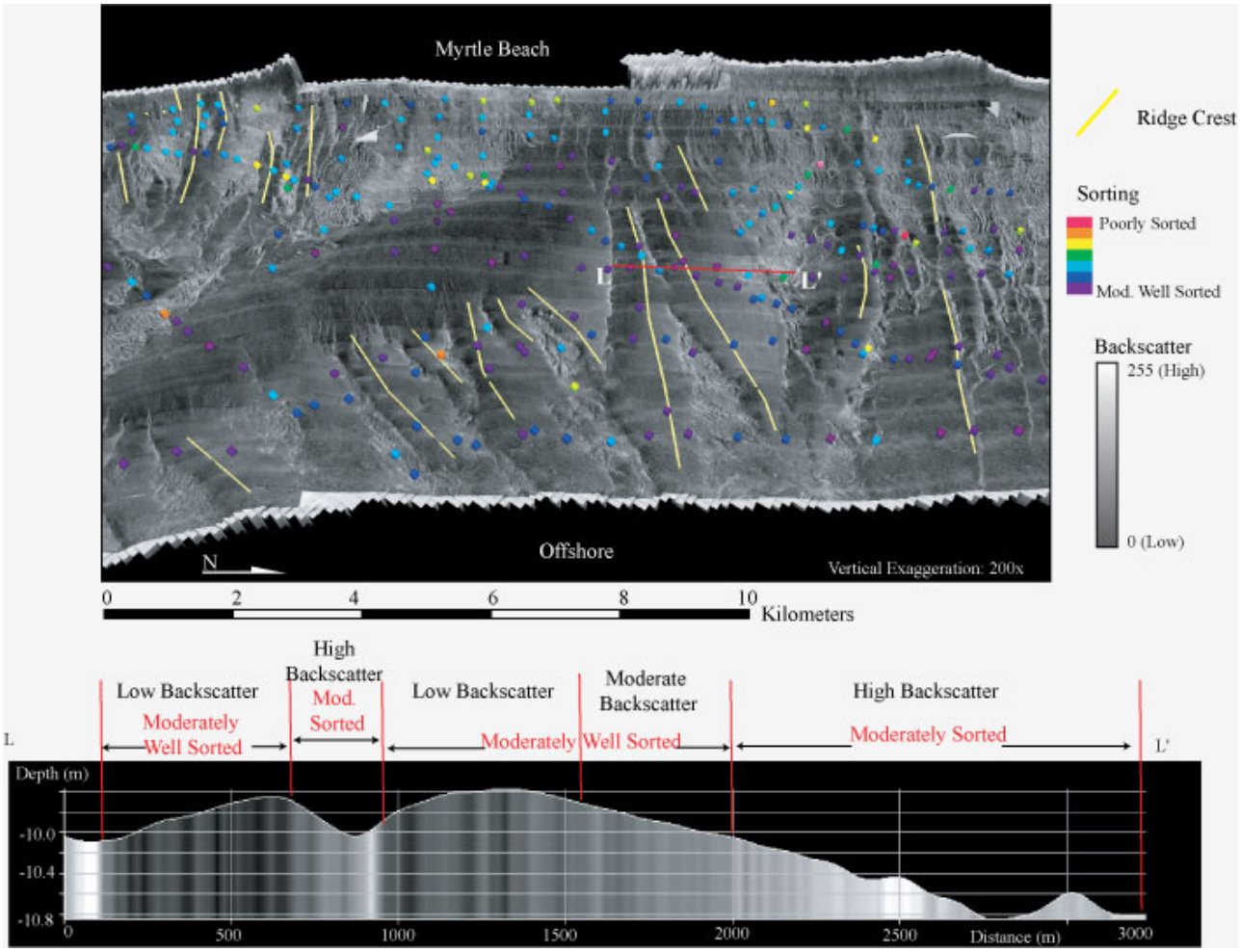

Figure 18. Top: Perspective view of sidescan-sonar imagery draped over bathymetry looking towards Myrtle Beach. The degree of sorting of surficial sediment samples is indicated by color-coded spheres. Vertical exaggeration is 200 x. Bottom: Shore-parallel bathymetric profile along a characteristic low-relief ridge showing variations in backscatter and sorting in relation to ridge morphology. Sorting improves moving from the NE side and trough to the crest and SW side.

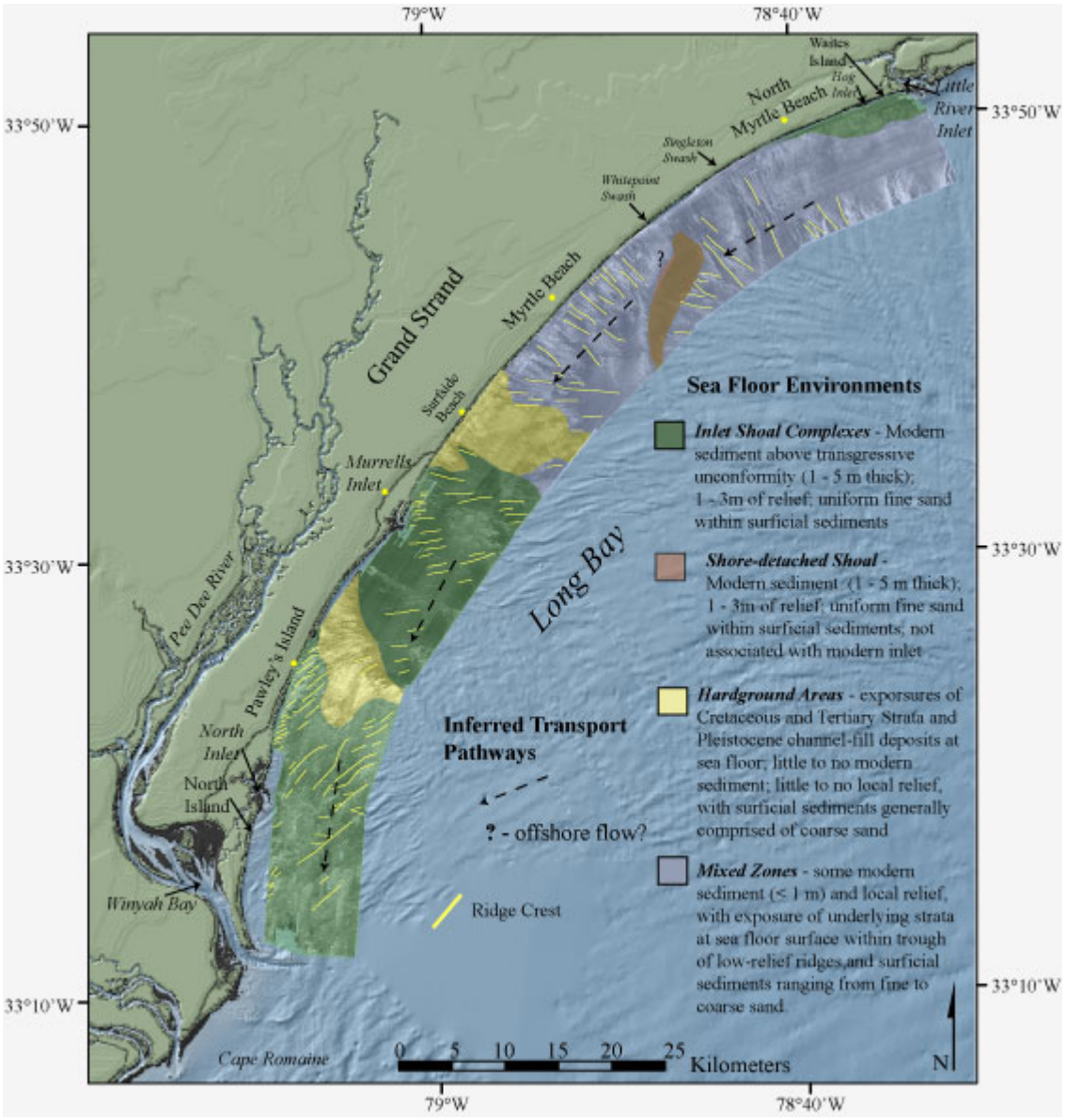

Figure 19. Map showing the four primary sea floor environments within Long Bay: inlet shoal complexes, shore-detached shoals, hardground and transition areas, and inferred sediment transport pathways based on seabed morphology and surficial textural distribution.

Table1: Feature Classification

Shoals

large features

> 5 km in length and width, < 1 m in height

Inlet-associated

Little River Inlet

Murrells Inlet

North Inlet

Shore-detached

offshore of Myrtle Beach

Ridges

smaller, low-relief features

< 5km in length, < 2 km in width, < 1.5 m in height

present throughout the study area

Classification of the primary morphologic features as defined within the text and mapped throughout the survey area. General morphology of features and their locations are provided. Shoals and ridge crests are identified within Figures 3 and 4, respectively.

Table 2. Summary of Ridge Morphology

Ridge Location	Ridge Length (km)	Ridge Width (km)	Ridge Height (m)	Mean crest Azimuth (degrees from North)
N. Myrtle Beach to Myrtle Beach – Offshore (> 9 m water depth)	1 – 2.5	0.5 – 1.5	0.5 – 1.0	**100**
Myrtle Beach - Nearshore (< 9 m water depth)	< 0.5 – 3	0.1 – 1.0	< 1.0	**125**
Murrells Inlet Shoal Complex	0.4 – 3	0.5 – 1.5	0.5 – 1.5	**85**
Pawley's Island to Winyah Bay **Shoal Complex**	**< 1 – 6**	**0.1 – 1.0**	**0.5 - > 3.0**	**60**

Description of the morphology, orientation, and location of low-relief ridges throughout the study area. Ridge lengths and widths are provided in kilometers, heights in meters, and orientations in degrees from North. Figure 5 identifies location of individual ridge crests.

Appendix A: Textural properties of grab samples collected within the survey area 2000 – 20002 by Coastal Carolina University. Table shows percent gravel, sand, silt, clay, mean grain size (mm), mean grain size (phi), sorting, skewness, kurtosis, longitude and latitude of sample locations.

Sample ID	% Gravel	% Sand	% Silt	% Clay	Mean Grain Size (mm)	Mean Grain Size (phi)	Sorting	Skewness	Kurtosis	Longitude	Latitude
GS-057	47.09	52.64	0.14	0.13	2.0562	-1.0400	1.93	-0.02	0.05	-79.05338	33.40735
GS-058	52.79	45.89	0.82	0.5	1.8150	-0.8600	1.85	0.78	5.02	-79.06401	33.38333
GS-059	0.15	99.20	0.35	0.3	0.1456	2.7800	0.71	0.99	25.74	-79.06110	33.41630
GS-060	36.12	62.78	0.62	0.49	1.5583	-0.6400	2.11	0.17	1.95	-79.06104	33.42291
GS-061	0.12	99.32	0.31	0.24	0.1593	2.6500	0.58	2.04	49.8	-79.06452	33.42643
GS-062	0.93	98.00	0.52	0.55	0.1895	2.4000	0.98	0.36	22.16	-79.06065	33.43258
GS-063	23.58	75.16	0.77	0.48	0.6783	0.5600	1.87	0.19	1.73	-79.06106	33.43757
GS-064	47.11	52.08	0.49	0.32	1.7654	-0.8200	2.66	0.06	-0.67	-79.06522	33.44070
GS-065	0.67	98.51	0.39	0.44	0.1661	2.5900	0.77	1.14	31.38	-79.06085	33.44235
GS-066	0.35	97.07	1.11	1.47	0.1560	2.6800	1.07	1.83	21.14	-79.05147	33.44556
GS-067	23.31	75.44	0.85	0.4	0.6329	0.6600	1.84	0.14	1.45	-79.07309	33.44228
GS-068	17.3	81.69	0.54	0.46	0.3560	1.4900	2.06	-0.44	1.17	-79.08714	33.44937
GS-069	0.1	99.36	0.32	0.22	0.2073	2.2700	0.74	1.03	19.65	-78.67122	33.74417
GS-070	0.32	98.96	0.39	0.33	0.1989	2.3300	0.83	0.96	19.46	-78.67630	33.74422
GS-071	0.33	99.06	0.31	0.3	0.1684	2.5700	0.75	0.94	25.27	-78.67855	33.74164
GS-072	2.54	97.09	0.21	0.16	0.6417	0.6400	0.88	1	20.62	-78.68378	33.74029
GS-073	2.08	97.60	0.19	0.13	0.6029	0.7300	0.84	1.02	19.96	-78.68472	33.74341
GS-074	0.05	98.87	0.50	0.59	0.1497	2.7400	0.7	2.73	50.52	-78.68817	33.73941
GS-075	0.02	99.48	0.35	0.15	0.1684	2.5700	0.74	0.17	15.83	-78.69104	33.73802
GS-076	0.1	97.14	1.64	1.12	0.1358	2.8800	0.97	1.91	22.67	-78.69317	33.73729
GS-077	2.96	90.12	4.40	2.52	0.3560	1.4900	2.16	0.76	2.95	-78.69763	33.73731
GS-078	1.57	97.63	0.44	0.36	0.6199	0.6900	0.95	2	30	-78.69986	33.73689
GS-079	0.63	98.87	0.32	0.18	0.4323	1.2100	0.89	1.16	15.69	-78.70301	33.73722
GS-080	0.01	99.47	0.31	0.21	0.2398	2.0600	0.69	1.75	28.79	-78.70583	33.73727
GS-081	1.35	97.77	0.54	0.34	0.1768	2.5000	1.01	0.02	10.82	-78.71225	33.73733
GS-082	3.87	95.55	0.32	0.26	1.0210	-0.0300	1.02	1.53	23.82	-78.71491	33.73627
GS-083	1.14	97.67	0.62	0.58	0.5396	0.8900	1.09	1.76	23.43	-78.71773	33.73565
GS-084	1.19	98.54	0.15	0.12	0.5864	0.7700	0.79	0.96	23.35	-78.72234	33.73516
GS-085	0.71	98.93	0.19	0.17	0.5105	0.9700	0.82	1.29	21.18	-78.72557	33.73424
GS-086	0.3	99.21	0.26	0.23	0.4475	1.1600	0.83	1.49	25.15	-78.72985	33.73340
GS-087	0.17	99.36	0.29	0.18	0.3015	1.7300	0.84	0.74	13.82	-78.73404	33.73299
GS-088	0.12	96.27	2.29	1.32	0.3276	1.6100	1.36	1.57	14.49	-78.74079	33.73222
GS-089	0.09	98.03	1.05	0.83	0.1560	2.6800	1.06	0.75	15	-78.74526	33.73211
GS-090	0.59	98.70	0.39	0.32	0.5249	0.9300	0.92	1.88	26.3	-78.74835	33.73142
GS-091	1.13	98.09	0.46	0.32	0.4475	1.1600	1.04	1.11	14.08	-78.75171	33.73162
GS-092	0.08	99.53	0.22	0.17	0.2813	1.8300	0.76	1.07	19.45	-78.75651	33.73130
GS-093	0.25	99.24	0.30	0.2	0.2238	2.1600	0.88	0.4	11.02	-78.76158	33.73107
GS-094	0.07	99.04	0.45	0.44	0.1518	2.7200	0.74	1.63	29.21	-78.76826	33.73124
GS-095	0.07	98.75	0.56	0.62	0.1358	2.8800	0.76	2.08	33.32	-78.77357	33.73106
GS-096	0.11	96.12	2.18	1.58	0.1303	2.9400	1.14	1.51	15.2	-78.77695	33.73224
GS-097	37.07	60.59	1.59	0.75	1.1487	-0.2000	2.11	0.45	2.6	-78.77813	33.73155
GS-098	21.84	77.75	0.21	0.21	0.9794	0.0300	1.33	0.52	5.16	-78.89549	33.65948

Sample ID	% Gravel	% Sand	% Silt	% Clay	Mean Grain Size (mm)	Mean Grain Size (phi)	Sorting	Skewness	Kurtosis	Longitude	Latitude
GS-099	20.28	77.30	1.42	1	0.6507	0.6200	2.06	0.24	2.72	-78.89262	33.66170
GS-100	31.71	67.63	0.37	0.28	1.1251	-0.1700	1.84	-0.05	2.02	-78.89016	33.66472
GS-101	4.05	95.55	0.21	0.18	0.2736	1.8700	1.1	-0.41	7.44	-78.88558	33.66662
GS-102	1.13	98.42	0.27	0.18	0.2415	2.0500	0.87	0.11	13.39	-78.88057	33.67087
GS-103	31.42	66.45	1.32	0.8	0.9202	0.1200	1.9	0.55	4.2	-78.87735	33.67192
GS-104	5.68	92.57	1.02	0.73	0.3164	1.6600	1.41	0.35	7.38	-78.87474	33.67582
GS-105	1.61	98.04	0.20	0.15	0.2793	1.8400	0.86	-0.18	17.01	-78.87202	33.67857
GS-106	1.63	97.62	0.41	0.34	0.2316	2.1100	0.95	0.4	14.48	-78.86892	33.68128
GS-107	0.98	98.66	0.19	0.17	0.2606	1.9400	0.7	0.8	31.2	-78.86553	33.68413
GS-108	3.61	96.05	0.19	0.15	0.4061	1.3000	0.99	0.07	9.32	-78.86251	33.68817
GS-109	1.34	98.21	0.29	0.16	0.1908	2.3900	0.9	-0.13	9.54	-78.85849	33.68976
GS-110	21.55	77.31	0.68	0.46	0.5987	0.7400	1.79	0.15	1.87	-78.85561	33.69236
GS-111	16.43	82.74	0.47	0.35	0.5141	0.9600	1.74	-0.24	2.24	-78.85194	33.69821
GS-112	2.12	97.28	0.33	0.27	0.2045	2.2900	1.01	-0.13	9.81	-78.84893	33.69961
GS-113	0.18	98.97	0.42	0.43	0.1895	2.4000	0.87	1.21	17.95	-78.84720	33.70094
GS-114	18	81.20	0.46	0.35	0.5864	0.7700	1.71	-0.03	2.21	-78.84435	33.70204
GS-115	13.56	86.03	0.23	0.17	0.6736	0.5700	1.25	0.11	5.38	-78.84233	33.70314
GS-116	15.25	84.22	0.27	0.26	0.5396	0.8900	1.64	-0.13	2	-78.83907	33.70471
GS-117	4.7	94.50	0.46	0.34	0.2102	2.2500	1.28	-0.49	6.3	-78.83625	33.70564
GS-118	0.73	98.90	0.21	0.16	0.2483	2.0100	0.75	0.61	20.14	-78.83367	33.70743
GS-119	1.62	97.74	0.32	0.32	0.5070	0.9800	0.97	1.35	20.93	-78.83124	33.70849
GS-120	4.81	94.70	0.26	0.23	0.4763	1.0700	1.1	0.44	8.36	-78.82820	33.71012
GS-121	26.48	72.60	0.55	0.37	0.9461	0.0800	1.62	0.29	4.46	-78.82548	33.71091
GS-122	15.79	83.67	0.31	0.24	0.3322	1.5900	2.1	-0.53	0.85	-78.82082	33.71201
GS-123	1.03	96.97	1.05	0.96	0.1528	2.7100	1.19	0.43	10.64	-78.81677	33.71279
GS-124	24.76	73.03	1.25	0.96	0.5510	0.8600	2.23	0.13	0.86	-78.81396	33.71325
GS-125	3.06	96.25	0.39	0.3	0.1817	2.4600	1.34	-0.94	9.66	-78.81139	33.71328
GS-126	0.33	99.28	0.22	0.18	0.1961	2.3500	0.83	0.34	11.49	-78.80804	33.71411
GS-127	3.58	96.09	0.20	0.13	0.5434	0.8800	0.95	0.5	10.93	-78.80544	33.71375
GS-128	9.83	89.67	0.25	0.25	0.5212	0.9400	1.42	-0.16	5.1	-78.80122	33.71513
GS-129	5.98	93.42	0.32	0.28	0.2285	2.1300	1.5	-0.63	4.51	-78.79687	33.71628
GS-130	1.45	97.85	0.36	0.34	0.3789	1.4000	1.03	0.8	13.68	-78.86262	33.63013
GS-131	0.9	98.68	0.24	0.18	0.2698	1.8900	0.83	0.53	17.02	-78.85656	33.63343
GS-132	1	98.44	0.36	0.2	0.3610	1.4700	1	0.57	8.77	-78.85098	33.63713
GS-133	0.7	98.98	0.20	0.12	0.4698	1.0900	0.84	0.92	12.91	-78.84480	33.64056
GS-134	2.67	96.87	0.30	0.17	0.4234	1.2400	1.03	0.38	7.54	-78.83780	33.64301
GS-135	0.43	99.05	0.33	0.19	0.1756	2.5100	0.75	0.53	17.61	-78.83041	33.64860
GS-136	1.54	97.85	0.40	0.21	0.2588	1.9500	1.08	0.04	7.15	-78.82493	33.64666
GS-137	7.44	91.89	0.48	0.19	0.3560	1.4900	1.7	-0.43	2.23	-78.81688	33.64756
GS-138	10.92	87.83	0.82	0.43	0.5783	0.7900	1.67	0.06	3.73	-78.80653	33.64965
GS-139	10.5	89.05	0.28	0.17	0.4090	1.2900	1.77	-0.66	3.03	-78.80250	33.65221
GS-140	0.56	99.00	0.28	0.16	0.1843	2.4400	0.79	-0.14	17.85	-78.79657	33.65512
GS-141	0.01	99.56	0.28	0.15	0.1975	2.3400	0.71	0.82	16.19	-78.79228	33.65753
GS-142	0.33	99.40	0.18	0.09	0.2449	2.0300	0.81	-0.01	12.36	-78.78655	33.66146
GS-143	0.78	98.79	0.30	0.13	0.2466	2.0200	0.86	0.1	11.46	-78.78351	33.66404
GS-144	0.46	99.27	0.19	0.09	0.2813	1.8300	0.81	0.17	9.63	-78.77777	33.66880
GS-145	0.62	99.02	0.24	0.12	0.5322	0.9100	0.87	0.92	12.48	-78.77063	33.67275

Sample ID	% Gravel	% Sand	% Silt	% Clay	Mean Grain Size (mm)	Mean Grain Size (phi)	Sorting	Skewness	Kurtosis	Longitude	Latitude
GS-146	4.18	95.09	0.42	0.31	0.5434	0.8800	1.22	0.43	9.09	-78.77423	33.68165
GS-147	0.6	99.06	0.21	0.13	0.4263	1.2300	0.86	0.84	12.31	-78.78144	33.68206
GS-148	0.12	99.53	0.23	0.13	0.1768	2.5000	0.64	0.69	20.67	-78.78857	33.68148
GS-149	0.06	99.41	0.33	0.21	0.1661	2.5900	0.78	0.36	15.96	-78.79498	33.68159
GS-150	0.38	98.33	0.67	0.62	0.1377	2.8600	0.81	1.61	30.4	-78.80035	33.68235
GS-151	28.08	71.02	0.54	0.36	0.5743	0.8000	2.5	-0.23	-0.63	-78.80321	33.68217
GS-152	1.34	98.12	0.34	0.21	0.2793	1.8400	0.89	0.37	15.83	-78.80938	33.68272
GS-153	1.68	97.81	0.33	0.18	0.4234	1.2400	0.97	0.47	11.82	-78.81389	33.67561
GS-154	1.68	97.70	0.40	0.22	0.3789	1.4000	1.06	0.35	9.62	-78.81507	33.67057
GS-155	1.57	98.11	0.20	0.12	0.3869	1.3700	0.94	0.24	9.41	-78.81492	33.66384
GS-156	0.57	99.05	0.26	0.11	0.3686	1.4400	0.91	0.6	7.67	-78.81478	33.65608
GS-157	0.7	98.89	0.27	0.15	0.6242	0.6800	0.81	1.7	26.42	-78.81259	33.65066
GS-158	4.84	94.76	0.23	0.17	0.6329	0.6600	1.13	0.11	10.35	-78.81424	33.64234
GS-159	1.79	97.88	0.22	0.11	0.6598	0.6000	1.01	0.79	7.76	-78.81362	33.63473
GS-160	2.21	97.40	0.25	0.15	0.4633	1.1100	1.06	0.52	6.44	-78.82913	33.62812
GS-161	0.67	99.07	0.18	0.08	0.4323	1.2100	0.92	0.4	6.48	-78.84255	33.62313
GS-162	0.45	99.18	0.24	0.12	0.3015	1.7300	0.95	0.26	5.39	-78.85290	33.61925
GS-163	1.23	98.09	0.36	0.32	0.2717	1.8800	0.95	0.55	14.59	-78.87674	33.62927
GS-164	0.02	99.50	0.30	0.18	0.2176	2.2000	0.8	0.56	12.58	-78.87256	33.63354
GS-165	0.42	98.89	0.40	0.29	0.1560	2.6800	0.76	0.6	21.98	-78.86911	33.63891
GS-166	0.34	99.28	0.23	0.15	0.2382	2.0700	0.82	0.36	11.03	-78.86619	33.64250
GS-167	0.22	99.23	0.33	0.22	0.1843	2.4400	0.82	0.22	14.7	-78.86185	33.64735
GS-168	0.26	99.30	0.25	0.19	0.2285	2.1300	0.75	0.77	19.79	-78.85748	33.65265
GS-169	0.77	98.92	0.21	0.1	0.3635	1.4600	0.85	0.45	8.61	-78.85445	33.65627
GS-170	2.33	97.38	0.17	0.12	0.4414	1.1800	0.97	0.18	8.28	-78.85289	33.65965
GS-171	35.53	63.94	0.29	0.24	1.2311	-0.3000	1.8	0.11	1.31	-78.84599	33.66166
GS-172	2.57	97.02	0.30	0.11	0.3763	1.4100	1.07	0.19	3.96	-78.84024	33.66114
GS-173	1.04	98.34	0.39	0.23	0.2316	2.1100	0.95	0.2	10.44	-78.83302	33.66207
GS-174	3.58	95.93	0.33	0.16	0.3869	1.3700	1.18	0.11	3.87	-78.82779	33.66217
GS-175	6.21	93.20	0.34	0.25	0.4665	1.1000	1.26	-0.12	7.23	-78.81496	33.68327
GS-176	1.08	98.42	0.27	0.23	0.2031	2.3000	0.74	0.43	28.12	-78.82042	33.68272
GS-177	0.45	99.23	0.18	0.14	0.2852	1.8100	0.86	0.52	9.79	-78.82494	33.68292
GS-178	18.54	80.97	0.31	0.18	0.5625	0.8300	1.8	-0.6	2.45	-78.82997	33.68276
GS-179	0.5	99.05	0.28	0.16	0.2238	2.1600	0.74	0.72	18.68	-78.83467	33.68308
GS-180	0.59	98.90	0.29	0.22	0.2382	2.0700	0.77	0.89	23.19	-78.84157	33.68380
GS-181	0.59	99.11	0.18	0.12	0.2146	2.2200	0.65	0.06	29.68	-78.85805	33.65947
GS-182	0.4	99.11	0.29	0.21	0.2382	2.0700	0.78	0.64	21.44	-78.86461	33.65977
GS-183	0.96	98.64	0.22	0.18	0.1948	2.3600	0.83	0.09	14.41	-78.86583	33.66551
GS-184	2.53	96.99	0.31	0.17	0.2624	1.9300	1.05	-0.22	7.27	-78.86859	33.66546
GS-185	0.97	98.67	0.23	0.13	0.1768	2.5000	0.6	-0.14	41.97	-78.87411	33.65897
GS-186	0.6	98.98	0.26	0.16	0.2088	2.2600	1	-0.48	7.9	-78.87605	33.66037
GS-187	10.21	88.87	0.46	0.46	0.3322	1.5900	1.67	-0.22	2.74	-78.89127	33.64864
GS-188	17.07	82.30	0.34	0.29	0.7071	0.5000	1.57	-0.11	4.3	-78.89617	33.64920
GS-189	8.97	90.75	0.17	0.11	0.5704	0.8100	1.31	-0.48	5.43	-78.89861	33.65101
GS-190	2.66	96.90	0.23	0.21	0.2606	1.9400	0.9	-0.2	17.92	-78.97697	33.54481
GS-191	0.13	99.32	0.27	0.28	0.1358	2.8800	0.65	1.21	34.71	-78.97778	33.54120
GS-192	0.35	98.78	0.39	0.48	0.1528	2.7100	0.76	1.52	34.35	-78.97752	33.53694

Sample ID	% Gravel	% Sand	% Silt	% Clay	Mean Grain Size (mm)	Mean Grain Size (phi)	Sorting	Skewness	Kurtosis	Longitude	Latitude
GS-193	15.32	84.26	0.23	0.19	0.4538	1.1400	1.44	-0.56	3.91	-78.97899	33.53060
GS-194	29.75	69.60	0.39	0.26	0.7371	0.4400	2.18	-0.37	0.51	-78.97944	33.52438
GS-195	14.11	85.47	0.28	0.14	0.4147	1.2700	1.56	-0.69	3.63	-78.97839	33.51713
GS-196	0.09	99.59	0.19	0.13	0.1756	2.5100	0.49	1.56	62.98	-78.98876	33.50309
GS-197	2.52	97.12	0.25	0.11	0.3763	1.4100	1.04	0.07	4.87	-78.97692	33.50375
GS-198	0.58	95.24	2.29	1.89	0.1882	2.4100	1.44	0.99	9.53	-78.97640	33.49777
GS-199	0.19	99.43	0.24	0.13	0.1528	2.7100	0.49	1.88	63.75	-78.97655	33.49190
GS-200	3.1	96.71	0.12	0.07	0.3143	1.6700	0.93	-0.68	8.94	-78.97639	33.48603
GS-201	0.12	99.40	0.33	0.15	0.1604	2.6400	0.6	0.46	38.28	-78.97615	33.47741
GS-202	0.1	99.51	0.24	0.15	0.1856	2.4300	0.57	1.37	37.58	-78.97577	33.46962
GS-203	0.22	99.35	0.28	0.16	0.1684	2.5700	0.52	1.75	58.45	-78.98419	33.45785
GS-204	16.65	82.59	0.47	0.29	0.3737	1.4200	1.75	-0.28	0.91	-78.99410	33.46207
GS-205F	12.92	86.13	0.61	0.34	0.3463	1.5300	1.87	-0.4	1.75	-78.79393	33.73168
GS-206	9.12	90.50	0.22	0.16	0.7270	0.4600	1.15	0.14	8.85	-78.79103	33.73160
GS-207	3.93	95.30	0.42	0.36	0.1895	2.4000	1.24	-0.52	8.2	-78.78667	33.73175
GS-208	15.6	83.79	0.35	0.27	0.3143	1.6700	1.87	-0.4	0.59	-78.78205	33.73143
GS-210	0.52	98.85	0.33	0.29	0.1856	2.4300	0.8	0.7	21.26	-78.76763	33.74531
GS-211	1.16	98.08	0.40	0.36	0.3186	1.6500	0.97	0.89	16.14	-78.75132	33.74836
GS-212	0.41	98.76	0.53	0.3	0.2624	1.9300	0.84	1.26	21.23	-78.74065	33.74964
GS-213A	9.4	89.55	0.62	0.43	0.2892	1.7900	1.58	-0.55	4.99	-78.72775	33.74871
GS-214	7.53	91.83	0.41	0.23	0.7120	0.4900	1.05	0.72	15.08	-78.72675	33.75204
GS-215	6.15	93.32	0.37	0.16	1.1096	-0.1500	0.85	2.05	34.97	-78.71996	33.75161
GS-216	0.44	98.79	0.54	0.22	0.1882	2.4100	0.81	0.56	16.4	-78.71619	33.75218
GS-217	0.44	98.41	0.69	0.45	0.1426	2.8100	0.83	0.95	21.77	-78.71286	33.75263
GS-218	4.37	93.29	1.23	1.11	0.1649	2.6000	1.48	-0.38	10.73	-78.71015	33.75282
GS-219	1.26	98.23	0.33	0.18	0.2717	1.8800	0.87	-0.1	20.32	-78.70673	33.75321
GS-220	3.84	93.27	1.71	1.18	0.2517	1.9900	1.71	0.28	3.25	-78.70343	33.75361
GS-221	0.06	99.07	0.54	0.32	0.1406	2.8300	0.6	2.46	48.93	-78.70049	33.75418
GS-222	0.45	98.36	0.63	0.57	0.1466	2.7700	0.83	1.23	27.54	-78.69290	33.76233
GS-223	24.05	75.48	0.29	0.17	1.1408	-0.1900	1.65	-0.01	2.31	-78.68966	33.76428
GS-224	6.8	92.21	0.60	0.39	0.3415	1.5500	1.15	0.02	12.44	-78.68654	33.76612
GS-225	0.12	99.28	0.37	0.23	0.1456	2.7800	0.57	2.02	48.29	-78.68170	33.76805
GS-226	20.58	78.67	0.49	0.27	0.4665	1.1000	1.96	-0.46	1.17	-78.68292	33.77217
GS-227	1.09	97.97	0.59	0.36	0.1649	2.6000	0.79	0.23	34.76	-78.68722	33.77053
GS-228	7.24	92.11	0.40	0.26	0.4005	1.3200	1.17	-0.45	11.13	-78.69223	33.76785
GS-229	1.25	97.34	1.00	0.41	0.1456	2.7800	0.86	0.28	22.46	-78.69508	33.76581
GS-230	0.38	82.52	0.00	6.16	0.0769	3.7000	1.88	0.86	2.95	-78.69890	33.76231
GS-231	17.49	74.57	5.23	2.7	0.9593	0.0600	2.69	0.67	3.3	-78.70131	33.76212
GS-232	2.54	96.84	0.38	0.25	0.3143	1.6700	0.78	0.69	33.37	-78.70336	33.76095
GS-233	0.2	97.65	1.09	1.07	0.1456	2.7800	0.96	1.84	23.97	-78.70528	33.76017
GS-234	6.34	93.12	0.30	0.24	0.4665	1.1000	1.15	-0.73	14.71	-78.70702	33.75975
GS-235	4.15	95.32	0.31	0.23	0.3585	1.4800	0.88	0.09	22.02	-78.70891	33.75922
GS-236	2.2	96.23	0.94	0.63	0.1805	2.4700	1.23	-0.01	8.31	-78.71467	33.75733
GS-237	15.24	83.27	1.02	0.47	0.7738	0.3700	1.65	0.24	5.2	-78.72572	33.75565
GS-238	25.11	73.53	0.90	0.46	0.6462	0.6300	2.18	-0.36	1.35	-78.72476	33.75957
GS-239	8.88	90.05	0.70	0.37	0.2872	1.8000	1.62	-0.56	4.46	-78.72418	33.76221
GS-240	22.56	76.28	0.70	0.45	0.5141	0.9600	1.83	-0.14	1.76	-78.72389	33.76534

Sample ID	% Gravel	% Sand	% Silt	% Clay	Mean Grain Size (mm)	Mean Grain Size (phi)	Sorting	Skewness	Kurtosis	Longitude	Latitude
GS-241	36.13	62.48	0.87	0.52	0.9659	0.0500	2.94	-0.14	-0.81	-78.72301	33.76919
GS-242	0.54	96.41	1.91	1.13	0.1368	2.8700	1.04	1.47	18.48	-78.71671	33.77382
GS-243	7.09	92.12	0.45	0.33	0.5359	0.9000	1.25	-0.03	11.02	-78.71209	33.77397
GS-244	2.97	92.73	2.84	1.47	0.1539	2.7000	1.41	0.51	8.66	-78.70597	33.77483
GS-245	0.85	96.01	1.82	1.32	0.1507	2.7300	1.15	1.3	16.37	-78.70369	33.77452
GS-246	1.9	97.68	0.29	0.13	0.4147	1.2700	0.88	0.48	12.9	-78.70114	33.77510
GS-247	14.99	82.50	1.40	1.11	0.3392	1.5600	1.82	0.07	3.85	-78.69773	33.77649
GS-248	0.48	98.41	0.68	0.42	0.1518	2.7200	0.73	1.44	34.26	-78.69359	33.77780
GS-249	2	97.33	0.42	0.26	0.1604	2.6400	0.97	-1.29	26.19	-78.69077	33.77889
GS-250	1.39	97.94	0.40	0.27	0.1780	2.4900	0.96	-0.25	13.75	-78.68729	33.78024
GS-251	0.78	98.37	0.47	0.38	0.1895	2.4000	0.91	0.46	16.32	-78.69561	33.78652
GS-252	1.27	96.52	1.29	0.92	0.1476	2.7600	1.1	0.41	19.6	-78.70779	33.77907
GS-253A	25.58	71.98	1.72	0.72	0.6552	0.6100	2.31	-0.06	0.83	-78.71601	33.78007
GS-254A	12.05	85.61	1.39	0.95	0.4475	1.1600	1.81	0.23	4.13	-78.72234	33.77978
GS-255	1.45	96.57	1.20	0.78	0.1934	2.3700	1.16	0.75	11.28	-78.72730	33.77876
GS-256	1.4	75.23	0.00	7.72	0.0830	3.5900	2.29	0.53	0.91	-78.73016	33.77728
GS-257	2.43	97.09	0.28	0.2	0.3345	1.5800	1.03	0.19	9.07	-78.73395	33.77554
GS-258	4.91	91.16	2.17	1.76	0.2755	1.8600	1.64	0.84	8.03	-78.73711	33.77419
GS-259	2.28	96.40	0.68	0.63	0.1560	2.6800	1.08	-0.17	17.42	-78.73939	33.77323
GS-260	0.85	97.60	0.91	0.64	0.3978	1.3300	1.06	1.77	23.02	-78.74181	33.77188
GS-261	4.3	94.67	0.54	0.5	0.3869	1.3700	1.16	0.57	13.45	-78.74451	33.77042
GS-262	0.49	97.60	0.90	1.01	0.1446	2.7900	0.96	1.55	22.89	-78.74710	33.76899
GS-263	1.91	97.77	0.17	0.15	0.1604	2.6400	0.81	-1.05	24.13	-78.99610	33.56195
GS-264	0.27	99.03	0.33	0.37	0.1719	2.5400	0.63	2.2	62.01	-78.99186	33.56435
GS-265	1.17	96.25	1.35	1.23	0.1756	2.5100	1.18	1.08	14.33	-78.98837	33.56725
GS-266	2.25	96.77	0.47	0.5	0.1571	2.6700	1.02	-0.15	16.31	-78.98433	33.57033
GS-267	1.69	97.68	0.36	0.27	0.1684	2.5700	0.91	-0.27	17.14	-78.98072	33.57335
GS-268B	11.12	88.19	0.42	0.27	0.3896	1.3600	1.63	-0.14	1.28	-78.97734	33.57664
GS-269	17.82	80.40	1.18	0.6	0.5359	0.9000	1.85	0.03	2.54	-78.97379	33.57971
GS-270	0.13	99.38	0.33	0.16	0.1708	2.5500	0.39	5.04	185.62	-78.97052	33.58246
GS-271	14.12	85.49	0.21	0.17	0.5704	0.8100	1.44	-0.11	2.47	-78.96679	33.58659
GS-272	9.58	89.49	0.60	0.32	0.2661	1.9100	1.44	-0.54	4.79	-78.96351	33.58957
GS-273	4.4	94.96	0.38	0.25	0.2872	1.8000	1.21	-0.46	8.7	-78.96862	33.59764
GS-274	2.38	96.97	0.33	0.32	0.2146	2.2200	0.88	0.01	22.05	-78.96195	33.59879
GS-275	5.82	93.64	0.31	0.23	0.2365	2.0800	1.25	-0.76	7.6	-78.95267	33.59969
GS-276	6.56	93.02	0.29	0.13	0.2892	1.7900	1.18	-0.79	6.9	-78.94566	33.59983
GS-277	28.19	71.41	0.24	0.16	0.6598	0.6000	1.79	-0.31	0.38	-78.93828	33.60164
GS-278	9.43	90.12	0.24	0.21	0.3610	1.4700	1.42	-0.6	5.09	-78.93196	33.59767
GS-279	4.38	95.10	0.35	0.17	0.3015	1.7300	1.08	-0.27	7.86	-78.93081	33.60413
GS-280	27.31	72.08	0.35	0.26	0.6736	0.5700	2.05	-0.23	0.11	-78.92565	33.60404
GS-281	2.8	96.81	0.28	0.11	0.3186	1.6500	0.95	-0.24	9.3	-78.91913	33.60534
GS-282	6.69	91.71	0.98	0.62	0.2483	2.0100	1.48	-0.2	5.86	-78.91201	33.60660
GS-283	1.78	97.70	0.33	0.18	0.2912	1.7800	0.88	0.26	15.13	-78.90364	33.60754
GS-284	26.65	69.55	2.79	1.01	0.7120	0.4900	2.51	0.02	1	-78.89494	33.60877
GS-285	8.98	90.27	0.48	0.27	0.2793	1.8400	1.47	-0.35	2.49	-78.88749	33.61330
GS-286	2.65	95.04	1.52	0.79	0.1276	2.9700	1.24	-0.62	15.57	-78.88281	33.61884
GS-287	6.57	92.27	0.78	0.38	0.2932	1.7700	1.24	-0.09	8.02	-78.87862	33.62409

Sample ID	% Gravel	% Sand	% Silt	% Clay	Mean Grain Size (mm)	Mean Grain Size (phi)	Sorting	Skewness	Kurtosis	Longitude	Latitude
GS-288	0.06	99.33	0.37	0.24	0.2088	2.2600	0.76	1.12	19.44	-78.86631	33.61286
GS-289	1.59	96.16	1.32	0.94	0.1921	2.3800	1.23	0.65	9.55	-78.87051	33.60871
GS-290	0.5	98.91	0.39	0.2	0.1627	2.6200	0.63	0.96	38.04	-78.87520	33.60539
GS-291	3.23	96.24	0.36	0.17	0.3816	1.3900	1.2	0.19	3.38	-78.87942	33.60242
GS-292	0.95	98.79	0.19	0.08	0.3164	1.6600	0.72	0.52	16.16	-78.88432	33.59940
GS-293	10.05	89.57	0.24	0.14	0.3869	1.3700	1.37	-0.64	4.97	-78.88872	33.59700
GS-294	14.38	85.29	0.21	0.12	0.6199	0.6900	1.09	-0.09	6.1	-78.89355	33.59472
GS-295	2.68	96.79	0.33	0.21	0.3099	1.6900	0.82	0.56	24.81	-78.89949	33.59233
GS-296	2.52	97.06	0.23	0.19	0.4175	1.2600	1.04	0.45	9.12	-78.90550	33.59055
GS-297	2.41	97.13	0.28	0.18	0.2973	1.7500	0.94	-0.12	13.91	-78.91170	33.58875
GS-298	1.74	97.87	0.21	0.18	0.1649	2.6000	0.82	-0.85	24.71	-78.91808	33.58641
GS-299	7.01	92.31	0.45	0.24	0.3035	1.7200	1.16	-0.31	7.89	-78.92619	33.58531
GS-300	4.28	95.15	0.37	0.2	0.3276	1.6100	1.16	-0.38	8.18	-78.93312	33.59374
GS-301	12.4	87.22	0.25	0.13	0.3737	1.4200	1.37	-0.67	3.99	-78.93295	33.58784
GS-302	2.2	97.46	0.20	0.14	0.3585	1.4800	0.91	0.19	10.76	-78.93452	33.58333
GS-303	4.68	94.93	0.23	0.15	0.2698	1.8900	1.07	-0.69	9.95	-78.93907	33.57895
GS-304	1.74	97.96	0.18	0.12	0.2285	2.1300	0.83	-0.39	16.68	-78.94291	33.57430
GS-305	0.35	99.29	0.24	0.11	0.1843	2.4400	0.56	0.43	47.75	-78.94860	33.56926
GS-306	0.14	99.41	0.26	0.18	0.1792	2.4800	0.64	1.02	33.11	-78.95300	33.56584
GS-307	3.03	96.46	0.30	0.21	0.2073	2.2700	1.18	-1.31	15.91	-78.95633	33.56231
GS-308	0.38	97.63	1.01	0.98	0.1250	3.0000	0.88	1.88	28.75	-78.96140	33.55814
GS-309	2.65	96.66	0.35	0.34	0.1627	2.6200	1	-0.67	17.45	-78.90350	33.64360
GS-310	1.37	98.16	0.24	0.23	0.1593	2.6500	0.75	-0.47	32.86	-78.90580	33.64110
GS-311	14.21	85.44	0.24	0.11	0.4061	1.3000	1.37	-0.45	2.26	-78.90820	33.63790
GS-312	0.96	97.60	0.97	0.46	0.1684	2.5700	0.86	0.93	23.89	-78.91180	33.63600
GS-313	22.41	77.15	0.28	0.16	0.5176	0.9500	1.64	-0.27	0.83	-78.91500	33.63340
GS-314	1.16	98.08	0.43	0.33	0.2333	2.1000	0.92	0.52	17.93	-78.92030	33.62914
GS-315	0.66	98.77	0.31	0.26	0.1731	2.5300	0.64	1.19	48.72	-78.92229	33.62736
GS-316	53.81	43.92	1.62	0.65	1.2058	-0.2700	2.28	0.38	1.06	-78.92605	33.62524
GS-317	23.32	75.48	0.78	0.42	0.3078	1.7000	2.4	-0.52	0.18	-78.93321	33.62599
GS-318	18.12	81.28	0.37	0.22	0.3896	1.3600	1.72	-0.49	1.45	-78.93165	33.63284
GS-319	6.21	93.10	0.39	0.3	0.2588	1.9500	1.36	-0.34	4.48	-78.93036	33.63483
GS-320	2.51	94.23	1.89	1.37	0.1975	2.3400	1.33	0.82	11.55	-78.92790	33.63715
GS-321	5.37	94.27	0.21	0.14	0.3610	1.4700	0.97	-0.67	15.03	-78.92430	33.64056
GS-322	28.99	68.84	1.50	0.66	0.7270	0.4600	2.15	0.15	1.27	-78.91884	33.64392
GS-323	26.87	70.10	2.19	0.85	0.5864	0.7700	2.38	0	0.64	-78.91412	33.64874
GS-324	5.96	92.50	0.99	0.55	0.2207	2.1800	1.33	-0.22	7.37	-78.90711	33.65279
GS-325	0.63	99.01	0.24	0.13	0.2207	2.1800	0.72	0.31	19.62	-78.90140	33.65625
GS-326	8.2	90.56	0.72	0.52	0.3842	1.3800	1.52	0.08	4.46	-78.92557	33.62096
GS-328	15.25	84.07	0.44	0.25	0.3896	1.3600	1.52	-0.43	3.05	-78.92902	33.61256
GS-329	5.15	94.50	0.19	0.16	0.3487	1.5200	1.01	-0.49	11.69	-78.92998	33.60908
GS-330	9.96	89.75	0.20	0.09	0.7220	0.4700	1.1	-0.08	6.54	-78.91703	33.58008
GS-331	2.78	96.85	0.26	0.1	0.3164	1.6600	0.76	-0.26	22.07	-78.91768	33.57536
GS-332	1.63	98.03	0.21	0.14	0.2679	1.9000	0.83	0.03	13.24	-78.91753	33.57070
GS-333	0.57	98.96	0.32	0.15	0.2349	2.0900	0.67	0.93	28.04	-78.91799	33.56629
GS-334	0.78	98.72	0.35	0.15	0.2774	1.8500	0.77	0.57	19.37	-78.91845	33.56052
GS-335	7.61	92.04	0.22	0.13	0.3231	1.6300	1.16	-0.57	5.46	-78.91868	33.55546

Sample ID	% Gravel	% Sand	% Silt	% Clay	Mean Grain Size (mm)	Mean Grain Size (phi)	Sorting	Skewness	Kurtosis	Longitude	Latitude
GS-336	0.91	98.62	0.30	0.17	0.2088	2.2600	0.69	0.34	30.32	-78.91782	33.55146
GS-337	0.72	98.23	0.64	0.41	0.1696	2.5600	0.75	1.22	33.85	-78.91839	33.54724
GS-338	1.96	95.75	1.41	0.88	0.1743	2.5200	1.18	0.51	12.17	-78.91851	33.54237
GS-339	0.69	98.88	0.30	0.13	0.2606	1.9400	0.79	0.25	13.12	-78.91962	33.53721
GS-340	0.86	98.68	0.29	0.17	0.2932	1.7700	0.87	0.33	12.35	-78.92030	33.53054
GS-341	0.59	98.97	0.27	0.17	0.1731	2.5300	0.58	0.73	48.51	-78.93211	33.55857
GS-342	1.79	97.84	0.25	0.12	0.2952	1.7600	0.72	0.05	25.35	-78.93673	33.55160
r1c1	4.1	65.90	0.00		0.1630	2.6172	1.91	-0.298		-78.73341	33.78223
r2c1	9.85	54.22	0.00		0.2026	2.3031	2.374	-0.237		-78.73979	33.77868
r2c2	23.91	73.72	0.00		0.7979	0.3257	1.663	0.493		-78.72455	33.75907
r3c1	6.09	90.94	0.00		0.3192	1.6475	1.367	-0.787		-78.74335	33.77612
r3c2	4.48	94.95	0.00		0.3780	1.4035	1.156	-0.713		-78.73156	33.75702
r4c1	1.75	91.54	0.00		0.2008	2.3165	1.141	-0.345		-78.75207	33.77020
r4c2	1.27	97.86	0.00		0.2223	2.1695	0.9	-1.471		-78.74579	33.76531
r4c3	1.32	98.00	0.00		0.2995	1.7395	0.878	-0.661		-78.74128	33.75963
r4c4	1.35	97.83	0.00		0.3154	1.6647	1.049	-0.475		-78.73437	33.75357
r4c5	6.83	92.02	0.00		0.5618	0.8318	1.138	-0.163		-78.72831	33.74663
r4c6	4.31	94.84	0.00		0.6146	0.7024	1.005	-0.014		-78.71865	33.73447
R5C2	0.3	98.32	0.00		0.2418	2.0481	0.773	-0.171		-78.74398	33.74993
R5C1	2.47	86.94	0.00		0.1769	2.4991	1.295	-0.606		-78.75719	33.76892
R6C1	1.88	96.77	0.00		0.2420	2.0472	0.995	-1.115		-78.76521	33.76480
R6C2	3.37	96.14	0.00		0.3920	1.3512	0.909	-0.942		-78.76086	33.76206
R6C3	1.72	97.74	0.00		0.2267	2.1409	0.96	-1.515		-78.75702	33.75722
r6c4	3.8	95.17	0.00		0.2293	2.1245	1.201	-1.477		-78.75118	33.75247
r6c5	0.37	98.71	0.00		0.2637	1.9229	0.718	-0.168		-78.74496	33.74574
r6c6	0.41	99.83	0.00		0.3147	1.6678	0.677	-0.938		-78.73771	33.73866
r7c8	1.34	98.53	0.00		0.5969	0.7444	0.784	0.355		-78.72023	33.71062
r7c7	0.1	99.45	0.00		0.3475	1.5247	0.771	0.371		-78.73473	33.72326
r7c6	0.23	98.80	0.00		0.2691	1.8937	0.781	0.178		-78.74246	33.73360
r7c5	0.27	98.38	0.00		0.1816	2.4610	0.724	-1.179		-78.75423	33.74214
r7c4	0.97	98.31	0.00		0.1955	2.3547	0.806	-1.936		-78.75997	33.74835
R7C3	5.17	92.98	0.00		0.2565	1.9632	1.249	-1.632		-78.76520	33.75322
R7C2	1.1	86.77	0.00		0.1944	2.3631	1.234	0.394		-78.76946	33.75859
R7C1	1.15	96.56	0.00		0.1895	2.3996	0.9	-1.185		-78.77031	33.76166
R8C1	8.77	74.66	0.00		0.2338	2.0968	1.872	-0.467		-78.78048	33.75596
R8C3	3.93	94.29	0.00		0.2000	2.3220	1.164	-2.075		-78.77373	33.74694
R8C4	-0.05	99.22	0.00		0.1880	2.4112	0.673	-0.532		-78.76763	33.74183
R8C5	0.15	98.56	0.00		0.2155	2.2143	0.724	-0.001		-78.76215	33.73605
r8c7	1.63	98.61	0.00		0.5141	0.9599	0.812	-0.411		-78.74278	33.71579
R8C8	3.52	76.10	0.00		0.2753	1.8608	1.91	0.468		-78.73551	33.70695
R9C9	0.5	97.90	0.00		0.3780	1.4034	0.95	0.371		-78.73500	33.69710
R9C8	1.25	98.38	0.00		0.4413	1.1802	0.84	-0.088		-78.74578	33.70692
R9C7	0.96	98.52	0.00		0.3685	1.4402	0.815	-0.005		-78.75190	33.71309
R9C6	0.58	98.69	0.00		0.2571	1.9596	0.72	-0.671		-78.75754	33.72005
r9c5	0.38	90.66	0.00		0.1715	2.5441	0.953	0.714		-78.76631	33.72995
R9C4	1	97.84	0.00		0.1781	2.4889	0.84	-2.177		-78.77297	33.73835
r9c3	3.26	96.44	0.00		0.3069	1.7041	1.095	-0.952		-78.77876	33.74531

Sample ID	% Gravel	% Sand	% Silt	% Clay	Mean Grain Size (mm)	Mean Grain Size (phi)	Sorting	Skewness	Kurtosis	Longitude	Latitude
r9c2	4.86	93.95	0.00		0.3684	1.4408	1.218	-0.681		-78.78303	33.74984
r9c1	7.9	78.58	0.00		0.2576	1.9568	1.85	-0.219		-78.78486	33.75276
r10c1	22.7	76.44	0.00		0.5334	0.9068	1.882	-0.566		-78.79384	33.74752
R10C2	9.55	88.76	0.00		0.2818	1.8272	1.546	-1.305		-78.79098	33.74417
R10C3	1.17	98.15	0.00		0.2309	2.1144	0.979	-1.197		-78.78795	33.74107
R10C4	8.22	91.18	0.00		0.3389	1.5610	1.427	-1.118		-78.78357	33.73662
R10C5	19.32	80.17	0.00		0.5880	0.7662	1.704	-0.202		-78.77979	33.73306
R10C6	3.38	94.96	0.00		0.1842	2.4405	1.089	-2.572		-78.77600	33.73064
r10c7	0.51	98.54	0.00		0.1716	2.5425	0.633	-1.92		-78.77631	33.72102
r10c8	0.39	99.21	0.00		0.1970	2.3437	0.688	-1.6		-78.76111	33.71579
r10c9	9.63	89.55	0.00		0.6475	0.6270	1.227	-0.197		-78.75411	33.70702
r10c10	0.87	98.92	0.00		0.3931	1.3470	0.83	-0.451		-78.74802	33.70139
r10c11	2.92	96.45	0.00		0.5212	0.9401	0.888	0.266		-78.74220	33.69206
r11c13	5.1	94.49	0.00		0.6889	0.5376	0.91	-0.03		-78.74666	33.68428
r11c12	1	99.18	0.00		0.4796	1.0600	0.909	-0.177		-78.75113	33.68915
R11C11	3.97	95.16	0.00		0.5694	0.8126	1.029	0.105		-78.75844	33.69557
r11c10	2.31	97.25	0.00		0.3780	1.4037	0.931	-0.6		-78.76198	33.70082
r11c9	2.96	96.57	0.00		0.2259	2.1464	1.088	-2.001		-78.76609	33.70675
r11c8	0.35	99.10	0.00		0.1829	2.4511	0.683	-1.791		-78.77133	33.71251
r11c7	0.06	99.34	0.00		0.1749	2.5155	0.531	-1.134		-78.77617	33.71749
r11c6	0.42	98.21	0.00		0.1654	2.5961	0.642	-1.961		-78.78153	33.72242
r11c5	13.65	70.37	0.00		0.2642	1.9201	2.134	-0.428		-78.78738	33.72662
r11c4	21.94	77.81	0.00		0.9951	0.0070	1.249	0.053		-78.79036	33.73017
r11c3	6.84	92.43	0.00		0.3325	1.5886	1.409	-0.906		-78.79478	33.73524
r11c2	2.86	96.52	0.00		0.2604	1.9411	1.12	-1.137		-78.79881	33.73957
r11c1	4.67	94.64	0.00		0.2955	1.7586	1.155	-1.537		-78.80123	33.74368
r12c1	1.25	97.24	0.00		0.1964	2.3482	0.876	-1.493		-78.80636	33.73885
r12c2	13.14	86.46	0.00		0.3925	1.3493	1.62	-1.005		-78.80489	33.73484
r12c3	8.38	93.35	0.00		0.4662	1.1008	1.218	-1.585		-78.79929	33.72905
r12c4	19.68	79.94	0.00		0.7803	0.3579	1.494	0.01		-78.78955	33.72736
r12c5	34.66	65.76	0.00		1.1494	-0.2009	1.502	0.194		-78.79016	33.71821
r12c6	1.06	96.87	0.00		0.2305	2.1174	0.801	-0.973		-78.78544	33.71540
r12c7	1.19	98.80	0.00		0.1905	2.3920	0.782	-2.842		-78.77696	33.70864
r12c8	3.66	95.40	0.00		0.6580	0.6037	1.019	0.747		-78.76404	33.68729
r14c6	1.01	97.96	0.00		0.1681	2.5723	0.697	-3.135		-78.79171	33.70304
r14c5	0.93	15.48	0.00		0.0495	4.3369	1.574	-2.168		-78.79610	33.70798
r14c4	2.95	96.36	0.00		0.2219	2.1723	1.049	-1.884		-78.80131	33.71358
r14c3	3.34	95.63	0.00		0.2767	1.8534	1.044	-1.173		-78.80705	33.72128
r14c2	-0.9	99.29	0.00		0.2039	2.2942	0.665	3.151		-78.81393	33.72732
r14c1	1.21	96.68	0.00		0.2166	2.2069	0.968	-0.958		-78.81818	33.73216
r13c1	11.46	86.63	0.00		0.3977	1.3303	1.489	-0.935		-78.81128	33.73626
r15c1	3.34	96.30	0.00		0.2789	1.8422	1.057	-1.545		-78.82605	33.72614
r15c2	5.23	94.38	0.00		0.3051	1.7128	1.169	-1.556		-78.82141	33.72213
r15c3	15.39	84.17	0.00		0.9890	0.0159	1.142	0.679		-78.81610	33.71526
r15c4	11.98	86.94	0.00		0.2686	1.8965	1.69	-1.275		-78.81090	33.71136
r15c5	1.75	97.67	0.00		0.3657	1.4513	0.992	-0.089		-78.80222	33.70296
r15c6	5.21	93.74	0.00		0.1917	2.3831	1.175	-3.038		-78.79548	33.69704

Sample ID	% Gravel	% Sand	% Silt	% Clay	Mean Grain Size (mm)	Mean Grain Size (phi)	Sorting	Skewness	Kurtosis	Longitude	Latitude
r16c1	33.06	65.87	0.00		0.8484	0.2372	1.883	-0.092		-78.83279	33.72131
t1c1	1.15	85.57	0.00		0.1723	2.5369	1.296	-0.033		-78.84030	33.71763
t2c1	6.46	86.54	0.00		0.3442	1.5388	1.511	-0.006		-78.84339	33.71593
t3c1	1.44	81.33	0.00		0.1662	2.5890	1.408	-0.025		-78.84730	33.71208
t4c1	0.03	91.62	0.00		0.1950	2.3585	1.034	0.95		-78.85306	33.70656
t5c1	0	31.53	0.00		0.1098	3.1872	2.672	-0.795		-78.86055	33.70361
t6c1	9.43	67.15	0.00		0.2035	2.2967	2.053	-0.403		-78.86450	33.70180
t7c1	6.12	79.82	0.00		0.2613	1.9364	1.72	0.033		-78.86754	33.69927
t8c1	-0.34	66.12	0.00		0.1095	3.1910	1.403	0.348		-78.87126	33.69566
t9c1	45.74	51.92	0.00		1.3291	-0.4105	1.777	0.834		-78.87826	33.68802
t10c1	1.92	17.20	0.00		0.0479	4.3849	1.433	-2.548		-78.88210	33.68366
t12c1	21.15	77.65	0.00		0.5467	0.8711	1.725	-0.466		-78.89114	33.67506
t13c1	27.52	66.87	0.00		0.7997	0.3224	1.882	0.754		-78.90047	33.66522
t14c1	0	8.76	0.00		0.0443	4.4961	1.626	-2.917		-78.90639	33.66199
t15c1	24.26	76.30	0.00		0.8915	0.1656	1.407	-0.479		-78.91287	33.65761
t17c1	11.92	72.27	0.00		0.2943	1.7646	1.98	-0.206		-78.93256	33.64047
t18c1	18.76	74.53	0.00		0.5995	0.7381	1.896	0.43		-78.93677	33.63722
t19c1	17.06	75.42	0.00		0.3796	1.3974	1.863	-0.423		-78.93977	33.63462
t20c1	22.33	76.84	0.00		0.8284	0.2716	1.483	0.072		-78.94302	33.63055
t21c1	12.94	77.17	0.00		0.4302	1.2169	1.877	0.277		-78.94657	33.62685
t22c1	14.87	82.91	0.00		0.4189	1.2553	1.673	-0.784		-78.95037	33.62267
t23c1	5.11	93.66	0.00		0.3152	1.6657	1.213	-0.987		-78.95690	33.61501
t24c1	12.13	85.09	0.00		0.3401	1.5558	1.684	-0.968		-78.96339	33.60705
t24c2	16.19	82.81	0.00		0.5925	0.7552	1.569	-0.392		-78.96043	33.60522
t23c2	19.94	78.67	0.00		0.9611	0.0573	1.341	0.556		-78.95323	33.61322
t22c2	24.42	74.69	0.00		0.5488	0.8656	1.892	-0.493		-78.94510	33.62087
t21c2	1.07	97.42	0.00		0.1974	2.3409	0.78	-1.552		-78.94101	33.62459
t19c2	5.48	94.39	0.00		0.3752	1.4143	1.037	-1.667		-78.93417	33.63139
t17c2	3.04	96.16	0.00		0.2721	1.8779	0.967	-1.885		-78.92848	33.63790
t16c2	51.28	47.09	0.00		1.1400	-0.1890	2.173	0.451		-78.91612	33.64774
t15c2	24.39	73.86	0.00		0.5965	0.7454	1.822	-0.388		-78.90676	33.65536
t14c2	0.82	97.97	0.00		0.2396	2.0613	0.834	-0.773		-78.90356	33.66091
t13c2	16.19	63.46	0.00		0.3279	1.6086	2.251	-0.003		-78.89824	33.66654
t12c2	19.34	78.80	0.00		0.5305	0.9146	1.694	-0.432		-78.88903	33.67455
t11c2	16.7	67.22	0.00		0.4383	1.1900	2.135	0.362		-78.88343	33.67968
t10c2	2.31	93.12	0.00		0.2223	2.1691	1.097	-0.731		-78.87942	33.68245
t9c2	2.5	96.66	0.00		0.2847	1.8127	0.91	-1.359		-78.87491	33.68670
t8c2	0.33	97.20	0.00		0.1869	2.4198	0.778	-0.453		-78.86644	33.69292
t7c2	0.37	73.00	0.00		0.1420	2.8165	1.485	0.234		-78.86290	33.69626
t6c2	2.8	89.78	0.00		0.2204	2.1815	1.252	-0.484		-78.85903	33.69946
t5c2	4.85	92.49	0.00		0.3747	1.4163	1.201	-0.242		-78.85704	33.70133
t4c2	1.11	96.82	0.00		0.2228	2.1661	0.984	-0.928		-78.85117	33.70563
t3c2	3.14	89.28	0.00		0.2351	2.0888	1.357	-0.275		-78.84449	33.71085
t2c2	11.75	87.55	0.00		0.4853	1.0431	1.341	-1.019		-78.84043	33.71475
t1c2	1.17	97.26	0.00		0.2187	2.1927	0.903	-1.126		-78.83832	33.71687
w1c1	0.83	98.51	0.00		0.2402	2.0574	0.803	-1.191		-78.53883	33.81947
w1c2	0.24	99.24	0.00		0.3837	1.3820	0.83	0.388		-78.53383	33.80532

Sample ID	% Gravel	% Sand	% Silt	% Clay	Mean Grain Size (mm)	Mean Grain Size (phi)	Sorting	Skewness	Kurtosis	Longitude	Latitude
w1c3	1.12	99.01	0.00		0.3685	1.4402	0.861	-0.57		-78.53182	33.79550
w1c4	10.33	89.32	0.00		1.0236	-0.0336	0.925	0.369		-78.52150	33.77999
w2c3	0.11	99.75	0.00		0.3317	1.5919	0.655	-0.274		-78.54331	33.77680
w3c3	0.23	99.59	0.00		0.2690	1.8942	0.668	-0.623		-78.55990	33.77664
w3c2	0.72	98.24	0.00		0.3034	1.7208	0.856	-0.062		-78.56450	33.78713
w2c2	0.28	99.35	0.00		0.3280	1.6083	0.792	-0.113		-78.55265	33.79784
w3c1	1.3	99.07	0.00		0.2698	1.8901	0.847	-1.664		-78.57169	33.81803
w2c1	0	66.01	0.00		0.1209	3.0476	1.541	0.149		-78.56574	33.82734
w4c1	0.36	90.11	0.00		0.1575	2.6666	1.018	0.312		-78.59280	33.82611
w4c2	1.66	97.77	0.00		0.2323	2.1057	0.923	-1.546		-78.59053	33.81367
w4c3	2.89	96.72	0.00		0.4156	1.2667	1	-0.718		-78.58261	33.79583
w4c4	7.51	92.13	0.00		0.4345	1.2026	1.23	-1.248		-78.57099	33.77215
w5c1	7.94	91.51	0.00		0.8006	0.3209	0.996	0.238		-78.58086	33.77303
w6c5	0.14	99.72	0.00		0.3640	1.4581	0.709	-0.019		-78.58734	33.76078
w6c4	0.3	99.28	0.00		0.3467	1.5281	0.728	0.134		-78.59455	33.77850
w6c3	0.43	99.25	0.00		0.3698	1.4352	0.789	-0.047		-78.60276	33.79093
w6c2	1.07	98.63	0.00		0.2874	1.7990	0.824	-0.885		-78.60995	33.80684
w6c1	0.33	98.68	0.00		0.2694	1.8924	0.708	0.147		-78.61660	33.82338
w7c1	0.39	98.94	0.00		0.2697	1.8905	0.715	-0.461		-78.63373	33.81999
w8c1	7.73	91.68	0.00		0.4814	1.0546	1.271	-0.468		-78.65860	33.80737
w8c2	7.11	92.49	0.00		0.3701	1.4342	1.138	-1.814		-78.64683	33.79428
w8c3	2.54	96.96	0.00		0.2904	1.7837	0.956	-1.428		-78.63443	33.78710
w7c2	6.82	91.94	0.00		0.5687	0.8143	1.168	-0.255		-78.61663	33.76934
w8c4	0.4	99.24	0.00		0.3806	1.3936	0.81	-0.052		-78.62524	33.76002
w7c3	6.82	91.94	0.00		0.5687	0.8143	1.168	-0.255		-78.61147	33.75532
w9c6	0.05	99.85	0.00		0.2620	1.9322	0.641	-0.449		-78.64151	33.74340
w9c5	2.33	96.17	0.00		0.2915	1.7785	1.096	-0.849		-78.65088	33.75916
w9c4	1.16	98.53	0.00		0.2272	2.1381	0.804	-2.058		-78.66108	33.77499
w9c2	3.06	96.13	0.00		0.2685	1.8970	1.005	-1.743		-78.67690	33.79228
w9c1	6.77	90.24	0.00		0.2932	1.7699	1.373	-1.013		-78.68432	33.80095
t1c3	2.71	97.08	0.00		0.3148	1.6675	0.95	-1.596		-78.83585	33.71536
t2c3	9.27	89.85	0.00		0.3156	1.6639	1.465	-1.363		-78.83894	33.71276
t3c3	4.83	94.09	0.00		0.3054	1.7111	1.208	-1.232		-78.84285	33.70869
t4c3	0.98	98.34	0.00		0.2358	2.0841	0.81	-1.282		-78.84912	33.70427
t5c3	2.93	95.39	0.00		0.2850	1.8110	1.076	-0.957		-78.85504	33.69984
t6c3	2.1	97.47	0.00		0.2872	1.7998	0.851	-1.573		-78.85604	33.69745
t7c3	6.33	93.38	0.00		0.4184	1.2571	1.23	-0.821		-78.85979	33.69445
t8c3	1	97.72	0.00		0.2340	2.0954	0.883	-0.884		-78.86410	33.69171
t9c3	1.67	97.14	0.00		0.2559	1.9662	0.923	-1.222		-78.87355	33.68526
t10c3	2.81	95.01	0.00		0.2545	1.9743	1.018	-1.117		-78.87891	33.68226
t11c3	2.17	94.88	0.00		0.2192	2.1894	1.056	-1.194		-78.88167	33.67815
t12c3	7.84	91.77	0.00		0.3991	1.3253	1.254	-1.26		-78.88694	33.67349
t13c3	24.5	73.24	0.00		0.5106	0.9696	1.959	-0.503		-78.89704	33.66516
t14c3	0.49	98.14	0.00		0.2656	1.9127	0.851	-0.314		-78.90156	33.65946
t15c3	29.31	69.86	0.00		0.7610	0.3941	1.817	-0.147		-78.90538	33.65385
t16c3	15.6	83.38	0.00		0.5473	0.8695	1.617	-0.434		-78.91249	33.64817
t17c3	1.8	97.05	0.00		0.2872	1.8000	0.904	-0.813		-78.92561	33.63695

Sample ID	% Gravel	% Sand	% Silt	% Clay	Mean Grain Size (mm)	Mean Grain Size (phi)	Sorting	Skewness	Kurtosis	Longitude	Latitude
t19c3	3.48	96.22	0.00		0.3457	1.5325	0.911	-1.592		-78.93251	33.63018
t 21c3	2.9	97.56	0.00		0.2653	1.9145	0.979	-1.971		-78.93897	33.62389
t22c3	19.14	80.98	0.00		0.5902	0.7608	1.597	-0.784		-78.94237	33.61949
t23c3	15.61	84.01	0.00		0.5287	0.9195	1.566	-0.669		-78.95022	33.61269
t24c3	40.87	58.64	0.00		1.2713	-0.3463	1.74	0.547		-78.95870	33.60361
gs_1_nf0302	2.47	97.01	0.00		0.2356	2.0859	0.956	-2.144	9.998	-79.00208	33.52411
gs_2_nf0302	4	95.70	0.00		0.2240	2.1586	1.124	-2.228	8.378	-79.00802	33.51816
gs_3_nf0302	0.88	98.83	0.00		0.2253	2.1503	0.607	-2.961	23.928	-79.01430	33.51324
gs_4_nf0302	1.41	98.26	0.00		0.1792	2.4803	0.858	-1.915	12.057	-79.01913	33.50808
gs_5_nf0302	0.75	98.50	0.00		0.1848	2.4364	0.7	-2.338	16.427	-79.02716	33.49872
gs_6_nf0302	1.09	98.36	0.00		0.1782	2.4883	0.773	-3.035	17.918	-79.03457	33.49073
gs_7_nf0302	1.33	97.78	0.00		0.1882	2.4100	0.832	-2.389	13.445	-79.03823	33.48593
gs_8_nf0302	0.33	99.06	0.00		0.2102	2.2498	0.663	-0.957	9.957	-79.04274	33.48107
gs_9_nf0302	4.32	95.04	0.00		0.2113	2.2423	1.177	-2.134	7.799	-79.04708	33.47643
gs_10_nf030	0.57	98.92	0.00		0.1818	2.4595	0.633	-2.649	19.758	-79.05503	33.46787
gs_11_nf030	0.5	98.94	0.00		0.1744	2.5199	0.62	-2.638	19.556	-79.06188	33.46033
gs_12_nf030	1.32	98.18	0.00		0.1859	2.4272	0.76	-2.891	16.583	-79.06545	33.45540
gs_13_nf030	0.84	98.53	0.00		0.1860	2.4263	0.745	-2.488	14.505	-79.06678	33.45314
gs_14_nf030	4.26	95.21	0.00		0.2048	2.2879	1.082	-3.044	13.189	-79.06947	33.44996
gs_15_nf030	66.01	32.83	0.00		2.0397	-1.0283	1.627	1.603	4.985	-79.07526	33.44376
gs_16_nf030	26.05	72.90	0.00		0.8162	0.2930	1.733	0.282	2.187	-79.06898	33.43945
gs_17_nf030	11.46	88.32	0.00		0.4478	1.1590	1.431	-0.77	2.615	-79.06207	33.43449
gs_18_nf030	1.36	98.10	0.00		0.2105	2.2479	0.78	-2.545	14.338	-79.05607	33.42952
gs_19_nf030	0.42	98.73	0.00		0.1949	2.3594	0.638	-1.585	14.699	-79.04970	33.43384
gs_20_nf030	0.36	99.06	0.00		0.1973	2.3417	0.596	-1.468	14.185	-79.04642	33.43762
gs_21_nf030	0.85	98.40	0.00		0.2141	2.2235	0.69	-1.671	12.755	-79.04061	33.44370
gs_22_nf030	0.91	98.47	0.00		0.2172	2.2029	0.719	-1.937	12.876	-79.03034	33.45594
gs_23_nf030	0.54	99.05	0.00		0.2643	1.9199	0.588	-1.112	13.085	-79.02457	33.46211
gs_24_nf030	10.36	89.33	0.00		0.6424	0.6385	1.179	-0.705	3.743	-79.02115	33.46614
gs_25_nf030	3.09	96.23	0.00		0.2122	2.2365	0.97	-2.533	11.266	-79.01743	33.47093
gs_26_nf030	1.04	97.87	0.00		0.1859	2.4273	0.852	-2.064	10.481	-79.01273	33.47619
gs_27_nf030	0.3	99.06	0.00		0.1785	2.4862	0.617	-2.089	15.174	-79.00439	33.48559
gs_28_nf030	0.07	99.25	0.00		0.2209	2.1784	0.522	0.234	9.825	-78.99980	33.49066
gs_29_nf030	0.48	98.96	0.00		0.2629	1.9272	0.676	-0.631	8.427	-78.99588	33.49377
gs_30_nf030	0.87	98.66	0.00		0.2349	2.0897	0.676	-1.979	14.257	-78.99318	33.49784
gs_31_nf030	0.6	98.90	0.00		0.2231	2.1642	0.612	-2.148	19.232	-78.98839	33.50280
gs_32_nf030	0.44	99.07	0.00		0.2749	1.8629	0.71	-0.862	7.62	-78.97563	33.49715
gs_33_nf030	1.17	98.05	0.00		0.2252	2.1508	0.8	-1.933	11.423	-78.97238	33.49402
gs_34_nf030	0.13	99.48	0.00		0.2112	2.2431	0.522	-0.965	11.99	-78.97692	33.48477
gs_35_nf030	0.31	99.31	0.00		0.2051	2.2853	0.581	-1.604	12.443	-78.97926	33.48015
gs_36_nf030	0.94	98.05	0.00		0.1900	2.3963	0.752	-1.899	12.007	-78.98551	33.47257
gs_37_nf030	7.9	91.80	0.00		0.3890	1.3621	1.404	-0.825	3.04	-78.99345	33.46438
gs_38_nf030	3.65	96.24	0.00		0.2948	1.7620	1.037	-1.776	6.586	-79.00006	33.45637
gs_39_nf030	3.13	96.76	0.00		0.2902	1.7849	0.99	-1.732	6.223	-79.00552	33.45107
gs_40_nf030	0.57	99.28	0.00		0.2564	1.9635	0.628	-1.67	10.011	-79.00977	33.44524
gs_41_nf030	0.82	98.91	0.00		0.1964	2.3478	0.7	-2.466	13.855	-79.01524	33.43889
gs_42_nf030	0.41	99.37	0.00		0.2048	2.2879	0.619	-1.94	12.475	-79.01980	33.43366

Sample ID	% Gravel	% Sand	% Silt	% Clay	Mean Grain Size (mm)	Mean Grain Size (phi)	Sorting	Skewness	Kurtosis	Longitude	Latitude
gs_43_nf030	4.97	95.01	0.00		0.3640	1.4580	1.061	-1.631	6.18	-79.02299	33.43010
gs_44_nf030	6.28	93.71	0.00		0.4362	1.1968	1.082	-1.17	4.317	-79.02616	33.42573
gs_45_nf030	0.32	99.68	0.00		0.2068	2.2734	0.552	-2.188	13.85	-79.03096	33.41994
gs_46_nf030	0.16	99.79	0.00		0.2091	2.2579	0.514	-1.397	9.935	-79.03317	33.41489
gs_47_nf030	0.61	98.98	0.00		0.1808	2.4675	0.657	-2.538	16.639	-79.03547	33.40670
gs_48_nf030	33.41	66.40	0.00		1.3551	-0.4384	1.185	0.711	3.939	-79.03772	33.39882
gs_49_nf030	25.25	74.71	0.00		1.2324	-0.3015	1.106	0.141	2.987	-79.03918	33.38973
gs_50_nf030	20.91	78.92	0.00		1.0113	-0.0162	1.217	0.141	3.146	-79.04137	33.38273
gs_51_nf030	18.02	81.80	0.00		0.9770	0.0336	1.165	0.167	3.106	-79.04542	33.37255
gs_52_nf030	25.51	74.33	0.00		1.1398	-0.1887	1.171	0.214	3.075	-79.04823	33.36361
gs_53_nf030	12.9	87.14	0.00		0.7973	0.3269	1.184	-0.262	2.601	-79.05219	33.35579
gs_54_nf030	9.54	90.26	0.00		0.5488	0.8656	1.261	-0.497	2.714	-79.05588	33.34970
gs_55_nf030	5.57	94.48	0.00		0.3697	1.4355	1.227	-1.128	3.601	-79.05860	33.34215
gs_56_nf030	4.59	94.94	0.00		0.5093	0.9734	1.143	-0.268	3.321	-79.06242	33.33419
gs_57_nf030	5.92	93.69	0.00		0.5558	0.8473	1.088	-0.306	3.733	-79.06454	33.32757
gs_58_nf030	2.29	97.55	0.00		0.3905	1.3568	0.938	-0.869	4.519	-79.06844	33.32078
gs_59_nf030	2.75	97.33	0.00		0.4427	1.1755	0.927	-0.79	3.516	-79.07036	33.31287
gs_60_nf030	5.32	89.60	0.00		0.3706	1.4320	1.459	0.138	3.534	-79.07367	33.30271
gs_61_nf030	0.7	99.01	0.00		0.2809	1.8320	0.796	-0.971	5.456	-79.08203	33.30044
gs_62_nf030	5.48	94.08	0.00		0.5617	0.8322	1.105	-0.353	4.304	-79.09496	33.30379
gs_63_nf030	6.43	93.29	0.00		0.4986	1.0042	1.159	-0.654	3.431	-79.09192	33.31299
gs_64_nf030	6.77	92.74	0.00		0.3326	1.5880	1.368	-1.051	3.453	-79.08795	33.32073
gs_65_nf030	6.66	92.63	0.00		0.3465	1.5290	1.329	-0.993	3.507	-79.08389	33.32891
gs_66_nf030	7.01	92.81	0.00		0.4891	1.0318	1.241	-0.448	2.709	-79.06693	33.33335
gs_67_nf030	4.11	95.67	0.00		0.3449	1.5358	1.112	-1.059	4.253	-79.08965	33.34499
gs_68_nf030	5.5	94.40	0.00		0.4977	1.0065	1.111	-0.616	3.64	-79.07554	33.34958
gs_69_nf030	4.4	95.16	0.00		0.2763	1.8556	1.16	-1.716	6.136	-79.07227	33.35723
gs_70_nf030	14.82	85.01	0.00		0.7672	0.3823	1.242	-0.128	2.738	-79.06840	33.36409
gs_71_nf030	11.4	87.87	0.00		0.3686	1.4401	1.641	-0.656	2.235	-79.06422	33.37655
gs_72_nf030	10.47	88.94	0.00		0.2854	1.8090	1.601	-1.33	3.689	-79.05905	33.38676
gs_73_nf030	19.64	79.97	0.00		1.0594	-0.0832	1.167	0.788	3.992	-79.05500	33.39607
gs_74_nf030	18.21	81.10	0.00		0.4070	1.2967	1.912	-0.699	2.076	-79.05070	33.40491
gs_75_nf030	14.3	84.13	0.00		0.3669	1.4465	1.822	-0.789	2.534	-79.05525	33.41424
gs_76_nf030	0.64	99.07	0.00		0.2056	2.2819	0.681	-2.501	14.756	-79.06108	33.41968
gs_77_nf030	4.25	94.97	0.00		0.2225	2.1682	1.281	-1.619	5.312	-79.06637	33.42377
gs_78_nf030	1.4	98.39	0.00		0.2035	2.2966	0.791	-2.787	13.8	-79.06870	33.42605
gs_79_nf030	7.31	92.46	0.00		0.3330	1.5862	1.331	-1.218	3.528	-79.07331	33.43181
gs_80_nf030	2.6	97.13	0.00		0.4787	1.0629	0.812	-0.552	8.023	-79.07846	33.42108
gs_81_nf030	6.17	93.57	0.00		0.5960	0.7465	0.917	-0.882	6.178	-79.08210	33.40286
gs_82_nf030	5.04	94.74	0.00		0.3768	1.4083	1.135	-1.194	4.643	-79.08258	33.39471
gs_83_nf030	12.56	87.29	0.00		0.6127	0.7068	1.261	-0.417	2.835	-79.08571	33.37986
gs_84_nf030	17.07	82.15	0.00		0.6712	0.5752	1.562	0.069	2.351	-79.08672	33.36585
gs_85_nf030	29.03	70.29	0.00		0.7779	0.3623	1.726	0.185	1.829	-79.08817	33.35307
gs_86_nf030		0.00	0.00		0.2310	2.1139	0.767	-1.928	10.097	-79.08965	33.34499
gs_87_nf030	6.25	93.58	0.00		0.4409	1.1816	1.164	-0.896	3.983	-79.09061	33.33710
gs_109_nf03	34.16	65.36	0.00		1.6010	-0.6790	1.127	1.444	7.19	-79.12162	33.38785
gs_110_nf03	8.45	91.27	0.00		0.7168	0.4803	1.118	-0.023	3.817	-79.12423	33.38032

Sample ID	% Gravel	% Sand	% Silt	% Clay	Mean Grain Size (mm)	Mean Grain Size (phi)	Sorting	Skewness	Kurtosis	Longitude	Latitude
gs_111_nf03	4.15	95.07	0.00		0.5362	0.8993	1.134	0.097	4.181	-79.12721	33.37471
gs_112_nf03	2.33	97.42	0.00		0.6042	0.7268	0.886	0.404	4.76	-79.12906	33.36864
gs_113_nf03	17.48	77.14	0.00		0.5987	0.7400	1.71	0.392	3.364	-79.13185	33.36132
gs_114_nf03	6.44	93.28	0.00		0.5895	0.7625	1.079	-0.207	3.867	-79.13244	33.35435
gs_115a_nf0	20.02	79.24	0.00		0.9965	0.0050	1.365	0.76	3.772	-79.12947	33.34733
gs_116_nf03	5.31	93.96	0.00		0.2600	1.9434	1.321	-1.51	4.912	-79.12749	33.34093
gs_117_nf03	5.9	93.97	0.00		0.5711	0.8082	1.187	-0.085	2.799	-79.12625	33.33554
gs_118_nf03	5.25	94.48	0.00		0.2787	1.8432	1.247	-1.585	5.241	-79.12386	33.32853
gs_120_nf03	5.46	93.85	0.00		0.5393	0.8909	1.134	0.059	3.657	-79.11981	33.31176
gs_121_nf03	0.6	98.87	0.00		0.3163	1.6606	0.847	-0.437	5.125	-79.11446	33.30383
gs_128_nf03	5.37	94.24	0.00		0.7234	0.4670	1.039	0.419	5.293	-78.56208	33.77671
gs_129_nf03	4.59	95.01	0.00		0.7248	0.4644	0.933	0.503	6.273	-78.56820	33.77480
gs_130_nf03	0.19	99.43	0.00		0.2717	1.8798	0.68	-0.112	5.728	-78.57590	33.77234
gs_131_nf03	0.24	99.55	0.00		0.3867	1.3706	0.688	0.283	5.707	-78.58480	33.77015
gs_132_nf03	0.31	99.53	0.00		0.4611	1.1167	0.677	0.026	5.397	-78.58964	33.76724
gs_133_nf03	0.27	99.42	0.00		0.3623	1.4648	0.732	0.125	4.806	-78.59565	33.76491
gs_134_nf03	0.56	99.17	0.00		0.3142	1.6702	0.817	-0.518	5.391	-78.60135	33.76117
gs_135_nf03	0.6	99.21	0.00		0.4168	1.2627	0.811	-0.381	4.676	-78.60621	33.75892
gs_136_nf03	22.26	76.95	0.00		0.5706	0.8094	1.715	-0.793	2.548	-78.61345	33.75670
gs_137_nf03	0.51	99.22	0.00		0.4856	1.0421	0.698	0.393	6.464	-78.61853	33.75560
gs_138_nf03	2.16	97.59	0.00		0.4353	1.2001	0.959	-0.701	5.16	-78.62480	33.75270
gs_139_nf03	0.13	99.48	0.00		0.3267	1.6138	0.691	-0.234	7.037	-78.63017	33.75085
gs_140_nf03	0.18	99.23	0.00		0.2237	2.1604	0.702	-0.823	7.687	-78.63529	33.74850
gs_141_nf03	0.83	98.86	0.00		0.5802	0.7854	0.749	0.781	6.542	-78.63908	33.74712
gs_142_nf03	0.07	99.54	0.00		0.2038	2.2951	0.592	-0.756	7.661	-78.64504	33.74641
gs_143_nf03	0.09	99.71	0.00		0.3175	1.6552	0.672	0.039	4.612	-78.65206	33.74335
gs_144_nf03	0.54	99.13	0.00		0.3484	1.5211	0.769	-0.203	5.135	-78.65538	33.74044
gs_145_nf03	0.14	99.58	0.00		0.2574	1.9578	0.692	-0.726	5.709	-78.66469	33.73631
gs_146_nf03	0.17	99.65	0.00		0.2166	2.2066	0.582	-1.395	10.704	-78.67236	33.73312
gs_147_nf03	0.33	99.42	0.00		0.5587	0.8398	0.726	1.142	6.764	-78.67809	33.73017
gs_148_nf03	0.31	99.21	0.00		0.1896	2.3990	0.64	-1.625	10.752	-78.68229	33.72759
gs_149_nf03	2.75	96.12	0.00		0.3790	1.3997	1.296	-0.19	2.71	-78.69021	33.72293
gs_150_nf03	2.32	97.55	0.00		0.7091	0.4959	0.695	-0.024	8.162	-78.69638	33.72006
gs_151_nf03	2.41	97.29	0.00		0.6159	0.6993	0.94	0.24	5.217	-78.70222	33.71630
gs_152_nf03	3.28	96.20	0.00		0.3117	1.6818	1.017	-1.389	7.473	-78.70876	33.71284
gs_153_nf03	1.34	98.39	0.00		0.6129	0.7064	0.833	0.442	5.307	-78.71546	33.70931
gs_154_nf03	0.28	99.42	0.00		0.3500	1.5146	0.866	-0.418	3.603	-78.72035	33.70586
gs_155_nf03	5.28	94.49	0.00		0.3998	1.3227	1.16	-1.037	4.397	-78.72511	33.70285
gs_156_nf03	2.02	97.85	0.00		0.5721	0.8057	0.883	-0.165	4.645	-78.73022	33.69874
gs_157_nf03	0.22	99.57	0.00		0.2708	1.8849	0.724	-0.752	4.864	-78.73605	33.69573
gs_158_nf03	1.55	98.28	0.00		0.3140	1.6710	0.962	-1.043	4.351	-78.74437	33.69071
gs_159_nf03	9.03	90.08	0.00		0.6786	0.5595	1.147	0.258	4.392	-78.75097	33.68480
gs_160_nf03	3.54	96.33	0.00		0.5481	0.8674	0.946	-0.266	3.209	-78.76815	33.68148
gs_161_nf03	1.02	98.61	0.00		0.4287	1.2220	0.997	-0.176	3.124	-78.76696	33.68360
gs_162_nf03	1.72	97.99	0.00		0.5832	0.7779	0.772	0.093	6.436	-78.76931	33.68895
gs_163_nf03	0.53	98.84	0.00		0.4468	1.1624	0.862	0.405	5.074	-78.76469	33.69463
gs_164_nf03	11.59	56.35	0.00		0.2975	1.7490	2.484	0.177	1.699	-78.75754	33.70003

Sample ID	% Gravel	% Sand	% Silt	% Clay	Mean Grain Size (mm)	Mean Grain Size (phi)	Sorting	Skewness	Kurtosis	Longitude	Latitude
gs_165_nf03	0.31	99.46	0.00		0.3725	1.4248	0.762	-0.146	4.671	-78.75267	33.70338
gs_166_nf03	0.41	99.35	0.00		0.3584	1.4802	0.811	-0.142	4.226	-78.74711	33.70719
gs_167_nf03	2.71	96.86	0.00		0.4660	1.1016	1.045	-0.005	4.012	-78.74186	33.71117
gs_168_nf03	0.86	98.78	0.00		0.5302	0.9154	0.906	0.557	4.482	-78.73851	33.71504
gs_169_nf03	0.39	99.59	0.00		0.4049	1.3044	0.848	0.001	2.858	-78.73216	33.71786
gs_170_nf03	3.22	96.31	0.00		0.5905	0.7601	0.926	0.122	5.303	-78.72764	33.72110
gs_171_nf03	2.07	97.67	0.00		0.7157	0.4826	0.765	0.827	7.069	-78.72260	33.72161
gs_172_nf03	2.55	97.14	0.00		0.5906	0.7598	0.94	0.032	5.466	-78.71708	33.72524
gs_173_nf03	3.75	95.87	0.00		0.7481	0.4186	0.903	0.576	5.679	-78.71199	33.72951
gs_174_nf03	0.08	99.32	0.00		0.1890	2.4034	0.614	-0.65	6.814	-78.70653	33.73136
gs_175_nf03	7.21	91.70	0.00		0.8198	0.2866	1.038	0.927	7.8	-78.69796	33.73562
gs_176_nf03	0.2	97.76	0.00		0.1808	2.4673	0.704	-0.667	10.355	-78.68792	33.74040
gs_177_nf03	0.16	96.91	0.00		0.1774	2.4949	0.724	-0.031	9.369	-78.67869	33.74544
gs_178_nf03	0.6	97.05	0.00		0.1998	2.3234	0.794	-0.617	9.575	-78.67016	33.74881
gs_179_nf03	0.14	99.40	0.00		0.2397	2.0609	0.667	-0.491	6.186	-78.65776	33.75565
gs_180_nf03	1.81	97.98	0.00		0.3863	1.3724	0.949	-0.692	4.858	-78.64657	33.75938
gs_181_nf03	0.14	99.55	0.00		0.3147	1.6679	0.753	-0.016	4.11	-78.63258	33.76518
gs_182_nf03	0.23	99.50	0.00		0.3815	1.3904	0.711	0.407	4.911	-78.62196	33.76920
gs_183_nf03	0.4	99.25	0.00		0.3562	1.4894	0.822	0.018	3.745	-78.61260	33.77142
gs_184_nf03	-0.02	99.38	0.00		0.3347	1.5793	0.807	0.174	4.226	-78.60211	33.77447
gs_185_nf03	0.23	99.46	0.00		0.3467	1.5281	0.73	0.022	5.11	-78.59340	33.77783
gs_186_nf03	1.58	98.07	0.00		0.6996	0.5153	0.729	0.725	9.799	-78.58222	33.78222
gs_187_nf03	0.46	98.92	0.00		0.3322	1.5900	0.854	0.089	4.282	-78.57332	33.78595
gs_188_nf03	5.75	93.87	0.00		0.5071	0.9795	1.201	-0.529	3.678	-78.56339	33.78884
gs_189_nf03	0.51	99.01	0.00		0.3221	1.6345	0.851	-0.432	5.015	-78.54863	33.79379
gs_190_nf03	0.1	99.64	0.00		0.3449	1.5356	0.771	0.04	3.731	-78.53585	33.79958
gs_191_nf03	0.12	99.57	0.00		0.2182	2.1963	0.612	-0.707	7.406	-78.53776	33.81058
gs_192_nf03	0.32	99.07	0.00		0.2363	2.0814	0.703	-0.713	7.912	-78.54399	33.81684
gs_193_nf03	0.64	98.77	0.00		0.3075	1.7013	0.847	-0.334	5.075	-78.55926	33.81249
gs_194_nf03	1.9	97.75	0.00		0.3266	1.6144	0.899	-1.198	7.451	-78.57415	33.80755
gs_195_nf03	0.47	99.17	0.00		0.2915	1.7782	0.802	-0.406	4.658	-78.58686	33.80286
gs_196_nf03	1.12	98.48	0.00		0.3541	1.4979	0.885	-0.329	4.661	-78.60400	33.79769
gs_197_nf03	0.51	99.24	0.00		0.3539	1.4987	0.789	-0.204	4.621	-78.61814	33.78938
gs_198_nf03	0.34	99.29	0.00		0.2396	2.0612	0.699	-0.813	7.48	-78.62934	33.78580
gs_199_nf03	2.52	97.11	0.00		0.2848	1.8120	0.966	-1.676	8.334	-78.64451	33.77861
gs_200_nf03	11.12	88.62	0.00		0.5563	0.8461	1.333	-0.666	3.007	-78.65418	33.77509
gs_201_nf03	6.26	93.38	0.00		0.5380	0.8943	1.125	-0.394	3.678	-78.66461	33.77063
gs_202_nf03	1.26	98.43	0.00		0.2859	1.8062	0.861	-1.061	6.683	-78.67058	33.76763
gs_203_nf03	2.03	97.73	0.00		0.2981	1.7462	1.077	-0.965	3.756	-78.68177	33.76232
gs_204_nf03	3.47	96.37	0.00		0.4965	1.0101	0.834	-1.1	8.683	-78.68605	33.76015
gs_205_nf03	0.6	99.05	0.00		0.2344	2.0930	0.725	-1.255	8.785	-78.69051	33.75750
gs_206_nf03	0.55	99.13	0.00		0.2243	2.1563	0.73	-1.22	7.786	-78.69720	33.75465
gs_207_nf03	0.22	98.31	0.00		0.1773	2.4958	0.677	-0.889	10.7	-78.69994	33.75186
gs_208_nf03	2.85	96.89	0.00		0.6437	0.6355	0.815	-0.057	7.294	-78.70287	33.75109
gs_209_nf03	0.51	98.34	0.00		0.1860	2.4267	0.72	-1.546	12.953	-78.70709	33.74745
gs_210_nf03	0.22	95.84	0.00		0.1641	2.6077	0.816	-0.602	8.727	-78.71227	33.74542
gs_211_nf03	18.3	81.18	0.00		0.4921	1.0229	1.713	-0.588	2.231	-78.71675	33.74249

Sample ID	% Gravel	% Sand	% Silt	% Clay	Mean Grain Size (mm)	Mean Grain Size (phi)	Sorting	Skewness	Kurtosis	Longitude	Latitude
gs_212_nf03	30.7	68.50	0.00		1.2370	-0.3069	1.41	0.422	3.473	-78.72236	33.73936
gs_213_nf03	0.99	98.73	0.00		0.4646	1.1059	0.695	0.079	7.632	-78.72779	33.73712
gs_214_nf03	0.13	99.58	0.00		0.3759	1.4114	0.665	0.226	5.832	-78.73337	33.73460
gs_215_nf03	0.96	97.17	0.00		0.2375	2.0743	1.078	-0.847	4.896	-78.73638	33.73160
gs_216_nf03	0.14	99.54	0.00		0.2331	2.1012	0.706	-0.761	5.625	-78.74099	33.72919
gs_217_nf03	2.39	97.18	0.00		0.5777	0.7915	0.848	0.246	6.902	-78.74443	33.72709
gs_218_nf03	0.3	99.36	0.00		0.4467	1.1627	0.855	0.278	4.156	-78.74819	33.72440
gs_261_nf03	1.59	97.28	0.00		0.2093	2.2562	0.877	-2.094	12.087	-78.99875	33.53083
gs_262_nf03	4.44	94.96	0.00		0.2484	2.0090	1.096	-2.028	8.007	-78.99434	33.53890
gs_263_nf03	3.19	96.40	0.00		0.2403	2.0570	0.99	-2.154	9.128	-78.98871	33.54875
gs_264_nf03	1.3	98.28	0.00		0.1922	2.3793	0.742	-2.726	16.091	-78.98192	33.55659
gs_265_nf03	0.83	99.04	0.00		0.2847	1.8124	0.694	-1.516	9.326	-78.97434	33.56266
gs_266_nf03	5.79	93.35	0.00		0.2364	2.0808	1.257	-2.198	8.15	-78.96961	33.56984
gs_267_nf03	0.75	98.82	0.00		0.2659	1.9110	0.717	-1.097	8.958	-78.95985	33.57729
gs_268_nf03	1.68	97.85	0.00		0.2767	1.8536	0.869	-1.35	7.411	-78.95005	33.58923
gs_269_nf03	7.89	91.82	0.00		0.4358	1.1982	1.195	-1.224	4.696	-78.93880	33.58874
gs_270_nf03	3.53	96.20	0.00		0.4022	1.3139	1.056	-0.863	4.204	-78.92633	33.57724
gs_271_nf03	5.99	93.60	0.00		0.3946	1.3417	1.201	-1.131	4.431	-78.93367	33.57073
gs_272_nf03	0.93	98.59	0.00		0.2880	1.7956	0.815	-1.094	7.076	-78.94126	33.56410
gs_273_nf03	0.25	99.37	0.00		0.2621	1.9318	0.622	-0.591	9.153	-78.94710	33.55687
gs_274_nf03	0.33	98.60	0.00		0.1901	2.3951	0.682	-0.966	9.195	-78.95395	33.55021
gs_275_nf03	0.6	99.00	0.00		0.2435	2.0383	0.724	-1.487	8.671	-78.95631	33.54615
gs_276_nf03	0.86	98.20	0.00		0.1839	2.4432	0.716	-2.267	15.939	-78.96167	33.53952
gs_277_nf03	19.54	79.77	0.00		0.9856	0.0209	1.289	0.611	3.819	-78.96627	33.52860
gs_278_nf03	6.86	92.69	0.00		0.5838	0.7765	1.179	-0.36	3.674	-78.96737	33.51077
gs_279_nf03	0.71	98.58	0.00		0.2228	2.1660	0.77	-1.579	10.005	-78.96471	33.50652
gs_280_nf03	0.82	98.51	0.00		0.3114	1.6832	0.842	-0.71	5.845	-78.96440	33.49957
gs_281_nf03	0.08	99.40	0.00		0.2375	2.0741	0.595	-0.433	8.011	-78.96061	33.48998
gs_282_nf03	4.37	95.27	0.00		0.5142	0.9597	0.988	-0.509	4.449	-78.95132	33.49893
gs_283_nf03	7.58	91.73	0.00		0.4522	1.1451	1.407	-0.36	2.564	-78.94141	33.51075
gs_284_nf03	2.38	97.03	0.00		0.4329	1.2079	0.907	-0.293	5.748	-78.93558	33.52126
gs_285_nf03	0.4	99.19	0.00		0.2904	1.7841	0.772	-0.85	5.889	-78.92937	33.52807
gs_286_nf03	2.83	96.76	0.00		0.4543	1.1382	1.022	-0.507	4.18	-78.92603	33.53466
gs_287_nf03	0.95	98.45	0.00		0.2689	1.8950	0.873	-0.91	4.968	-78.92181	33.54021
gs_288_nf03	1.23	98.08	0.00		0.2725	1.8759	0.855	-1.101	6.768	-78.91232	33.54758
gs_289_nf03	5.62	93.56	0.00		0.5853	0.7727	1.105	0.095	4.106	-78.90457	33.55279
gs_290a_nf0	0.37	99.18	0.00		0.2685	1.8971	0.767	-0.83	5.819	-78.89739	33.56105
gs_291_nf03	1.63	98.21	0.00		0.4471	1.1612	0.834	-0.346	4.776	-78.89231	33.56767
gs_292_nf03	3.45	96.17	0.00		0.4351	1.2005	1.034	-0.565	4.149	-78.88546	33.57248
gs_293_nf03	1.6	97.78	0.00		0.4463	1.1640	0.941	-0.057	4.663	-78.87305	33.58611
gs_294_nf03	1.73	97.58	0.00		0.4373	1.1933	0.958	0.02	4.349	-78.86147	33.59500
gs_295_nf03	0.36	98.78	0.00		0.3362	1.5727	0.825	0.108	5.296	-78.85760	33.59832
gs_296_nf03	1.12	98.35	0.00		0.3951	1.3397	0.954	0.01	3.523	-78.84863	33.60640
gs_297_nf03	1.01	98.79	0.00		0.4066	1.2983	0.93	-0.263	3.471	-78.83659	33.61477
gs_298_nf03	2.31	97.49	0.00		0.4515	1.1471	0.987	-0.154	4.179	-78.82152	33.62915
gs_299_nf03	23.16	76.62	0.00		0.8017	0.3189	1.516	-0.258	2.156	-78.83228	33.63866
gs_300_nf03	3.01	96.75	0.00		0.4997	1.0008	0.868	-0.436	5.355	-78.84500	33.64829

Sample ID	% Gravel	% Sand	% Silt	% Clay	Mean Grain Size (mm)	Mean Grain Size (phi)	Sorting	Skewness	Kurtosis	Longitude	Latitude
gs_301_nf03	0.41	99.27	0.00		0.2508	1.9957	0.706	-1.066	8.78	-78.85799	33.63907
gs_302_nf03	1.38	98.46	0.00		0.3127	1.6769	0.903	-0.938	4.316	-78.86719	33.63015
gs_303_nf03	0.18	99.51	0.00		0.2337	2.0971	0.618	-0.925	7.659	-78.87483	33.61845
gs_304_nf03	1.92	97.54	0.00		0.3063	1.7068	0.894	-1.171	7.152	-78.88768	33.60540
gs_305_nf03	22.35	76.34	0.00		0.9083	0.1387	1.515	0.281	3.339	-78.89644	33.58802
gs_306_nf03	3.22	96.07	0.00		0.3221	1.6342	1.021	-1.378	6.824	-78.90335	33.57671
gs_307_nf03	44.98	54.65	0.00		1.1254	-0.1704	1.957	0.063	1.346	-78.91355	33.58392
gs_308_nf03	0.89	98.28	0.00		0.2611	1.9374	0.742	-0.868	11.033	-78.92273	33.59627
gs_309_nf03	10.46	88.83	0.00		0.3897	1.3596	1.426	-1.063	3.668	-78.91493	33.60629
gs_310_nf03	0.44	98.75	0.00		0.2181	2.1968	0.697	-1.119	9.524	-78.90902	33.61490
gs_311_nf03	0.8	98.60	0.00		0.2524	1.9863	0.762	-1.36	9.331	-78.90386	33.62080
gs_312_nf03	1.16	98.32	0.00		0.2115	2.2413	0.778	-2.108	11.913	-78.89652	33.62897
gs_313_nf03	1.6	98.03	0.00		0.2686	1.8966	0.793	-1.779	10.682	-78.89171	33.63468
gs_314_nf03	0.62	99.18	0.00		0.2273	2.1373	0.683	-1.861	10.298	-78.88503	33.64067
gs_315_nf03	16.81	82.90	0.00		0.4803	1.0580	1.617	-0.866	2.751	-78.87943	33.64376
gs_316_nf03	2.11	97.98	0.00		0.2369	2.0779	0.878	-2.292	9.818	-78.87179	33.65177
gs_317_nf03	0.48	99.30	0.00		0.2233	2.1629	0.719	-1.417	7.6	-78.86602	33.65586
gs_318_nf03	13.31	88.67	0.00		0.4679	1.0958	1.354	-2.058	3.785	-78.85851	33.66421
gs_319_nf03	1.97	97.36	0.00		0.2429	2.0417	0.883	-1.772	10.148	-78.84867	33.67408
gs_320_nf03	3.13	96.39	0.00		0.3887	1.3631	0.99	-0.549	4.894	-78.83662	33.67916
gs_321_nf03	0.8	98.60	0.00		0.2146	2.2202	0.781	-1.553	8.842	-78.82650	33.67425
gs_322_nf03	0.14	99.51	0.00		0.2994	1.7399	0.756	-0.159	4.112	-78.81932	33.66703

Appendix B1. Descriptive logs of two cores collected from the shoreface-detached shoal offshore of Myrtle Beach. See Figure 6 for core locations. Shell and organic material were extracted from the cores and submitted for C-14 dating, yielding Holocene age of the shore-oblique shoal (Gayes, pers. comm.). Cores were described by E. Karbabanov May and August 2001.

Appendix B 1- Core Descriptions

Core ID: NF00-A1-6 **Total length (cm): 168**

description by: E. Karabanov **May 2001**

Lithology Photo Color

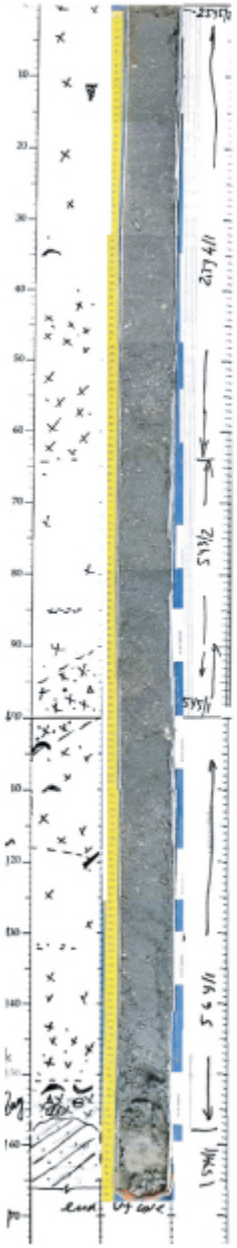

0-1 cm: grayish brown fine sand with shell fragments - oxidized surface layer.

1-151 cm: olive gray medium-fine sand with shell fragments and few whole shells. Sand is not carbonated.

1-45/50 cm: fine clean sand with small amount of shell fragments and rare shells that is well preserved.

45/50-65 cm: medium sand with fine and coarse sand and abundant shell fragments and few small shells - good preserved. There are black shell fragmesnts. The upper boundary obscure but lower boundary more visible.

65-90/95 cm: medium sand with fine and coarse sand and shell fragments (less then above). The amount of shell fragments increase down of layer. There are few black shell fragments. Some fine beds or lenses dark colored sand are present at 80-90 cm depth.

90/95-100/105 cm: coarse sand bed with fine and medium sand and some fine gravel grains and abundant shell fragments. Coarse sand grains are angular and subangular. Lower boundary eroded or bioturbated.

100/105-118/120 cm: same like 65-80 cm.

118/120 - 151 cm: medium sand with fine sand with shell fragments - more dense then above. The concentration of shell fragments increase down layer. There are some black shell fragments and black phosphate concertions. There is medium-fine sand bed with gradation boundaries at 131-132 cm depth. This layer gradually transform to next layer with biggest amount of shell fragments at depth 151 cm.

151-156/158 cm: shell detritus with medium/fine sand, coarse sand, black shell fragmetns, black phosphate concretions and clay/mud inclusion - clast. This layer represents the rest (coarse fractions) of sediments, when fine sediment are eroded and removed by currents - lag?

156/158-166 cm: dense cemented (carbonate cemetn??) olive gray silty sand/sandstone (fine-very fine with rare grains of coarse sand) with high carbonate content. This layer similar to observed in core #7 at **195-210 cm** depth and probably represents ancient (creatceous ??) sandstone rock that commonly exposed in sea floor in this area (Paul Gayes information).

*** Dated material (shell) extracted from 137 cm**

Appendix B2. Descriptive logs of two cores collected from the shoreface-detached shoal offshore of Myrtle Beach. See Figure 6 for core locations. Shell and organic material were extracted from the cores and submitted for C-14 dating, yielding Holocene age of the shore-oblique shoal (Gayes, pers. comm.). Cores were described by E. Karbabanov May and August 2001.

Appendix B 2- Core Descriptions

Core ID: NF01-50

Total length (cm): 128

description by: E. Karabanov **August 2001**

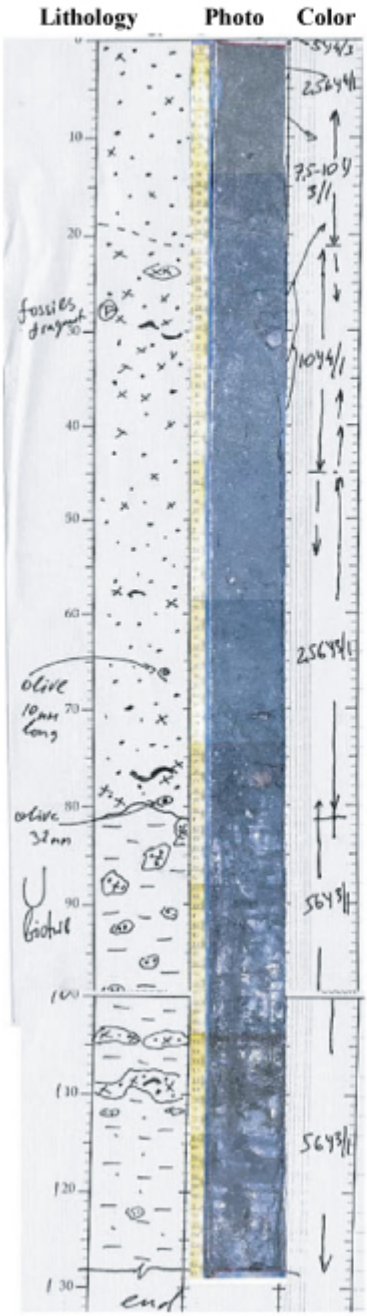

0-19/21 cm: fine to medium sand: 0 0.2 cm yellow gray-oxidized layer; 0.2 - 7 cm dark olive gran, 7-21 cm olive balck. There is sulfur smell (H2S). Some shell framgenst are present. Sediments are low carbonated just in shell fragments.

19/21-45-50 cm: gray medium sand with coarse and very coarse sand grains. There are also fine sand grains. Shell fragments are abundant. There are some small unbroken shells. Some obscure lamination is observerd - due change of color and grain size and shell fragments percentage.

45-50 - 81 cm: Upper sand layer gradually transform to dark olive gray fine sand (weith medium) at this depth. There are less shell fragments then above layer. There are some unbroken shells - small cockle, olive. Sand is low carbonated - just shell fragments. Bottom boundary is hard and eroded.

81-128 cm: olive dark gray (almost black) fine cary (mud) soft wet with silt and fine sand grains. Clay is highly bioturbated at 81-112 cm depth. There are many lenses with fine/medium sand with shell fragments like above layer. Clay is barren of shell fragments and low carboneated (except bioturbated lenses). Surface boundary eroded or bioturbated but no oxidized. So it was exposed on sea surface but not much time and always was covered by sand. Dark color of clay shows that clay is organic rich. This maybe represents freshwater lagoon or pond sedimentary environments. Similar not carbonated balck clay also observed in some cores from NF00.

*** Dated material (organic sediment) extracted from 81-128 cm**